NUREG/CR-1822
BMI-2069
R2

Steam-Water Mixing and System Hydrodynamics Program - Task 4

Quarterly Progress Report
July - September 1980

Manuscript Completed: October 1980
Date Published: November 1980

Prepared by
A. Segev, R. P. Collier

Battelle Columbus Laboratories
505 King Avenue
Columbus, OH 43201

Prepared for
Division of Reactor Safety Research
Office of Nuclear Regulatory Research
U.S. Nuclear Regulatory Commission
Washington, D.C. 20555
NRC FIN No. A4048

8012120590

PREVIOUS REPORTS IN THIS SERIES

Report No.	Period Covered	Date Issued
BMI-X-657	January - March 1975	April, 1975
BMI-1936	April - June 1975	August, 1975
BMI-1940	July - September 1975	November, 1975
BMI-NUREG-1945	October - December 1975	March, 1976
BMI-NUREG-1949	January - March 1976	May, 1976
BMI-NUREG-1962	April - June 1976	November, o976
BMI-NUREG-1964	July - September 1976	December, 1976
BMI-NUREG-1968	October - December 1976	February, 1977
BMI-NUREG-1972	January - March 1977	May, 1977
BMI-NUREG-1979	April - June 1977	September, 1977
BMI-NUREG-1987	July - September 1977	December, 1977
NUREG/CR-0034 (BMI-1993)	October - December 1977	March, 1978
NUREG/CR-0147 (BMI-2003)	January - March 1978	June, 1978
NUREG/CR-0526 (BMI-2011)	April - June 1978	November, 1978
NUREG/CR-0565 (BMI-2013)	July - September 1978	December, 1978
NUREG/CR-0845 (BMI-2028)	October - December 1978	May, 1979
NUREG/CR-0897 (BMI-2029)	January - March 1979	June, 1979
NUREG/CR-1557 (BMI-2038)	April - June 1979	June, 1980
NUREG/CR-1625 (BMI-2058)	July - September 1979	July, 1980
NUREG/CR-1657 (BMI-2062)	October - December 1979	August, 1980
NUREG/CR-1742 (BMI-2065)	January - March 1980	September, 1980
NUREG/CR-1743 (BMI-2067)	April - June, 1980	September, 1980

ABSTRACT

During this quarter we analyzed results from hot wall tests in the 2/15-scale model and compared the experimental filling curves to those predicted by the mechanistic model. The comparison shows a good agreement for both the large break tests and scaled size break tests.

SUMMARY

This report describes progress during the fourth quarter of FY'80 on the BCL Steam-Water Mixing and System Hydrodynamics Program.

During this quarter we concluded the analysis of hot wall tests conducted in the 2/15-scale model with scaled and oversized break leg. The experimental filling traces were compared with theoretical predictions obtained from a modified version of the mechanistic model. The major modification is in the hot wall calculation precedure. The present model is capable of predicting the entire filling trace and is not limited to time delay calculation. The comparison shows a reasonably good agreement for the penetration delay time and the penetration rate.

TABLE OF CONTENTS

LIST OF FIGURES

LIST OF FIGURES

(Continued)

LIST OF FIGURES
(Continued)

INTRODUCTION

The U. S. Nuclear Regulatory Commission is responsible for assessing and assuring the safety of nuclear reactors under abnormal conditions such as a postulated loss-of-coolant accident (LOCA), as well as under normal operating conditions. Prediction of the thermal-hydraulic behavior of the reactor system following such a LOCA is of particular interest, and NRC supports a very large research effort aimed at increasing that predictive capability. In the Steam-Water Mixing and System Hydrodynamics Program currently in progress at Battelle-Columbus Laboratories (BCL) both analytical and experimental work are directed toward a more thorough understanding and description of steam-water interaction and its influence on the effectiveness of emergency core cooling systems under LOCA conditions. The phenomena of ECC penetration and bypass are of primary interest.

Fiscal Year 1980 activities include definition of ECC bypass scaling relationships based on available data, development of a mechanistic model for ECC penetration, and performance and evaluation of experiments supporting ECC bypass analysis.

This Quarterly Progress Report summarizes the activities and progress made during the quarter ending September 30, 1980.

Progress for Quarter

July 1, 1980 - September 30, 1980

ANALYSIS

Objectives

The objectives of this task are to:

(1) Develop an improved theoretical understanding of steam-water interaction phenomena,

(2) Analyze and correlate the available experimental data,

(3) Evaluate and interpret experimental data from off-site steam-water mixing experimental efforts, and

(4) Use this knowledge to verify and improve current LOCA/ECC analysis methods.

Work During Quarter

During this quarter we concluded the analysis of hot wall tests conducted in the 2/15-scale model with scaled[1] and oversized[2] break legs. The experimental results were compared with theoretical predictions obtained from an upgrade version of the mechanistic model, resulting in a fairly good agreement. The modifications made in the theoretical model and the results obtained are described below.

Modifications of Mechanistic Model

The mechanistic model as presented in Reference 3 is somewhat limited in its application to hot wall experiments. In its original version the model is limited to the calculation of delivery delay time, measured experimentally by extrapolating the penetration curve to zero volume[4]. It does not address the problem of predicting the complete penetration curves. This has enabled us to obtain a relatively simple closed-form expression for the time delay used in the evaluation of the mechanistic model. Several problems may be identified regarding this approach. First, in the final analysis one cannot ignore the lower plenum filling period as it is an important process in the complete penetration phenomenon. Also, by considering only the time delay we ignore the transient filling period which precedes the steady part. This transient period may be significant in the theoretical description of the filling process. The second problem is associated with the restriction imposed by the assumption that the liquid film flow rate is constant during the delay time. This assumption does not hold when tests with ramped steam flow are considered since the liquid film flow rate changes with time in response to the transient in steam flow rate. For this type of flow an alternative procedure is required, in which the position of the liquid front in the downcomer is determined numerically at any given time.(3) The same approach is utilized here for hot wall tests with steady core steam flow.

For each time step the liquid flux of the penetrating liquid film ($K^*_{\ell i}$) is determined from the effective momentum correlation:

$$\{K^*_{gc} - f\lambda K^*_{\ell i} - f_1[\lambda(K^*_{\ell in} - K^*_{\ell i})D^{*1/2}]^{1/2} + Q^*\}^{1/2}(1 + K^*_{\ell i}) = (4C_a/L)^{1/4} \quad , (1)$$

where f_1 represents the condensation efficiency on the liquid being bypassed and f describes the effectiveness of energy transferred to the liquid film from the hot walls and from condensation. At the present time it is difficult to evaluate f analytically when simultaneous vaporization and condensation are involved. However, for two special cases an expression for f can be constructed. When the walls are adiabatic, only condensation is considered, and f is given by a correlation determined from experiments(5). When condensation is not present or when its effects are negligible relative to the wall heat flux, f is given by

$$f = [1 - \exp(-\frac{L - z_o}{\Delta\ell})]\,\frac{T_s - T_o}{T_\ell - T_{\ell i}} \quad , \qquad (2)$$

where $\Delta\ell$ is the significant boiling length and z_o is the point of net vapor generation, given by

$$z_o = \frac{W_{\ell i} C_p (T_o - T_{\ell i})}{P_h q_w} \quad . \tag{3}$$

The liquid temperature at z_o is determined from the correlations developed by Saha & Zuber[6].

The dimensionless heat flux Q^* is described by

$$Q^* = \frac{P_h \int_{z_o}^{z} q_w dz}{A[\rho_g{}^2 g\sigma(\rho_\ell - \rho_g)]^{1/4} h_{fg}} \quad , \tag{4}$$

where q_w is assumed to be conduction limited

$$q_w = \frac{k_w(T_w - T_s)}{\sqrt{\pi\alpha_w[t - t(z)]}} \quad , \tag{5}$$

and $t - t(z)$ is the time period that any wetted point on the wall has been in contact with the liquid film.

As can be readily shown, Equation (1) is a 6th order polynominal equation for $K^*_{\ell i}$. Attempts to solve this equation implicitly resulted in difficulties as the solution was very sensitive to changes in the coefficients during the iteration process. An alternative method has been used in which Equation (1) was solved explicitly for K^*_{gc} as $K^*_{\ell i}$ varied from zero to $K^*_{\ell in}$. The vectors for $K^*_{\ell i}$ and K^*_{gc} were then interpolated to obtain a certain value of $K^*_{\ell i}$, which corresponds to a given experimental value of K^*_{gc}.

The solution procedure is as follows: For each time step the value of $K^*_{\ell i}(t)$ is determined from Equation (1). Assuming that the film thickness is given by the Nusselt equation, the velocity and the distance the film travels during this time step are evaluated. Subsequently, $z_o(t)$ and $Q^*(t)$ are determined and substituted in Equation (1) to calculate $K^*_{\ell i}(t + \Delta t)$. When the liquid front reaches the end of the core barrel, penetration is assumed to commence.

Comparison With Experiments

Tests which examine the effects of superheated walls on ECC penetration behavior were conducted in the 2/15-scale model[1,2]. Figures (1) - (62) show the plenum filling traces from these tests with the predicted filling rates. In addition, the pressures in the lower plenum and in the containment are also given (the pressure p_V indicates the average pressure in the lower plenum). Figures (1) - (37) present results from tests with the scaled break leg. Figures (38) - (62) present results from tests with the oversized break leg. The arrows in those figures indicate the time at which ECC liquid injection was initiated.

As may be noticed, the pressure traces describe quite well the resultant vapor generation during the tests. Upon the injection of liquid, vapor is generated at the hot walls of the downcomer, resulting in a pressure increase. This pressure increase depends mainly on inlet liquid and steam flow rates, inlet liquid temperature, and initial wall temperature. The maximum pressure in the lower plenum may reach a value twice as large as the pressure in the containment. For a given set of test conditions, an increase in wall temperature results in an increase of lower plenum pressure, suggesting that a larger amount of steam was generated. It is interesting to note that even though more vapor is generated as wall temperature increases, no significant increase in time delay is observed. The explanation for that may be related to the competing effect of pressure on the penetration behavior. This point will be discussed later. After the pressure reaches its peak it then decreases gradually to near ambient pressure (in cases when cold liquid is injected), or decreases slightly in an oscillatory manner (in cases when hot liquid is injected).

A typical plenum filling curve is characterized by a time delay before filling is observed. During this time delay the liquid front moves in the downcomer and vapor is generated at the hot walls. As the film reaches the end of the downcomer the lower plenum begins to fill at a low rate, which is transient and controlled by the wall vapor generation. When the vapor generation decreases significantly (due to decrease in wall heat flux and/or an increase in z_o) a shift in the penetration rate is noticed. The rate increases and becomes steady, controlled only by the core steam flow.

As shown in Figures (1) - (62) the calculated penetration delay time coincides in most tests to the time at which liquid first reaches the lower plenum and the calculated penetration rates are also in satisfactory agreement with the experiments. From these tests and from the theoretical model we can evaluate the effects of the major variables on the plenum filling behavior.

Core Steam Flow - As core steam flow rate increases more liquid is bypassed, resulting in a longer delay time, a longer period of steam generation, and lower rate of steady penetration.

ECC Water Flow - The major effect of inlet liquid flow rate is on the condensation on the bypassed liquid (K^*_{cbp}). As $K^*_{\ell in}$ increases, K^*_{cbp} increases and consequently $K^*_{\ell i}$ increases, resulting in shorter time delays, a shorter transient period, and a larger steady penetration rate.

ECC Subcooling - Subcooling ($\Delta T_s = T_s - T_{\ell i}$) affects the condensation potential and net vaporization point z_o. An increase in ΔT_s results in an increase in condensation and z_o. The latter indicates that the boiling component of the wall heat flux decreases as liquid subcooling increases. This also can be shown from the expression for f (Equation 2). All these processes cause an enhancement of liquid penetration.

Pressure - As the pressure in the vessel increases, the liquid subcooling increases, the wall superheat decreases, and the effective dimensionless steam flux decreases, all resulting in a faster filling.

Wall Superheat - ($\Delta T_w = T_w - T_s$) When the wall superheat increases, more vapor is generated. If the pressure remains unchanged, the vapor generated increases the effective steam flow and the filling of the lower plenum is delayed. However, if the pressure in the lower plenum increases due to the enhanced vapor generation, the filling rate may increase and the time delay may decrease according to the pressure effects discussed above.

Plans for Future Work

During the next quarter, effort will be concentrated on comparing the prediction of the mechanistic model to the hot wall experimental results obtained in Creare's 1/15-scale model and to ramped steam flow tests conducted in Battelle's 2/15-scale model.

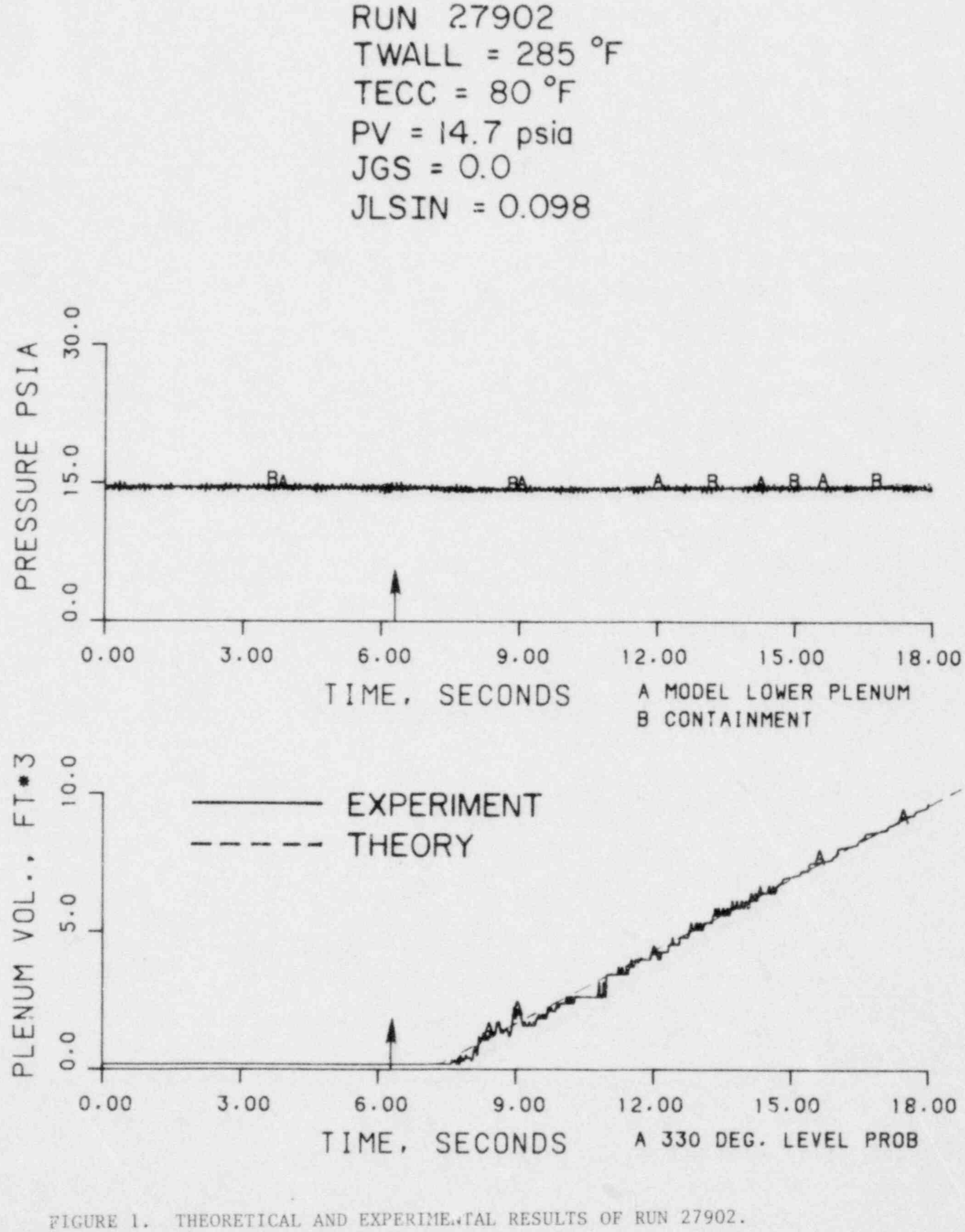

FIGURE 1. THEORETICAL AND EXPERIMENTAL RESULTS OF RUN 27902.

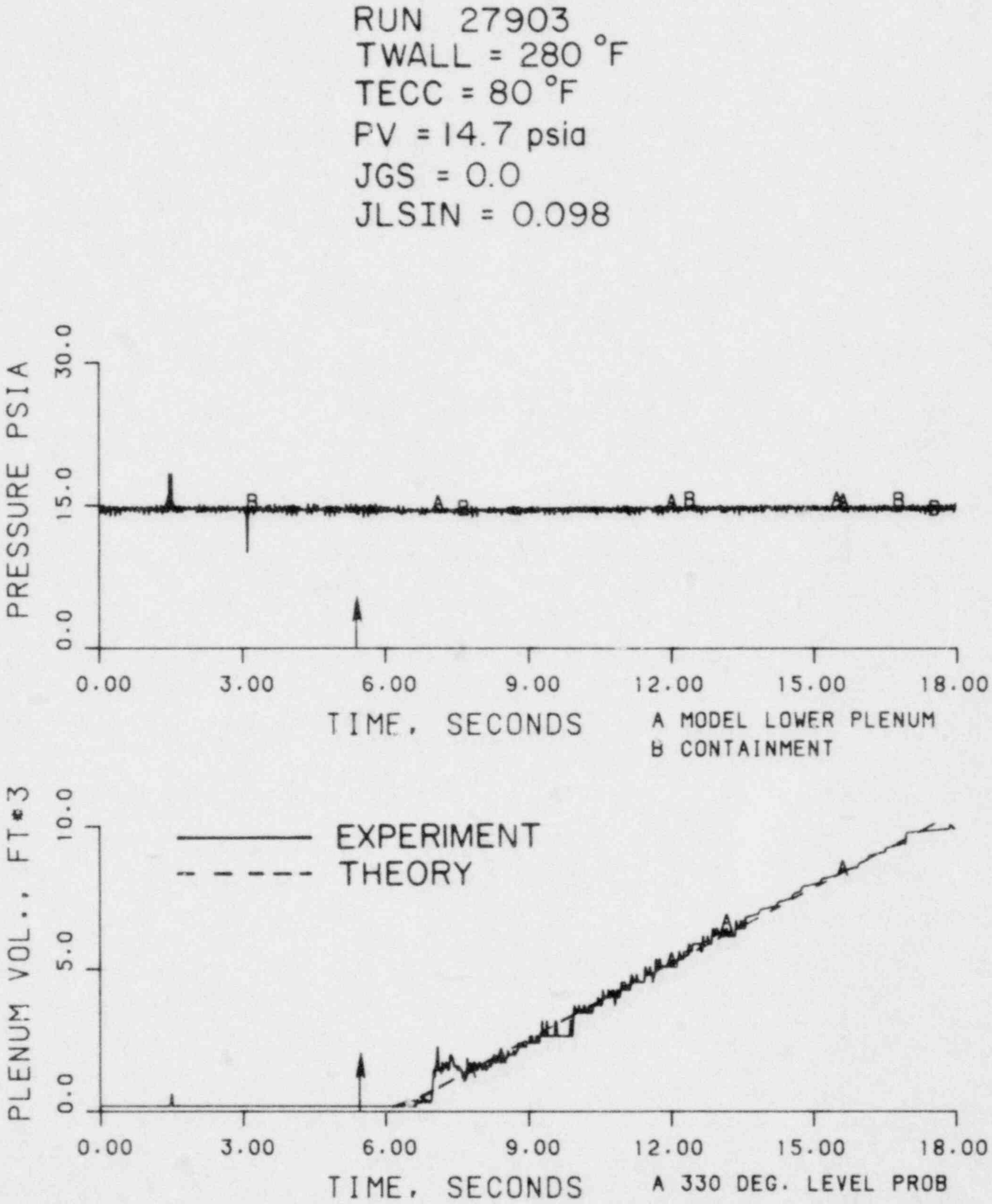

FIGURE 2. THERORETICAL AND EXPERIMENTAL RESULTS OF RUN 27903.

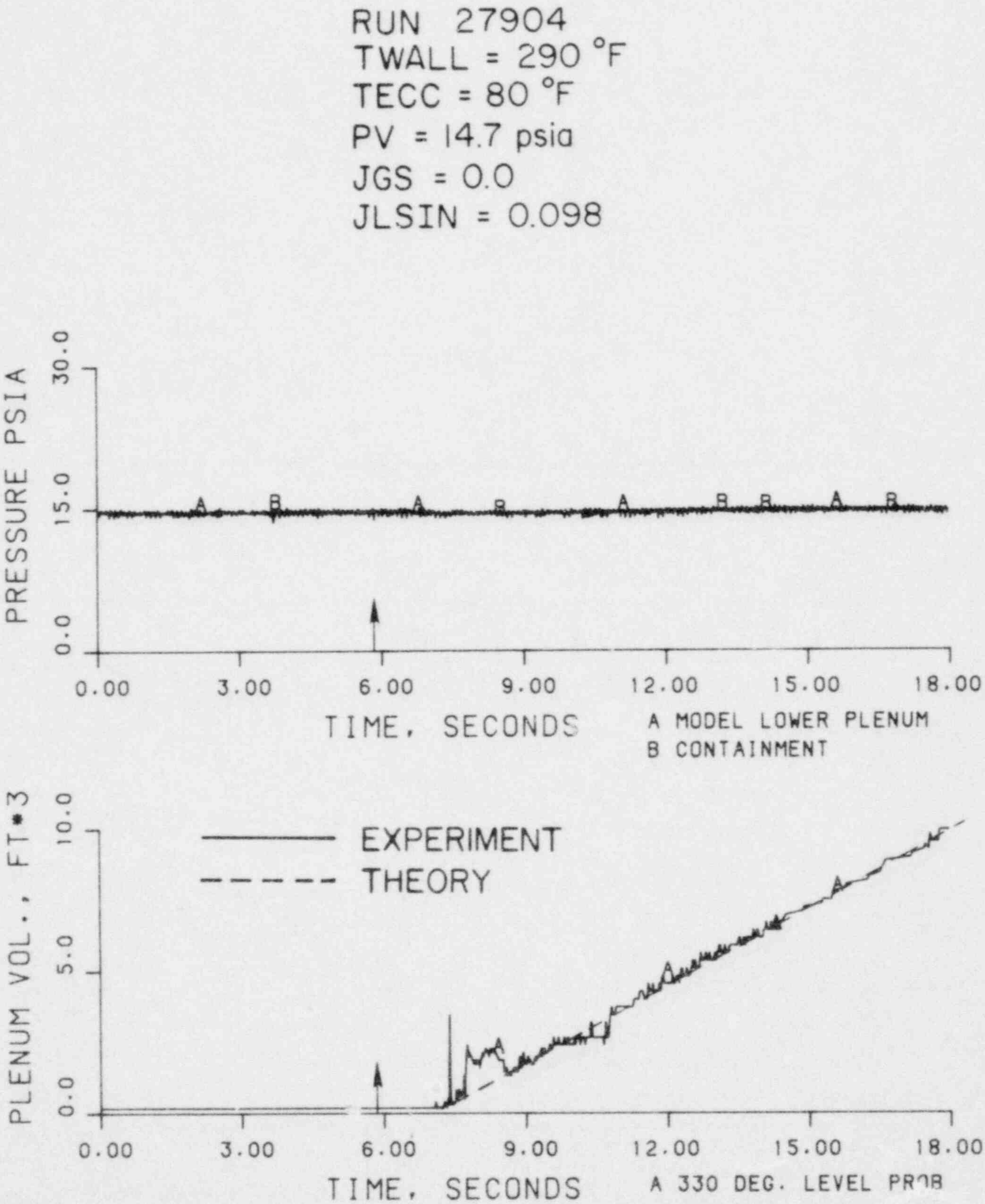

FIGURE 3. THEORETICAL AND EXPERIMENTAL RESULTS OF RUN 27904.

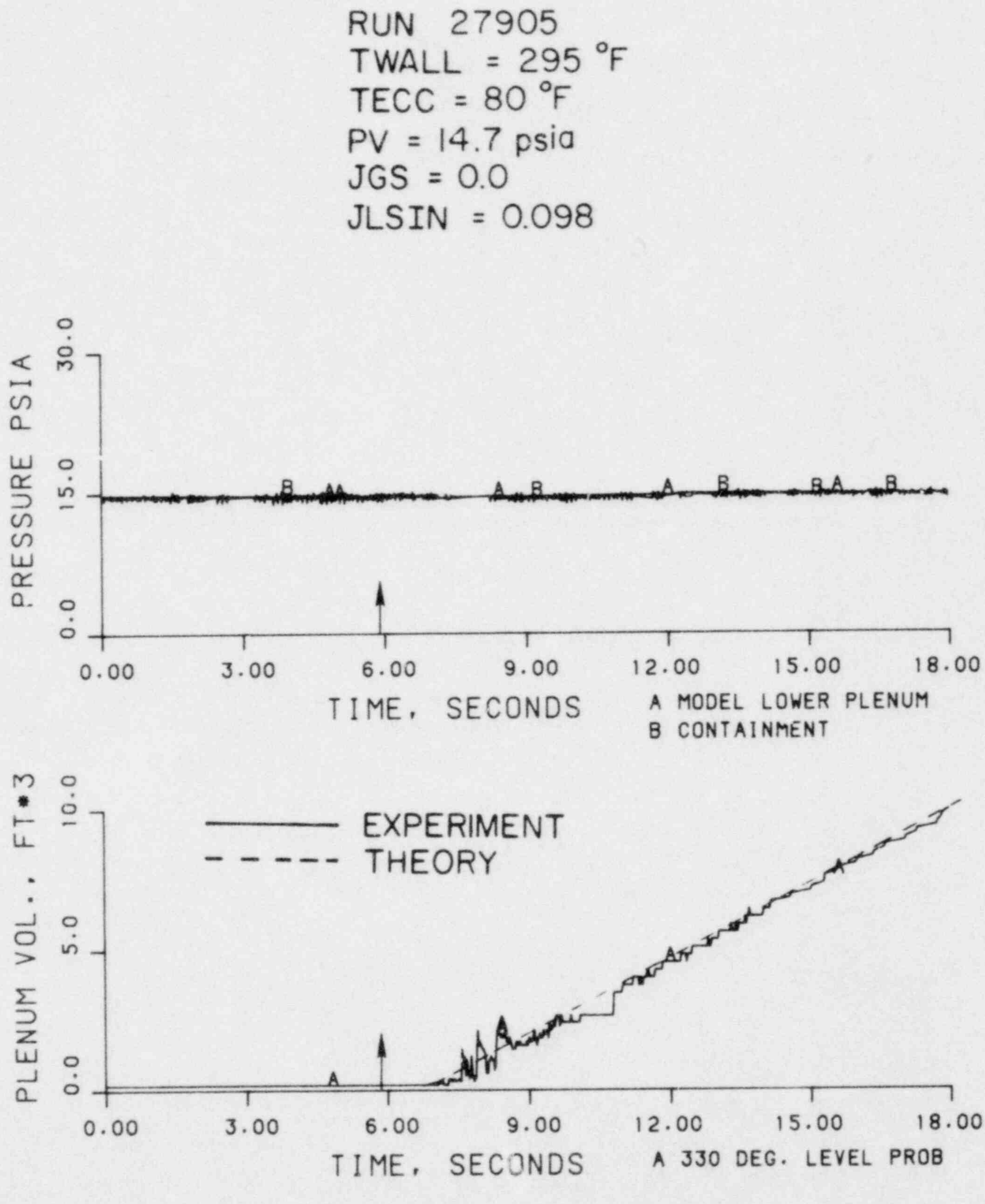

FIGURE 4. THEORETICAL AND EXPERIMENTAL RESULTS OF RUN 27905.

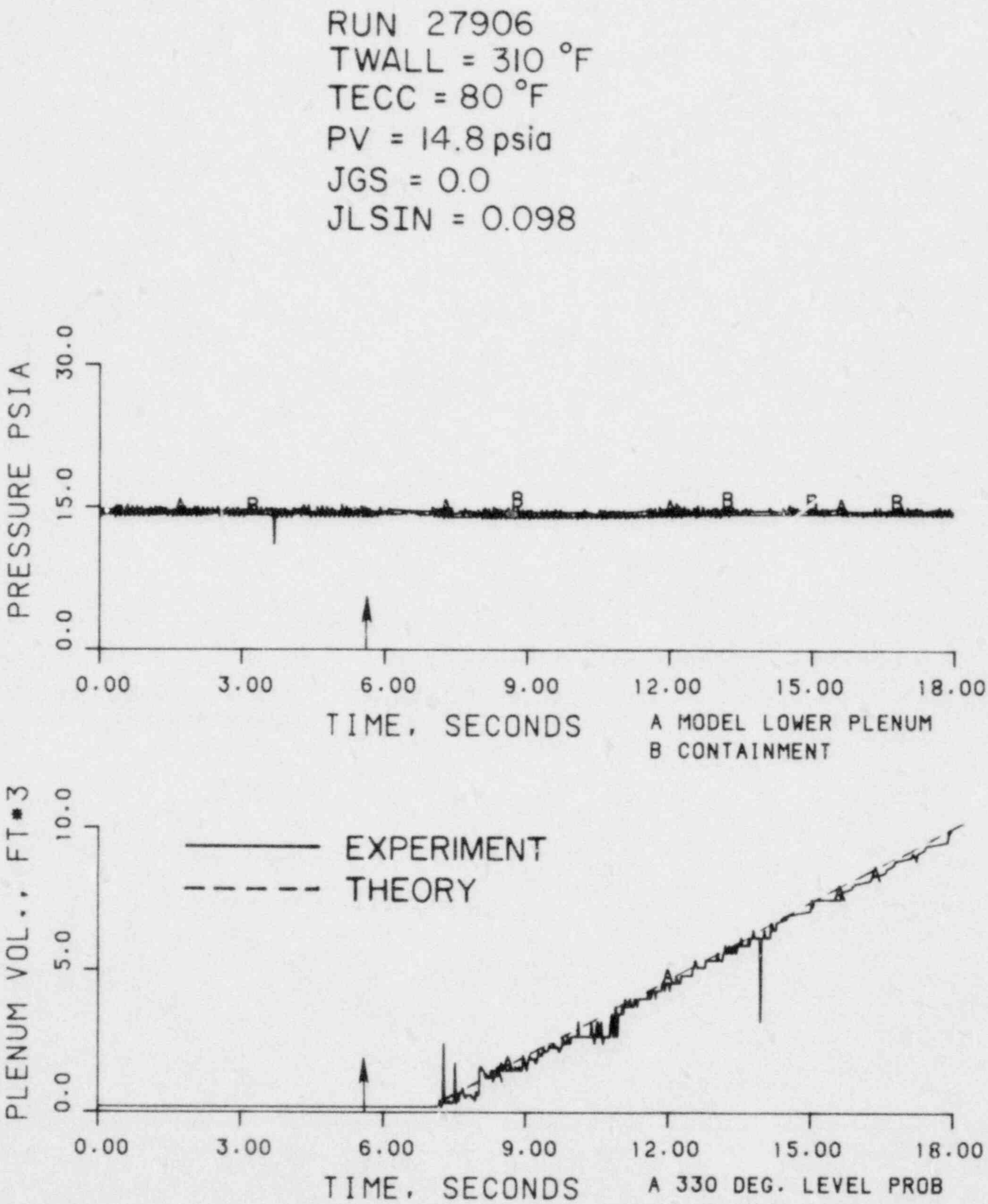

FIGURE 5. THEORETICAL AND EXPERIMENTAL RESULTS OF RUN 27906.

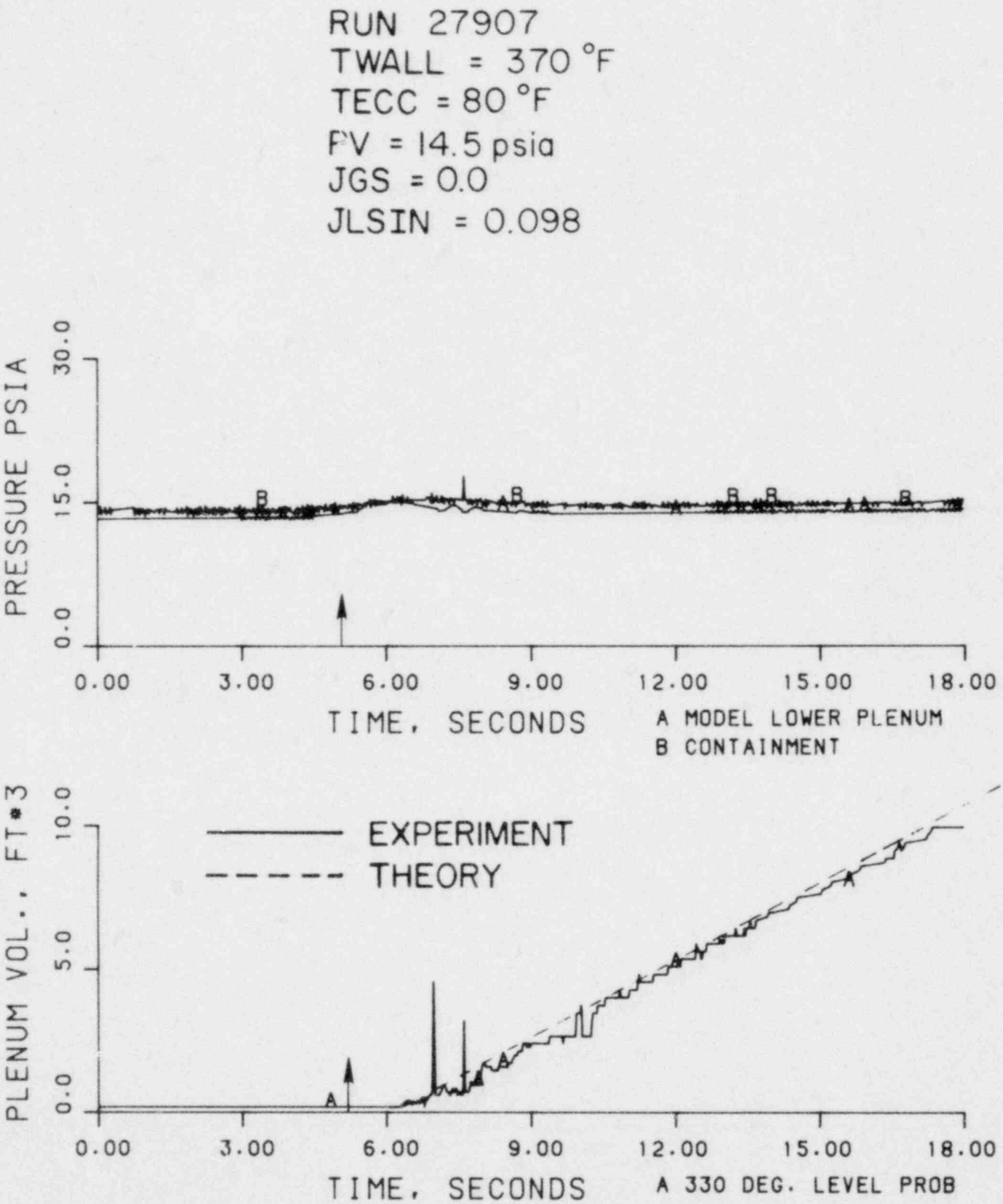

FIGURE 6. THEORETICAL AND EXPERIMENTAL RESULTS OF RUN 27907.

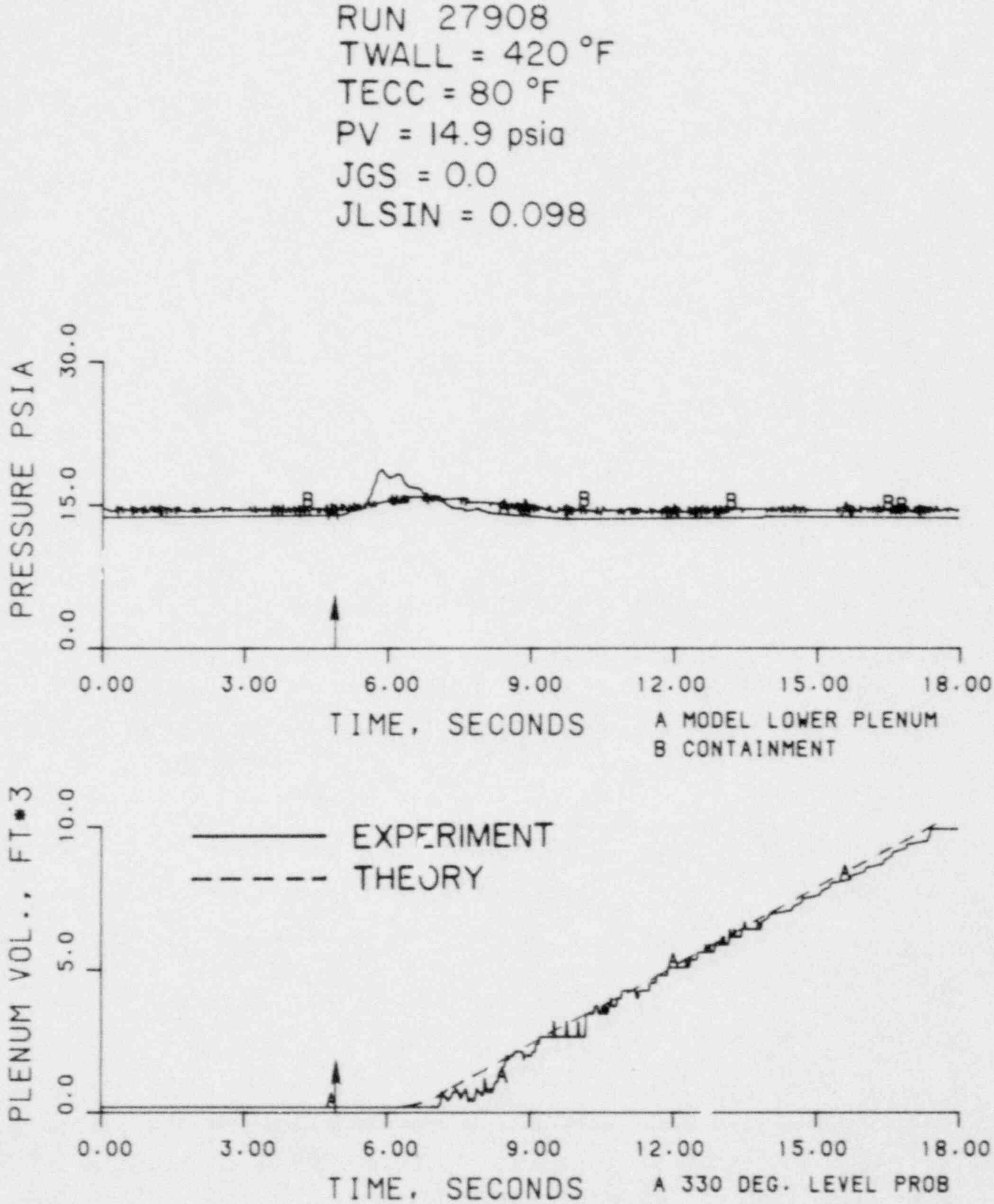

FIGURE 7. THEORETICAL AND EXPERIMENTAL RESULTS OF RUN 27908.

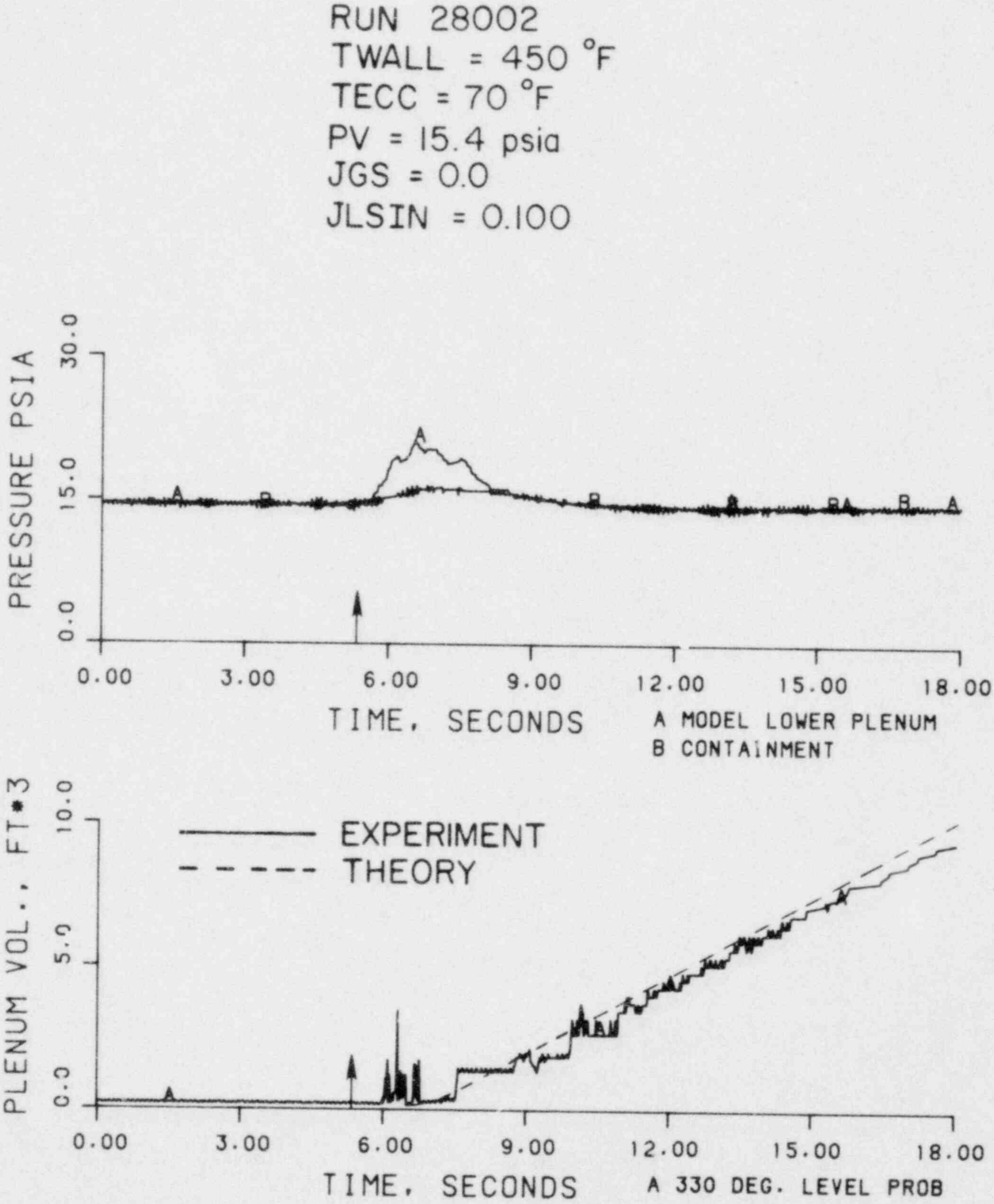

FIGURE 8. THEORETICAL AND EXPERIMENTAL RESULTS OF RUN 28002.

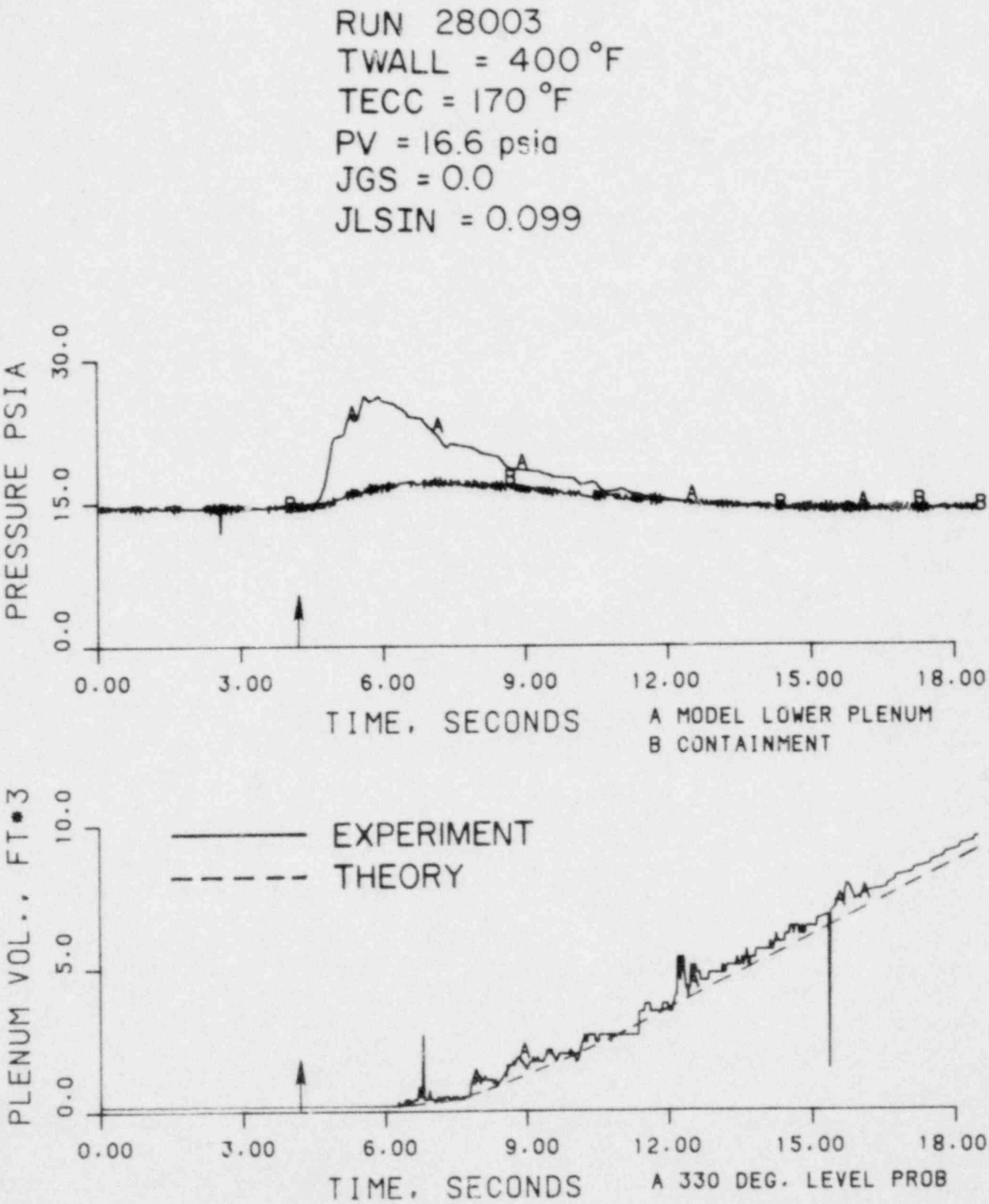

FIGURE 9. THEORFTICAL AND EXPERIMENTAL RESULTS OF RUN 28003.

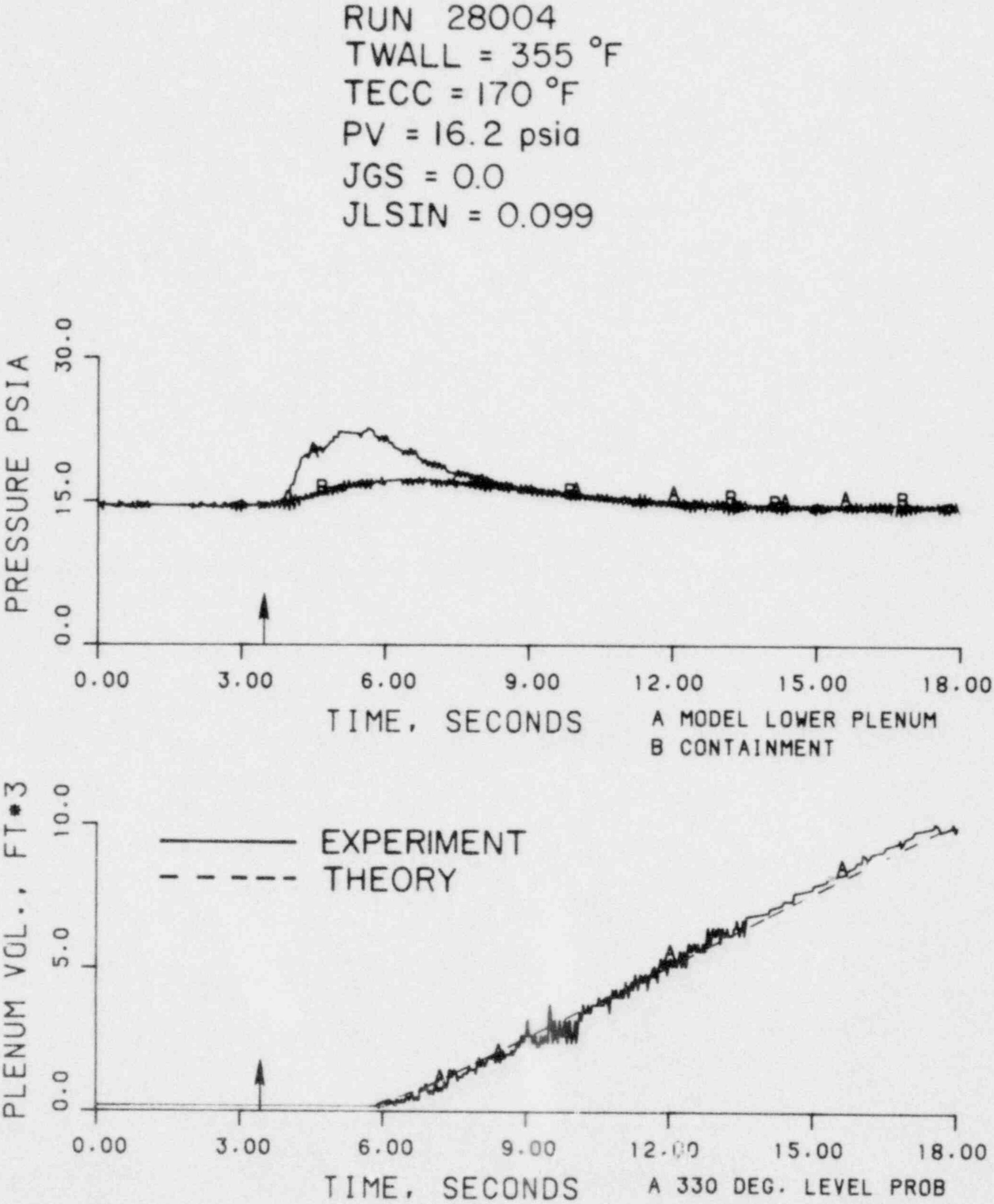

FIGURE 10. THEORETICAL AND EXPERIMENTAL RESULTS OF RUN 28004.

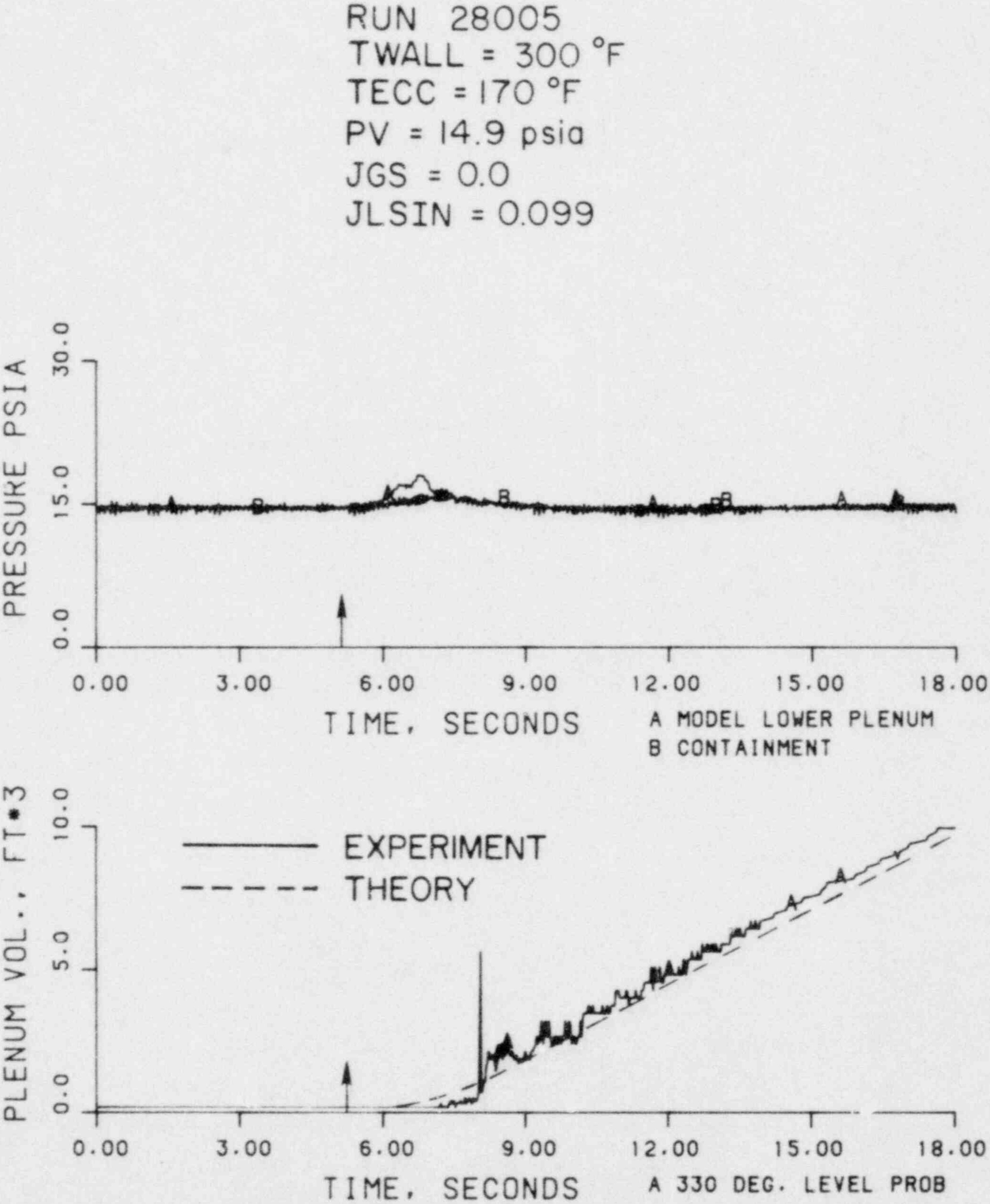

FIGURE 11. THEORETICAL AND FXPERIMENTAL RESULTS OF RUN 28005.

RUN 28010
TWALL = 300 °F
TECC = 208 °F
PV = 31.3 psia
JGS = 0.063
JLSIN = 0.092

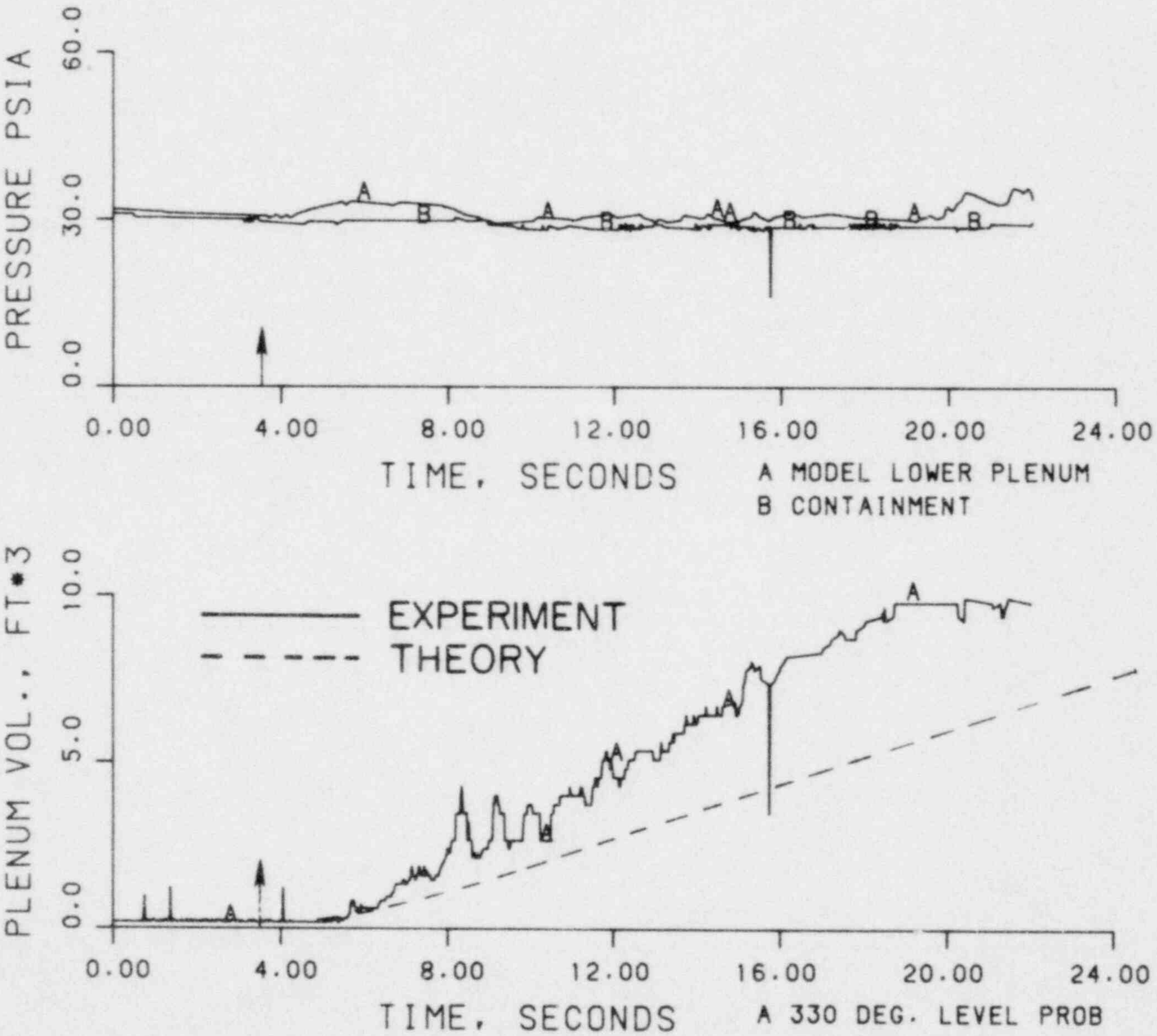

FIGURE 12. THEORETICAL AND EXPERIMENTAL RESULTS OF RUN 28010.

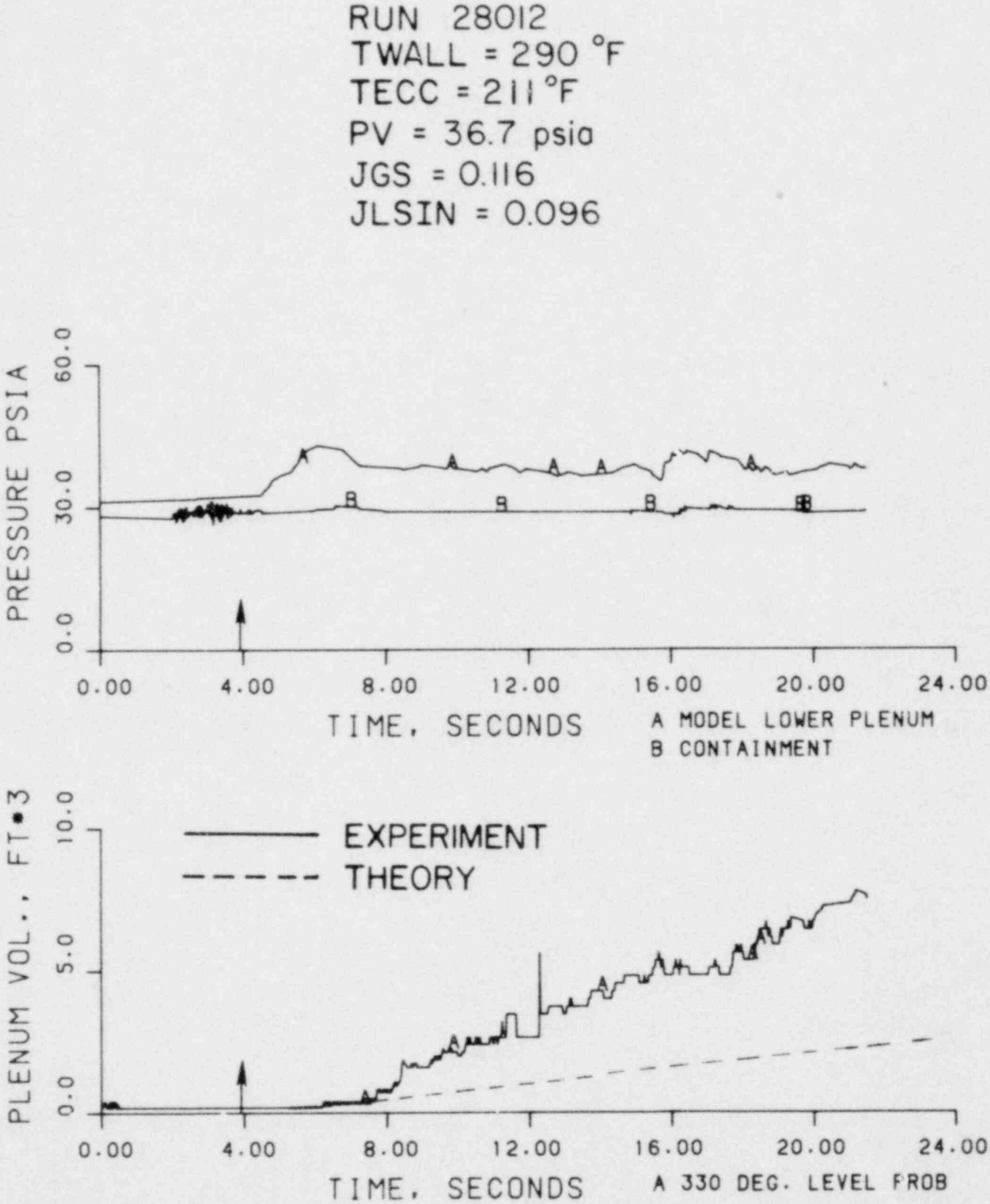

FIGURE 13. THEORETICAL AND EXPERIMENTAL RESULTS OF RUN 28012.

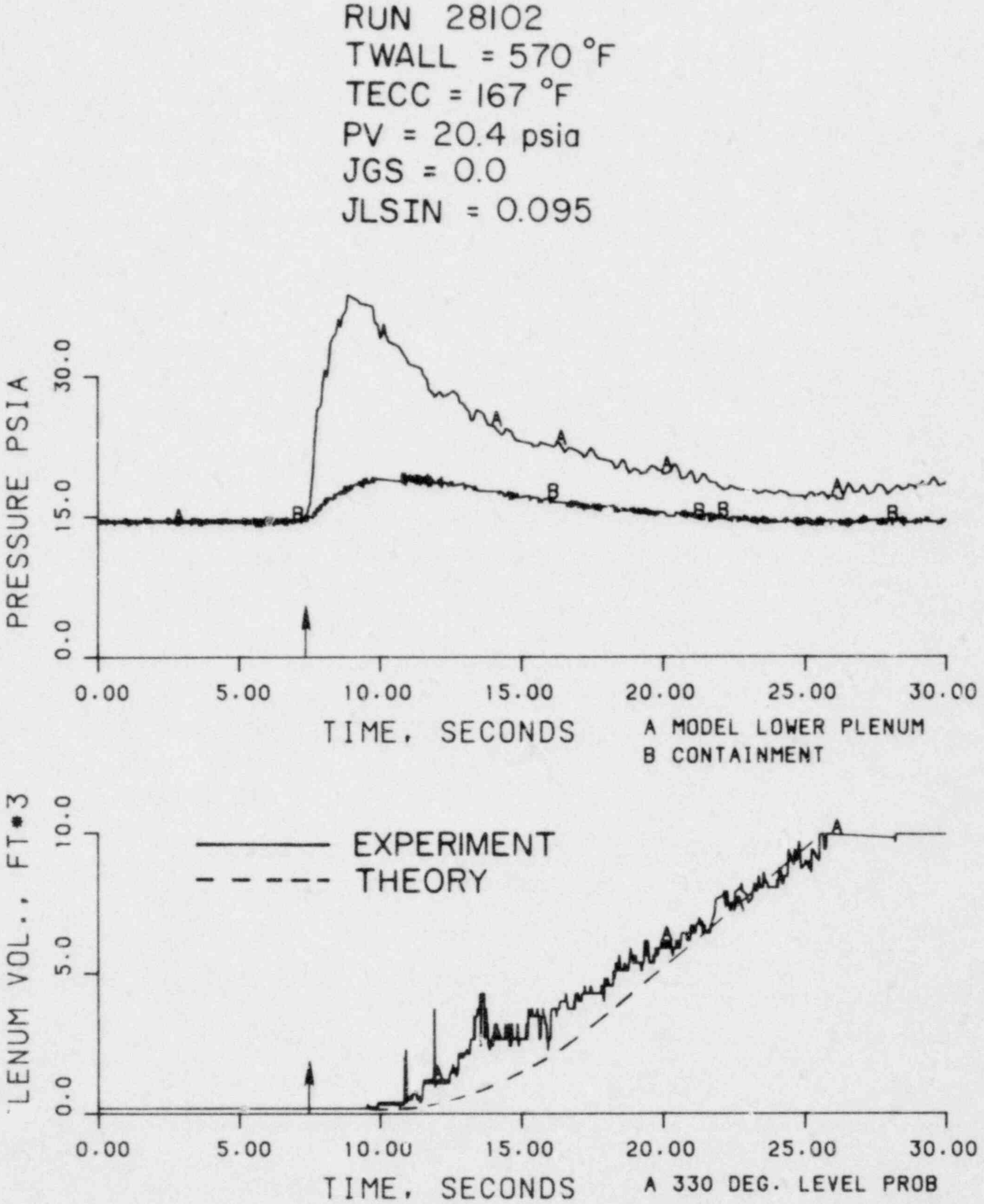

FIGURE 14. THEORETICAL AND EXPERIMENTAL RESULTS OF RUN 28102.

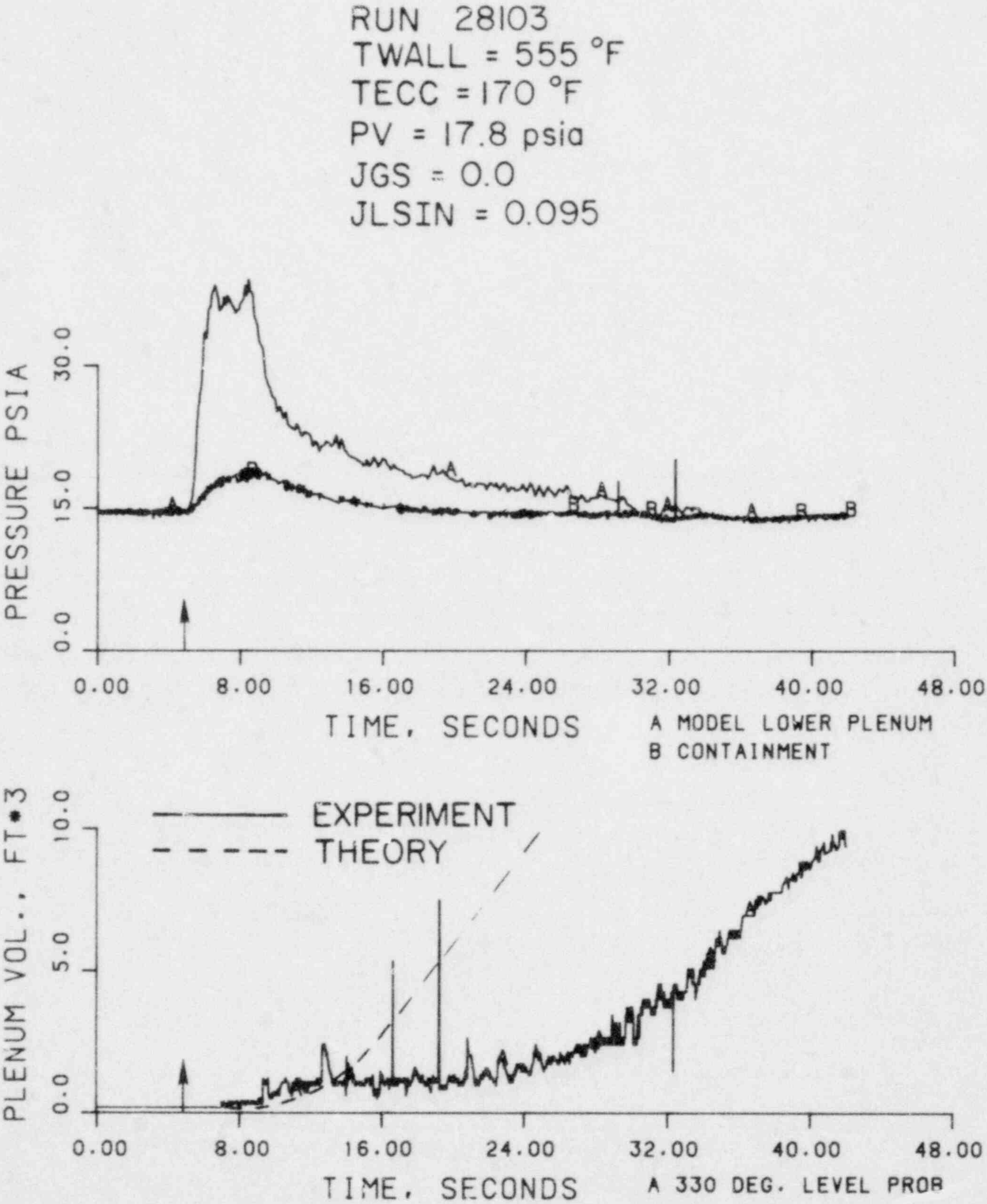

FIGURE 15. THEORETICAL AND EXPERIMENTAL RESULTS OF RUN 28103.

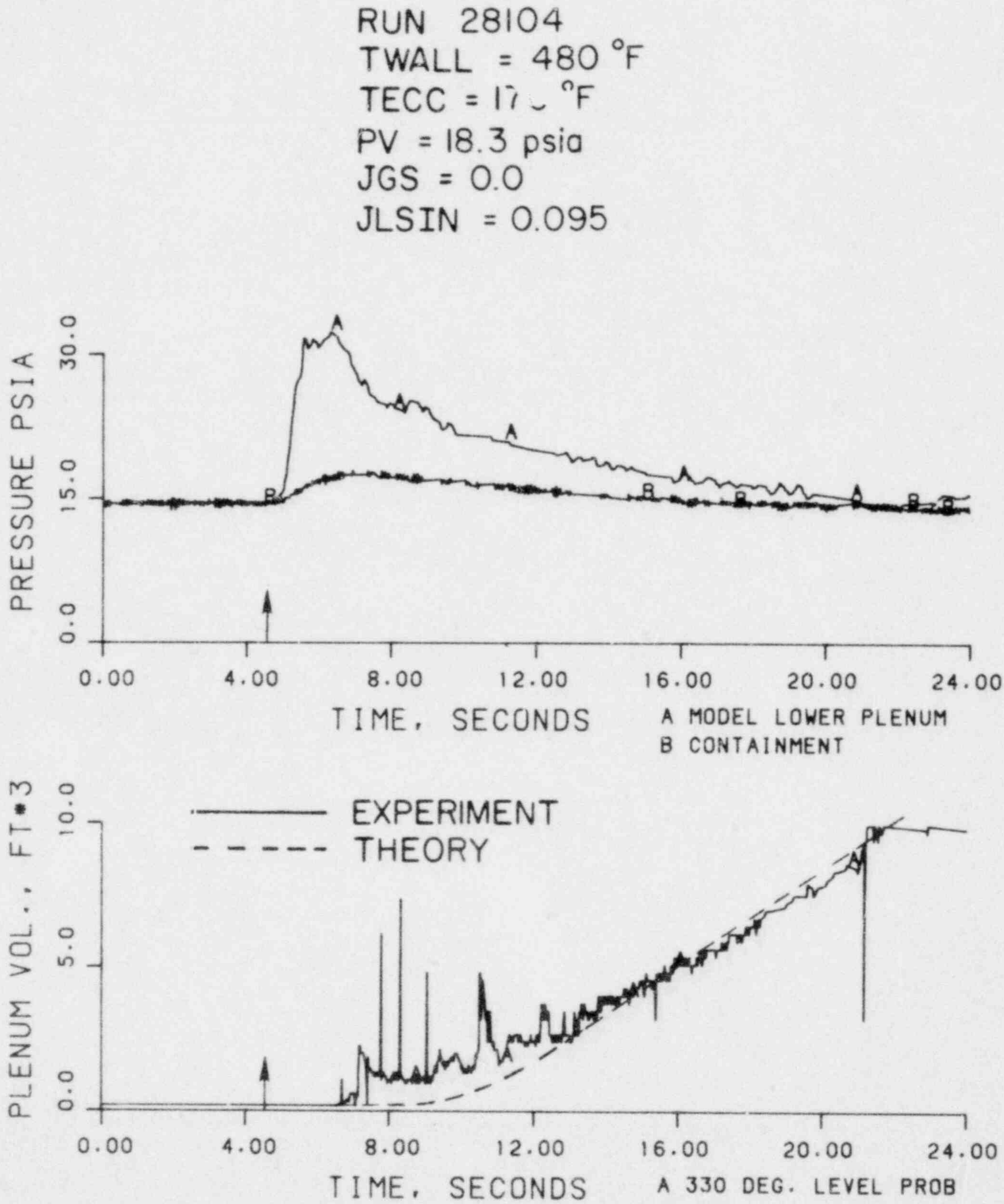

FIGURE 16. THEORETICAL AND EXPERIMENTAL RESULTS OF RUN 28104.

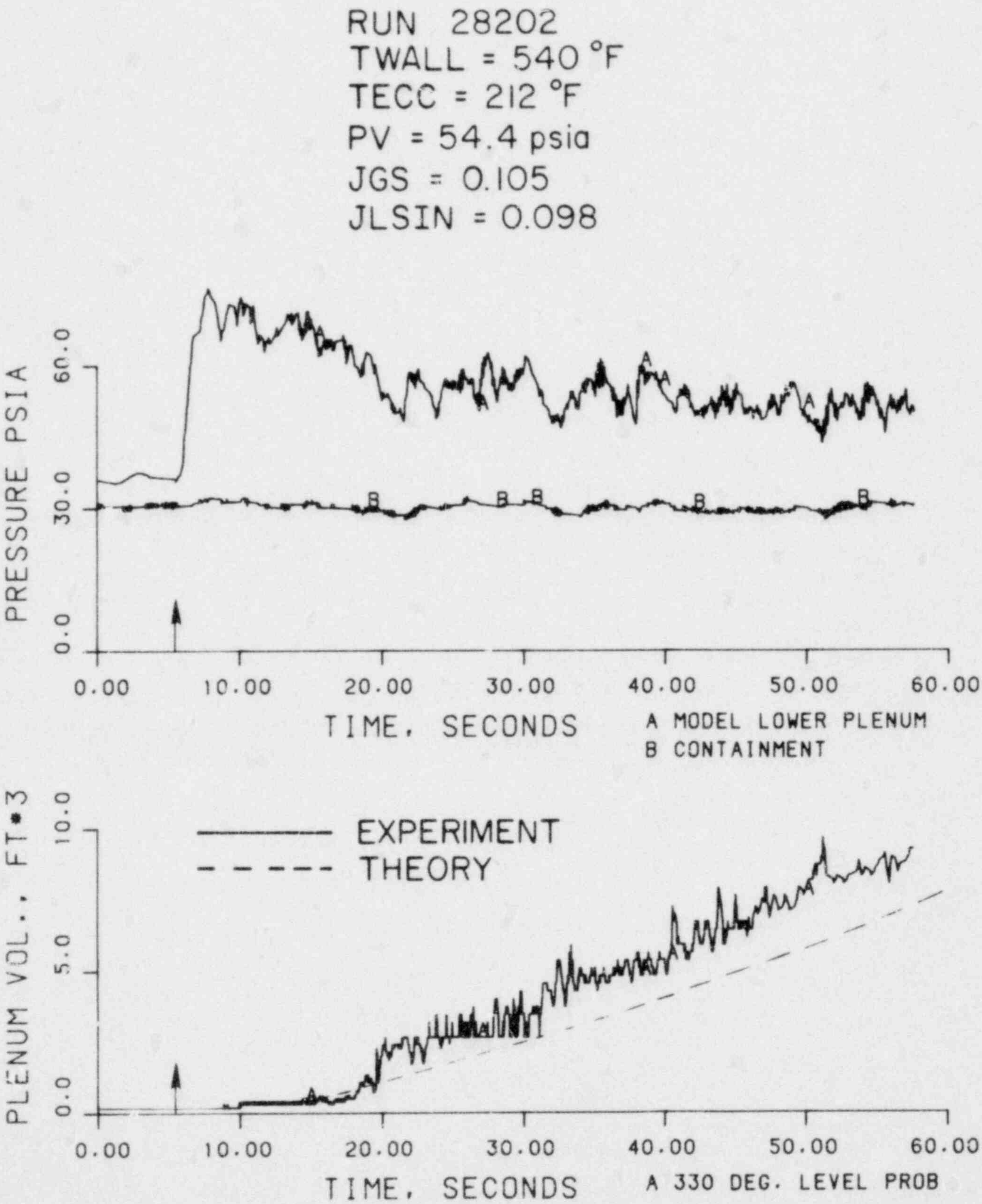

FIGURE 17. THEORETICAL AND EXPERIMENTAL RESULTS OF RUN 28202.

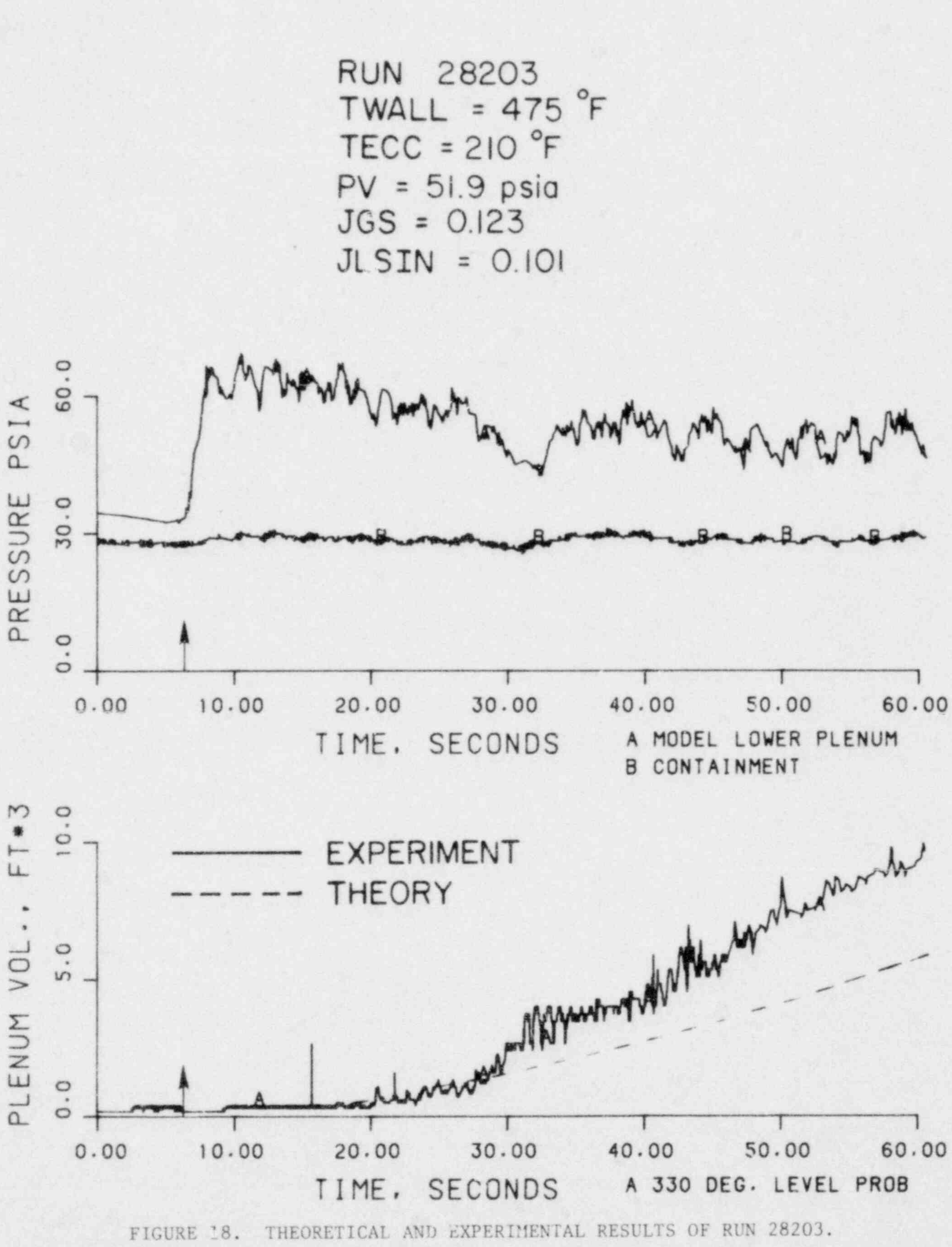

FIGURE 18. THEORETICAL AND EXPERIMENTAL RESULTS OF RUN 28203.

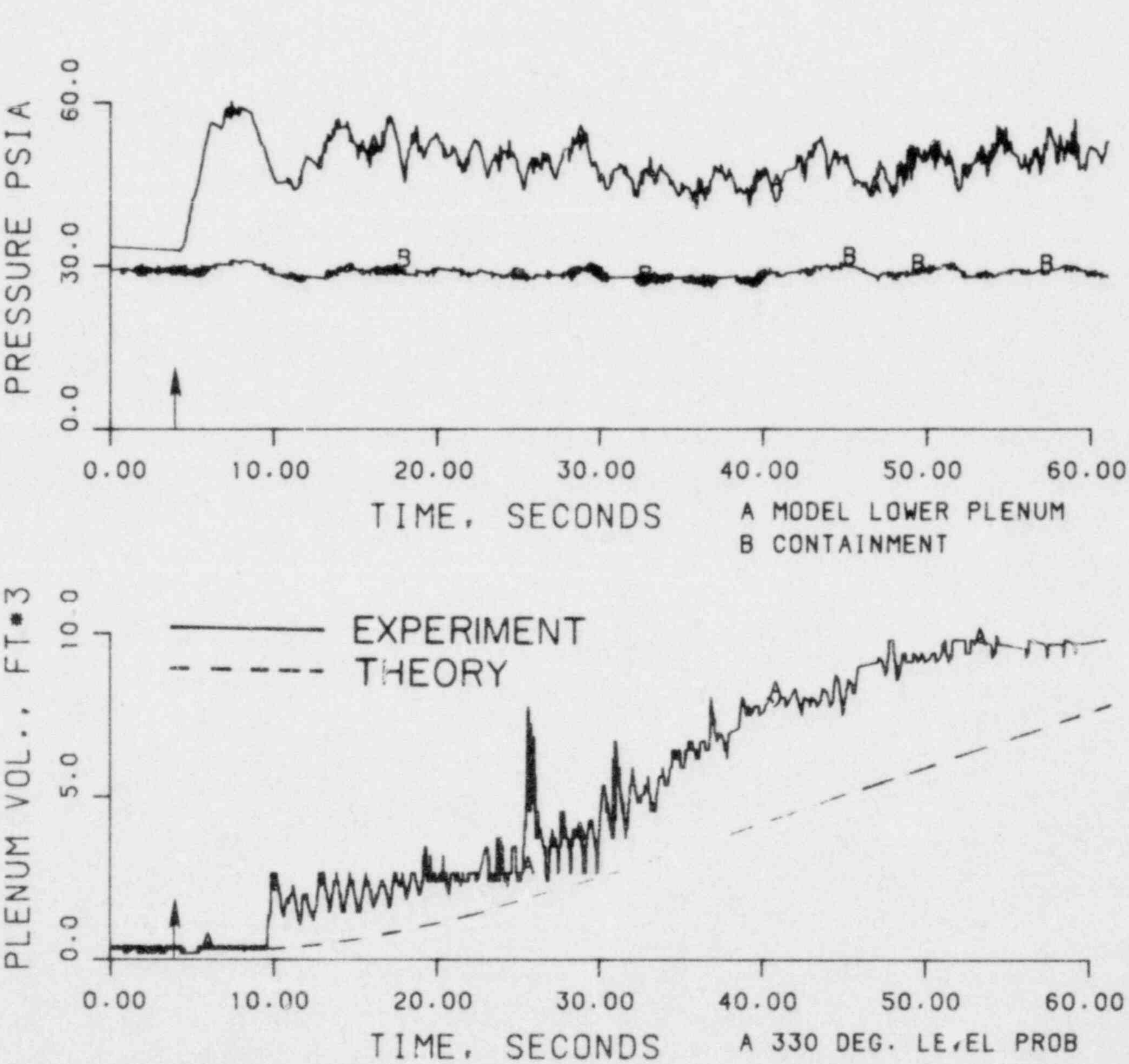

FIGURE 19. THEORETICAL AND EXPERIMENTAL RESULTS OF RUN 28204.

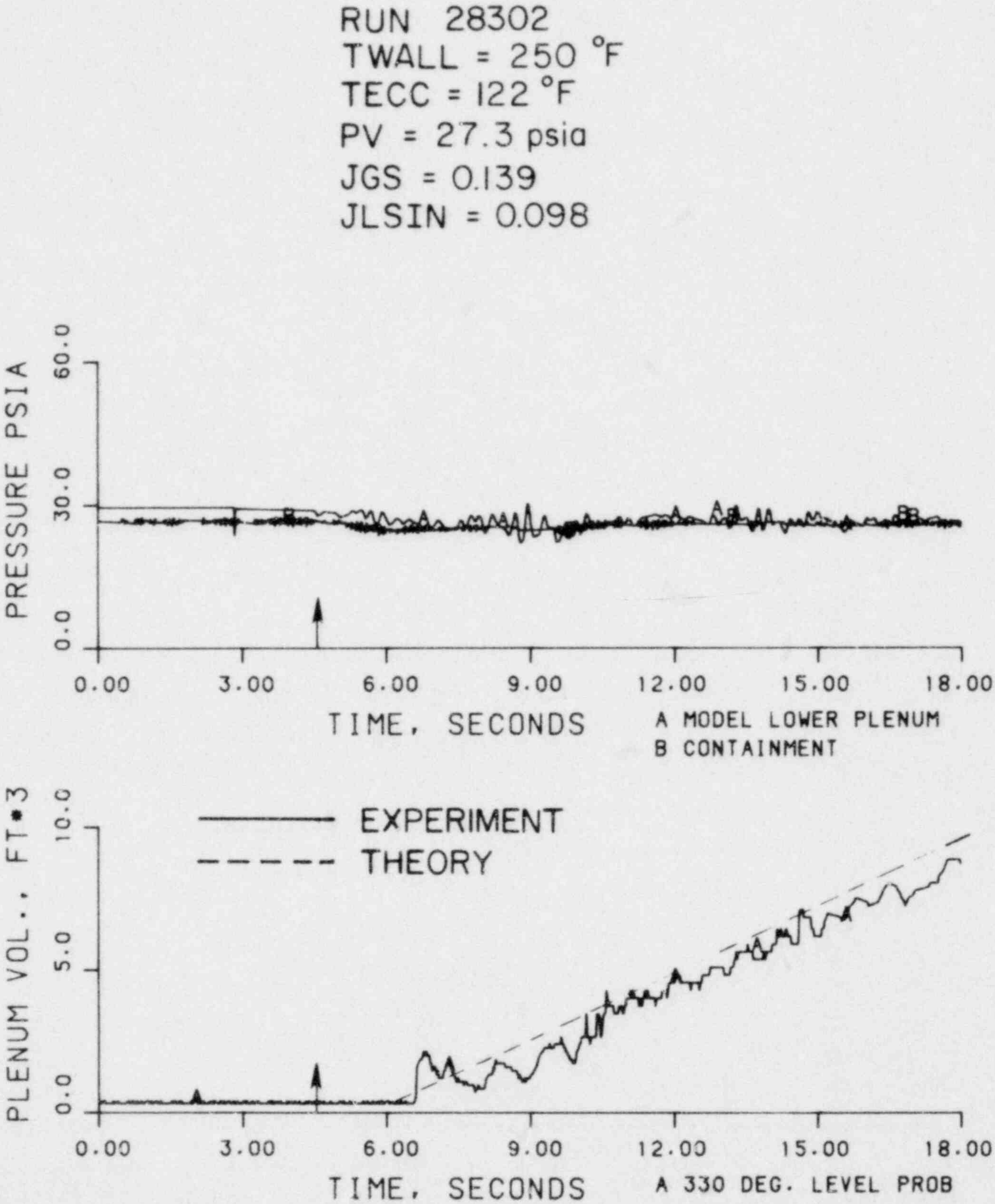

FIGURE 20. THEORETICAL AND EXPERIMENTAL RESULTS OF RUN 28302.

IMAGE EVALUATION TEST TARGET (MT-3)

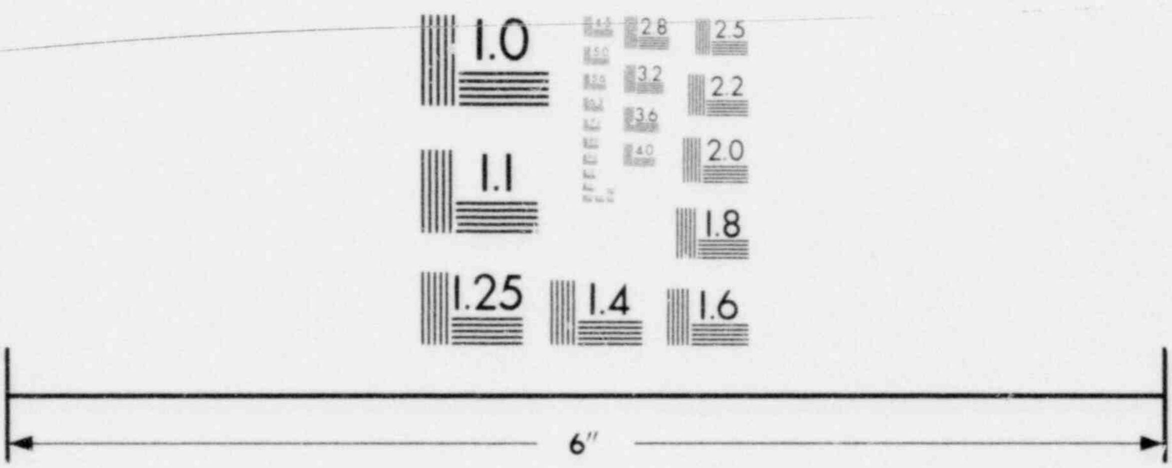

IMAGE EVALUATION TEST TARGET (MT-3)

6″

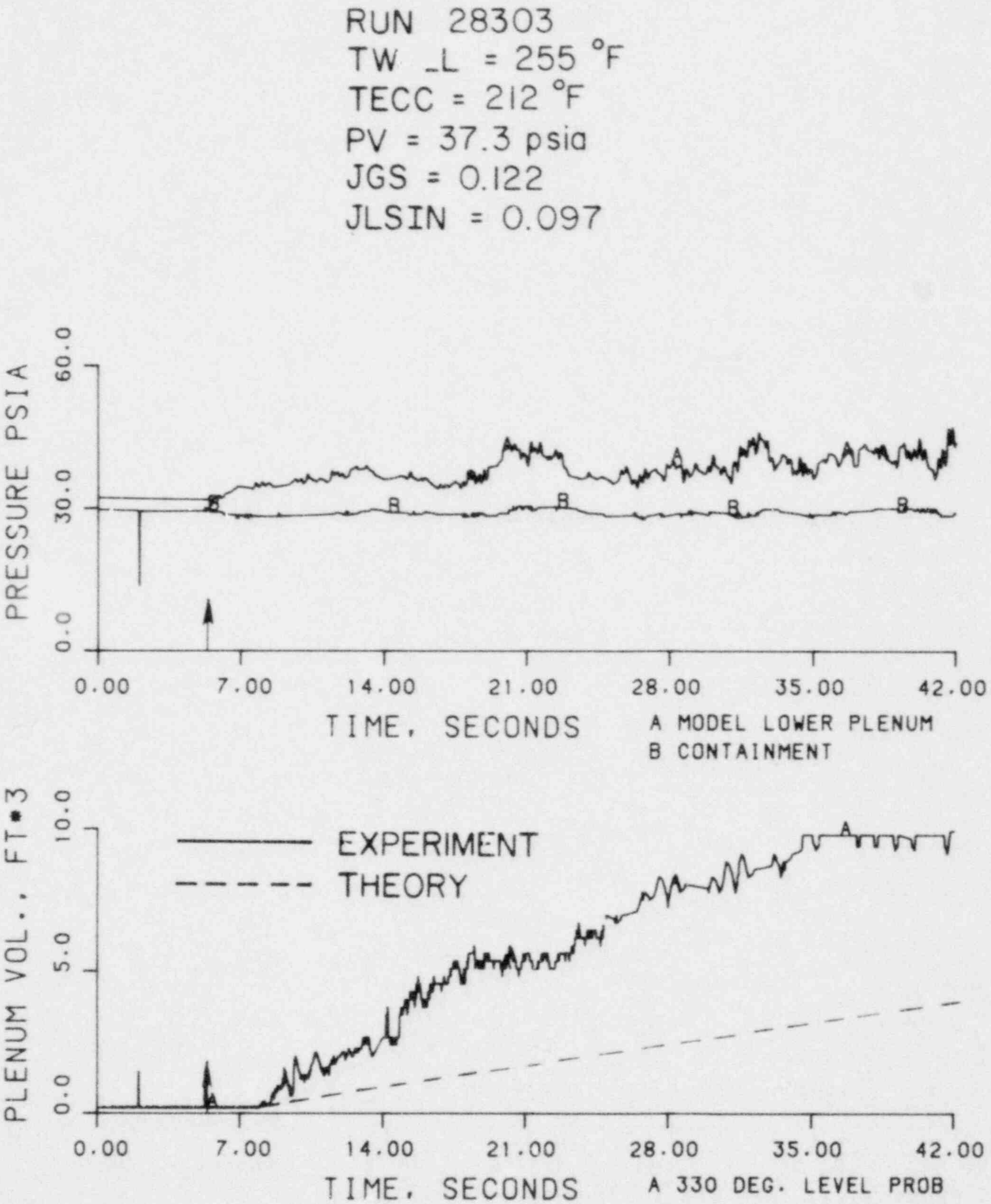

FIGURE 21. THEORETICAL AND EXPERIMENTAL RESULTS OF RUN 28303.

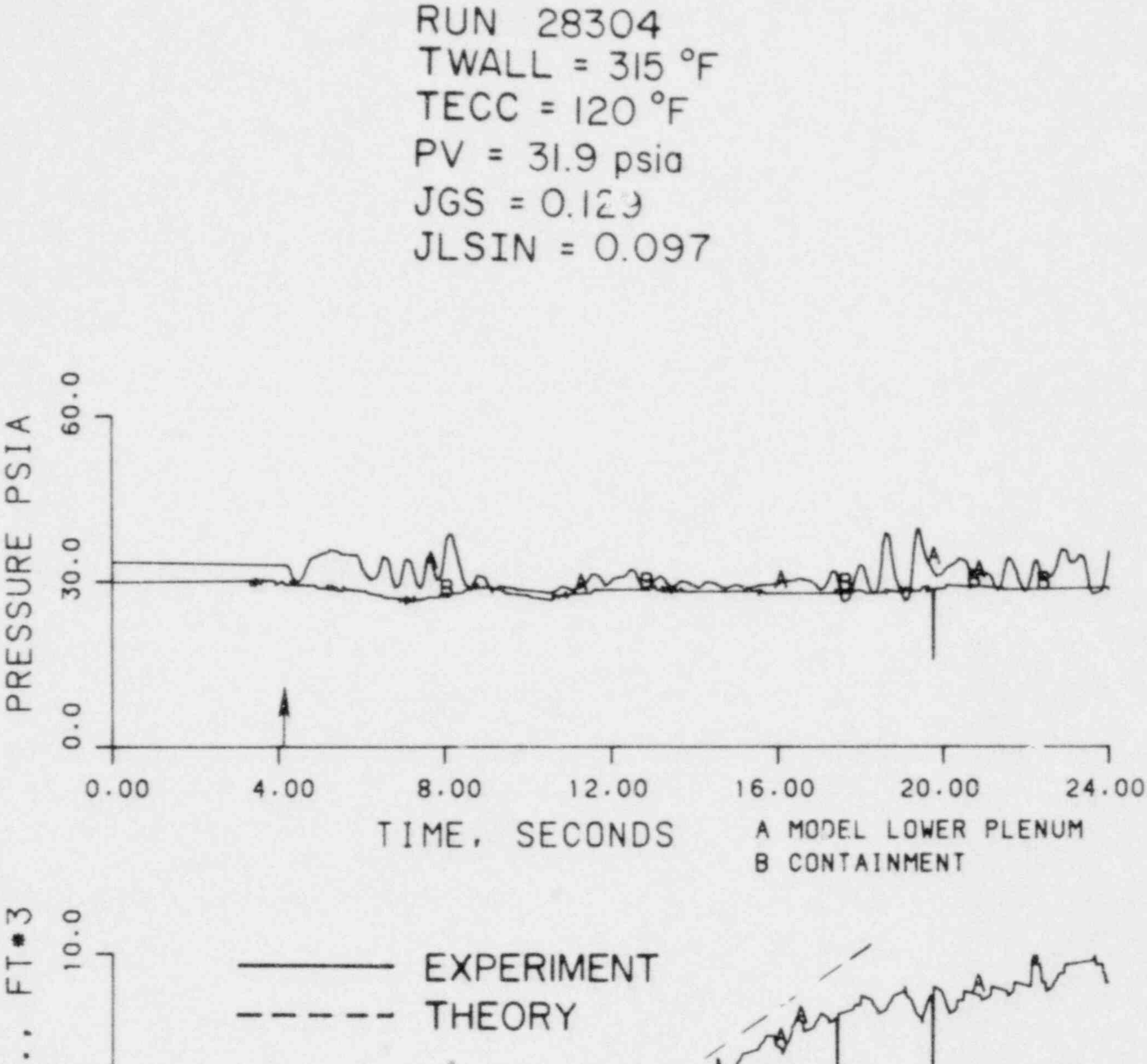

FIGURE 22. THEORETICAL AND EXPERIMENTAL RESULTS OF RUN 28304.

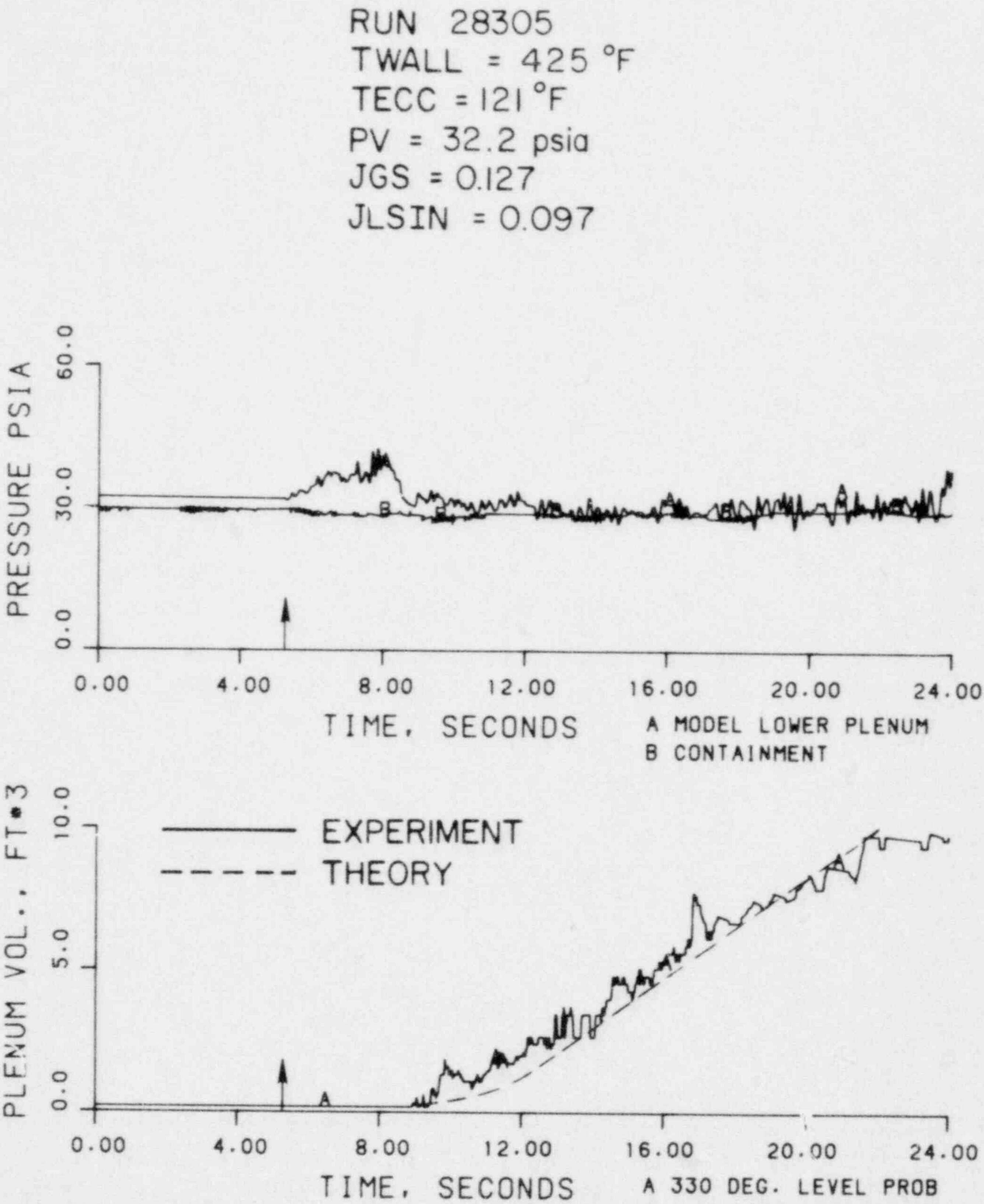

FIGURE 23. THEORETICAL AND EXPERIMENTAL RESULTS OF RUN 28305.

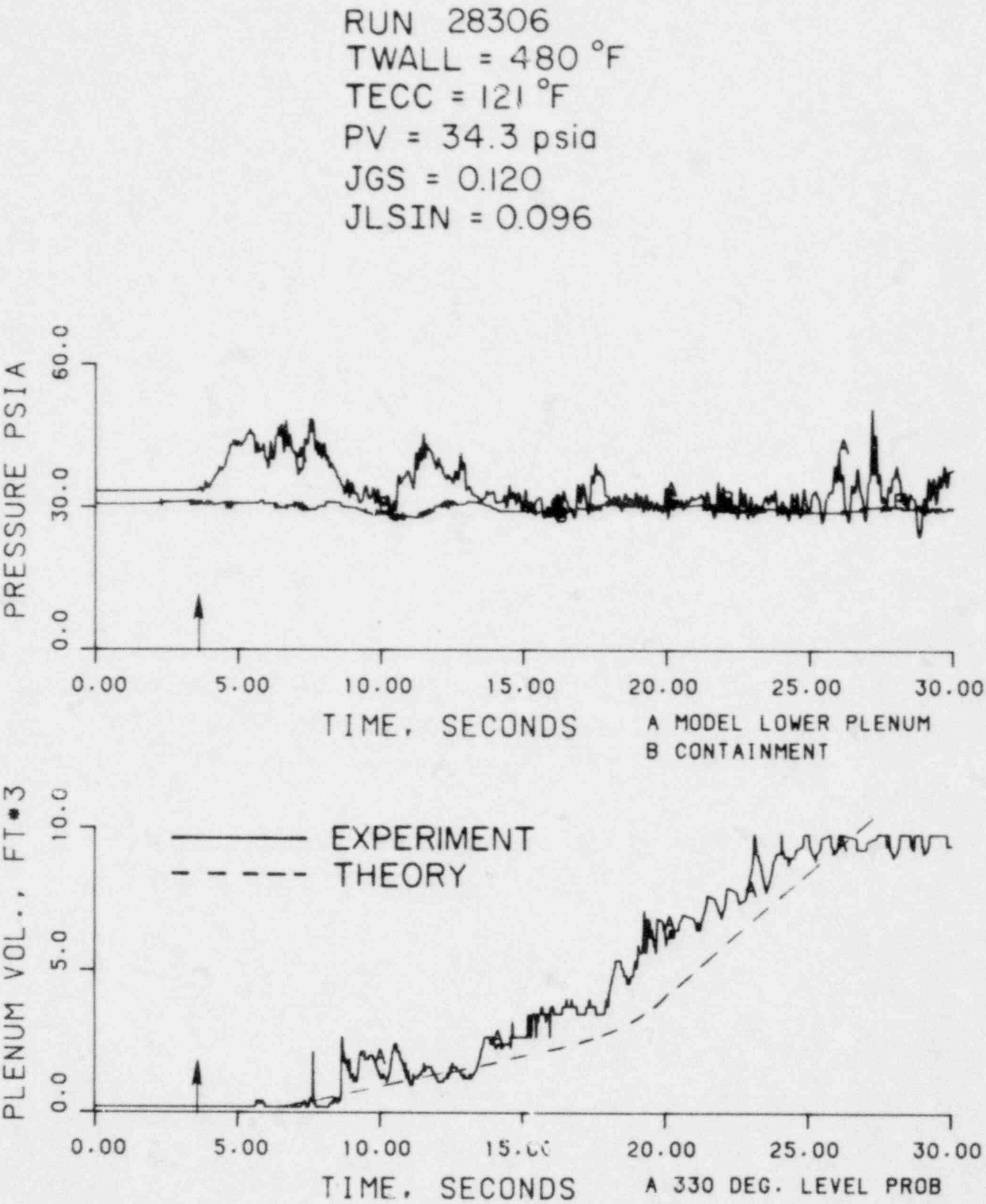

FIGURE 24. THEORETICAL AND EXPERIMENTAL RESULTS OF RUN 28306.

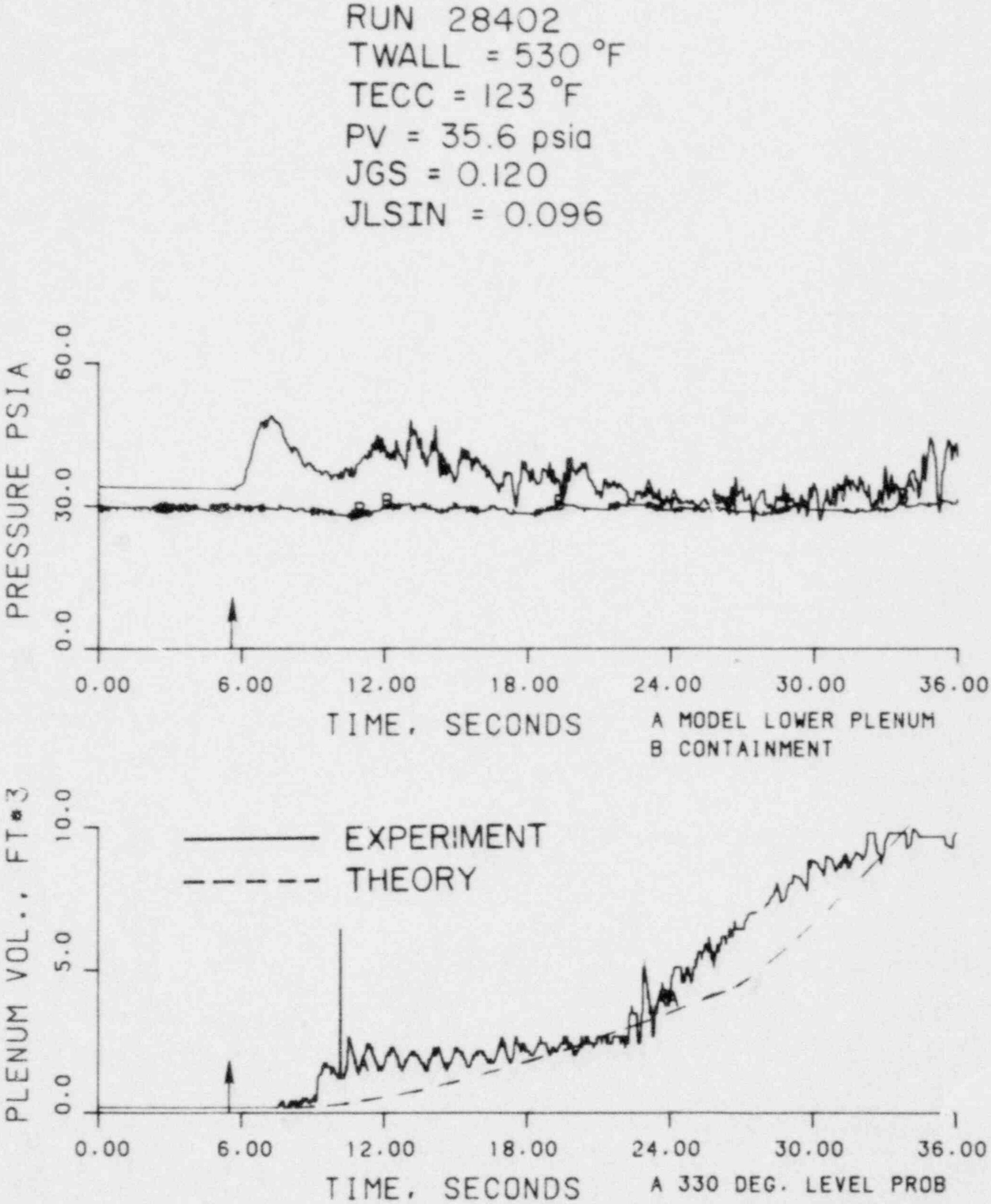

FIGURE 25. THEORETICAL AND EXPERIMENTAL RESULTS OF RUN 28402.

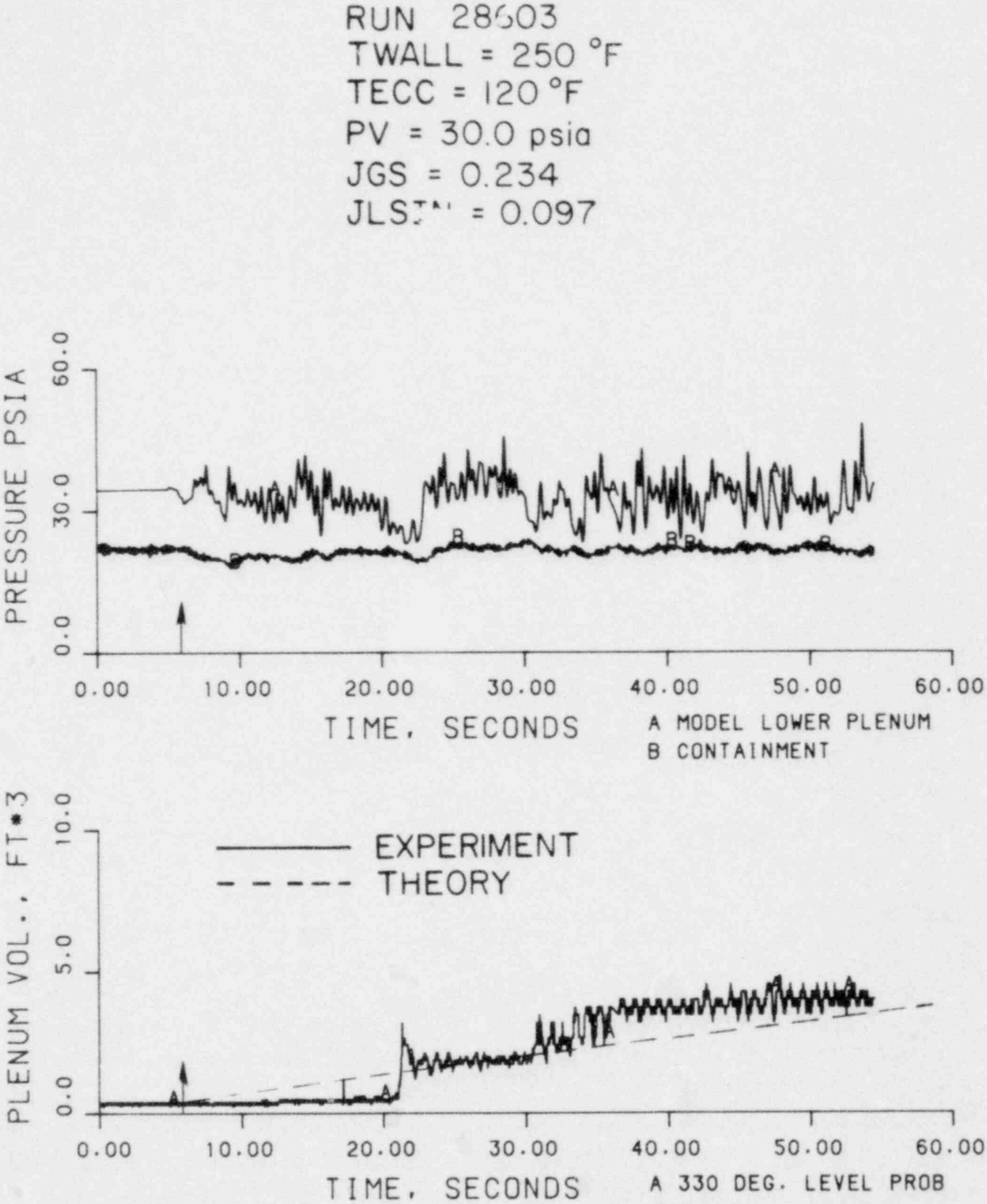

FIGURE 26. THEORETICAL AND EXPERIMENTAL RESULTS OF RUN 28603.

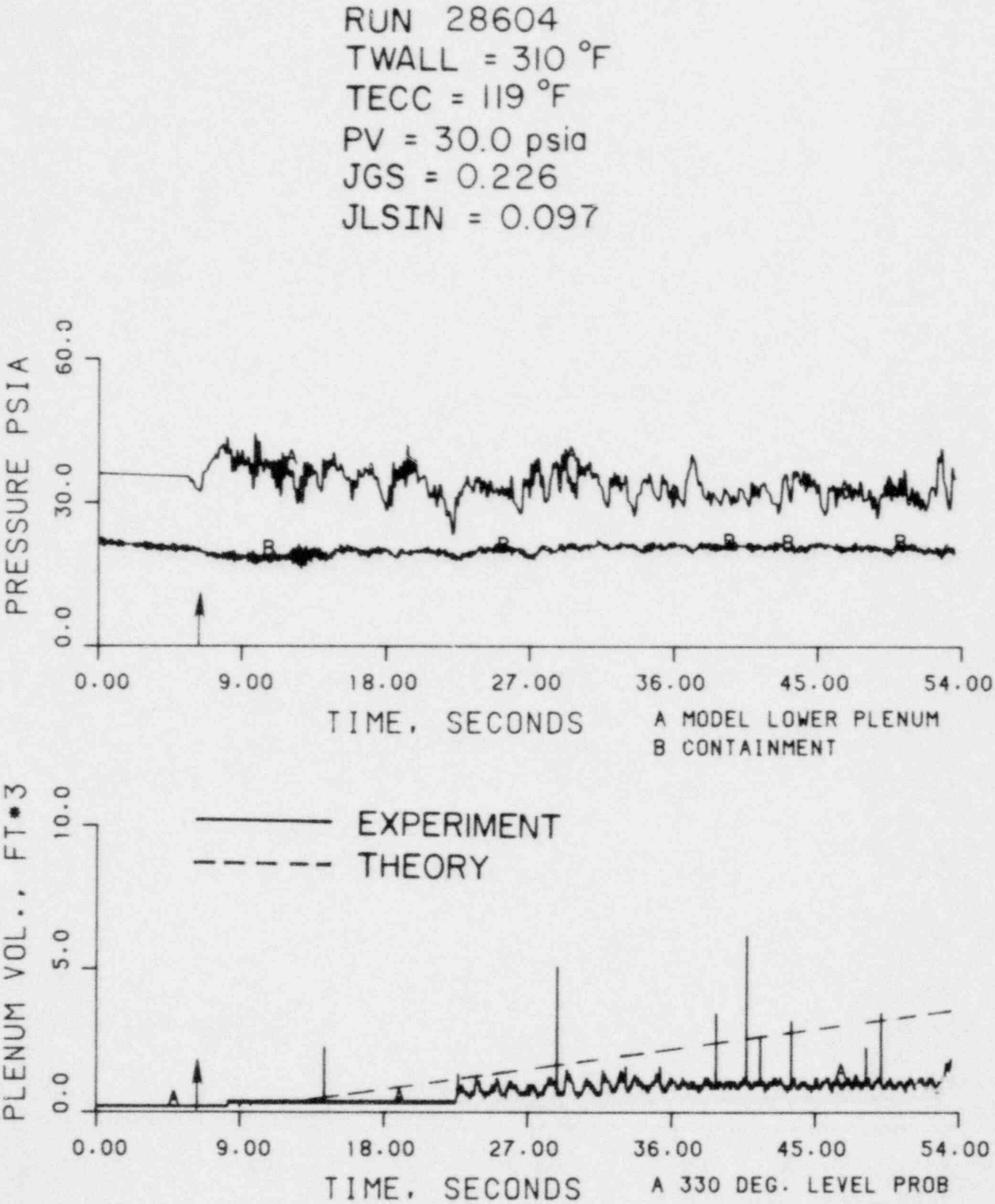

FIGURE 27. THEORETICAL AND EXPERIMENTAL RESULTS OF RUN 28604.

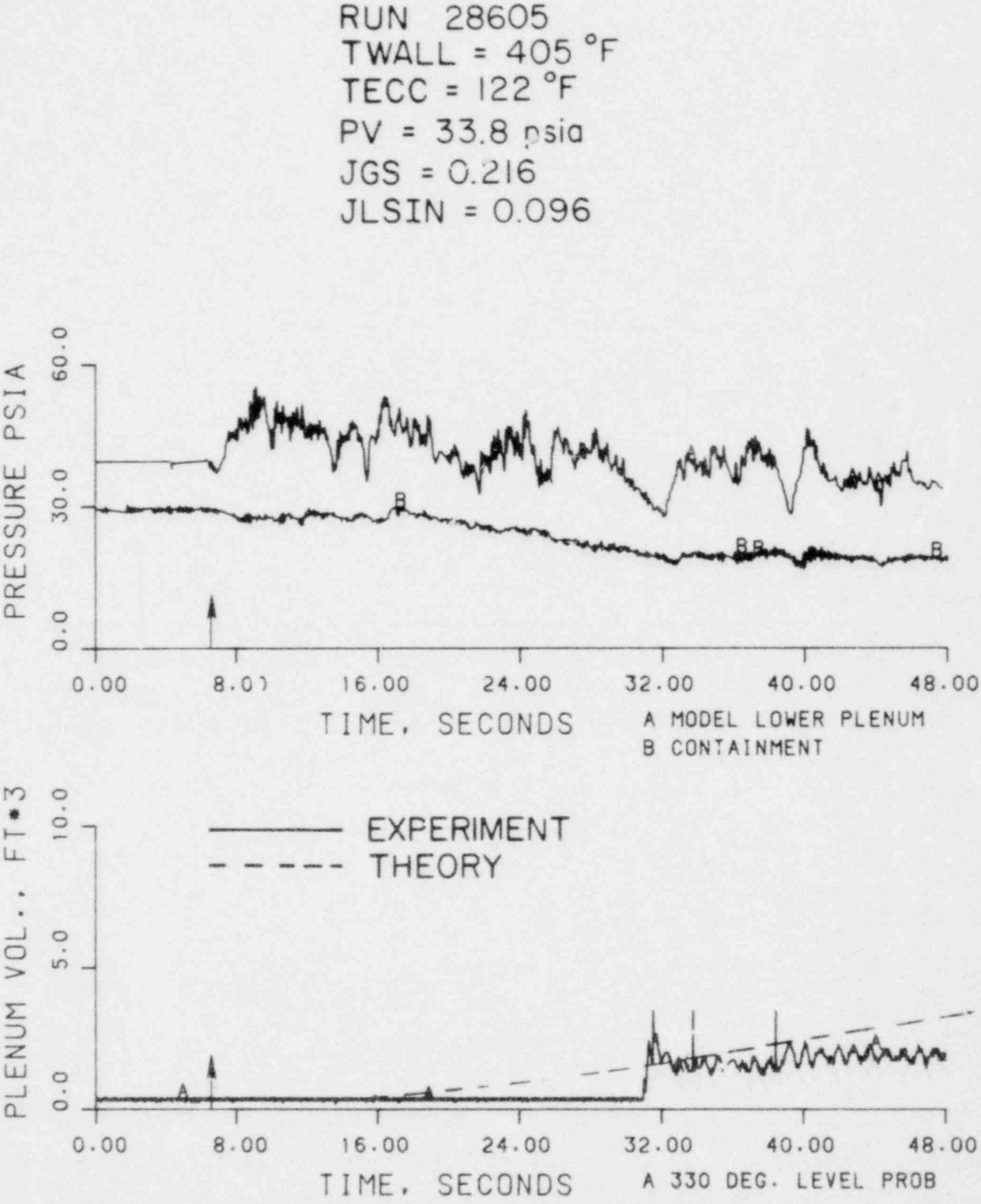

FIGURE 28. THEORETICAL AND EXPERIMENTAL RESULTS OF RUN 28605.

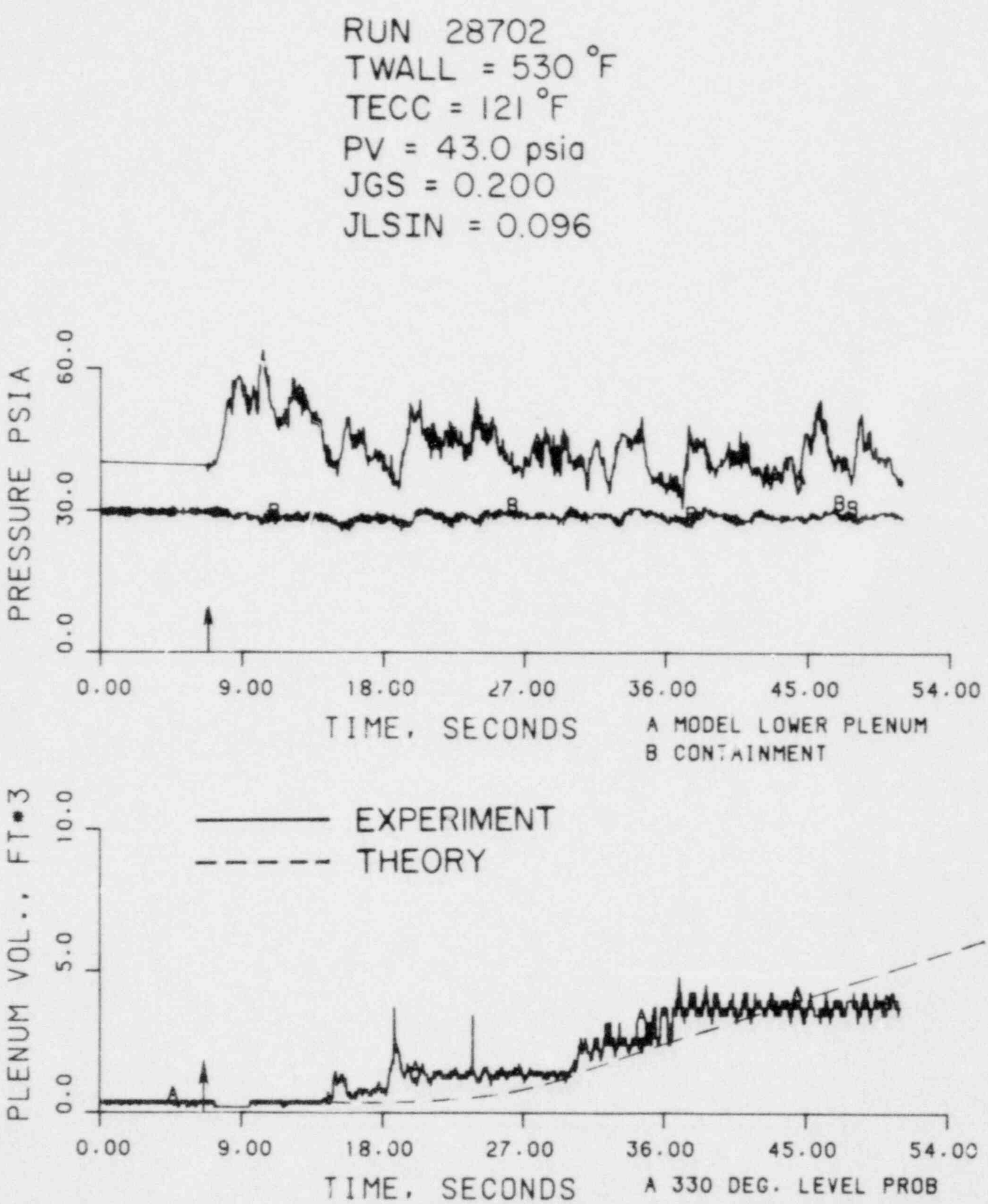

FIGURE 29. THEORETICAL AND EXPERIMENTAL RESULTS OF RUN 28702.

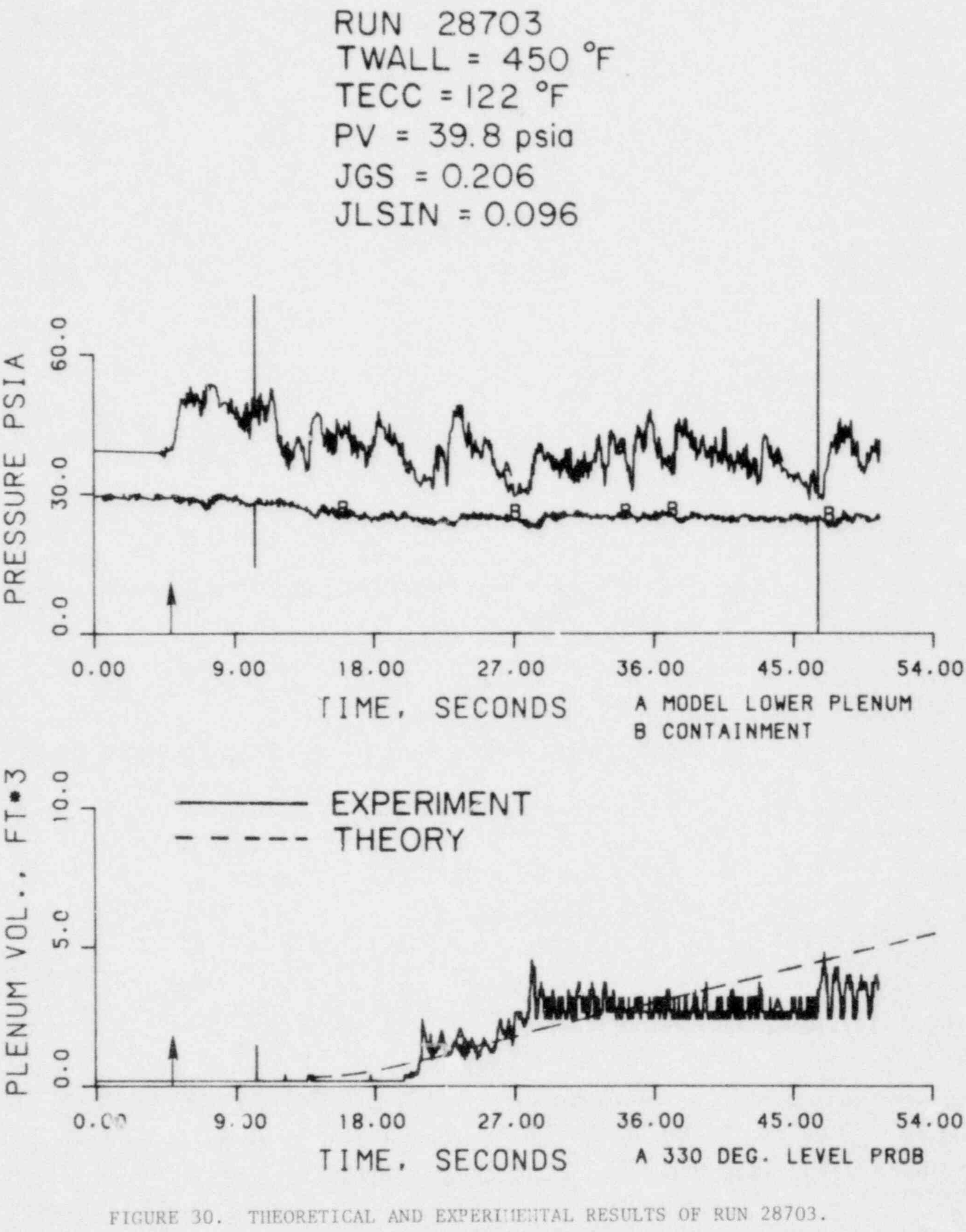

FIGURE 30. THEORETICAL AND EXPERIMENTAL RESULTS OF RUN 28703.

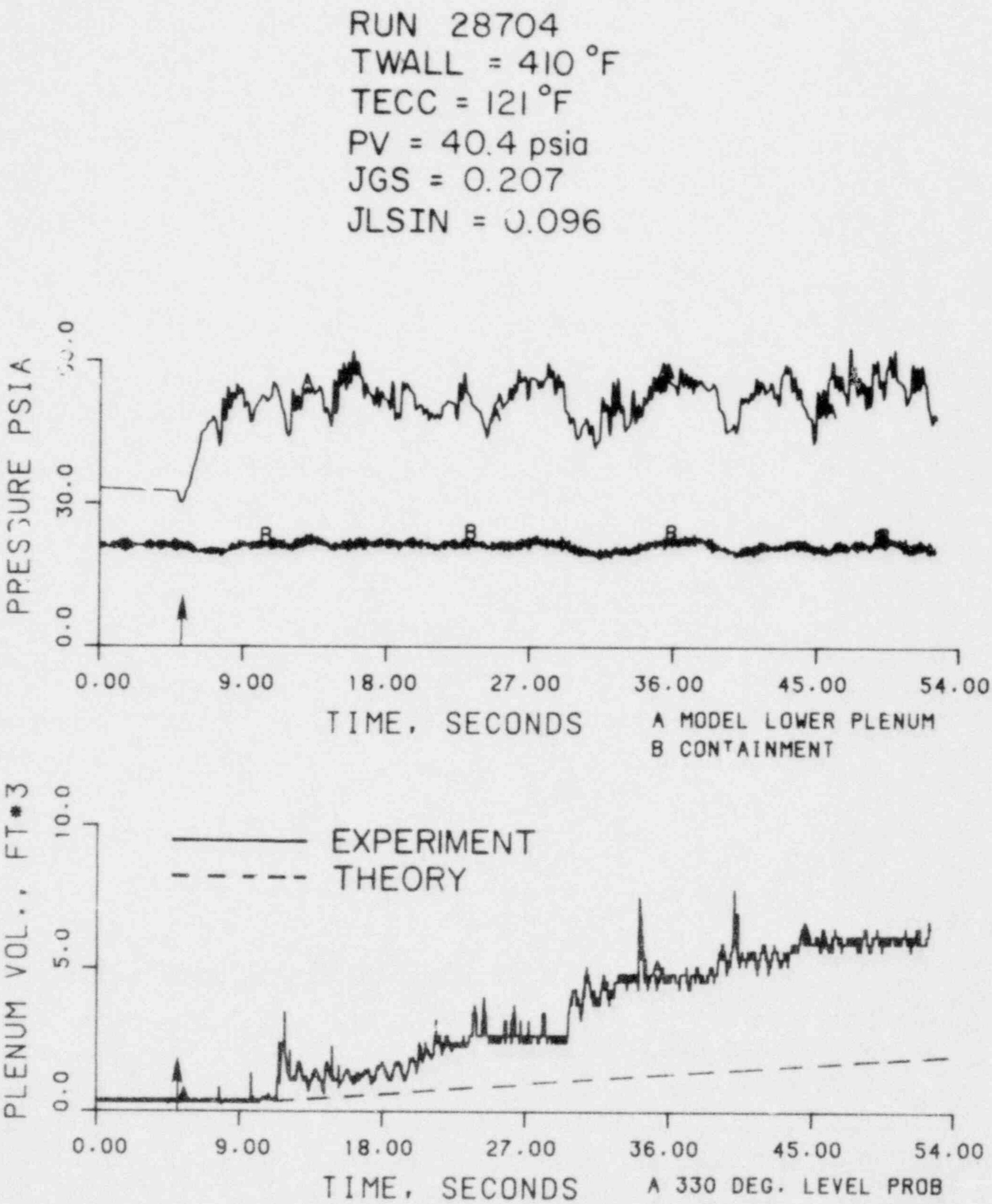

FIGURE 31. THEORETICAL AND EXPERIMENTAL RESULTS OF RUN 28704.

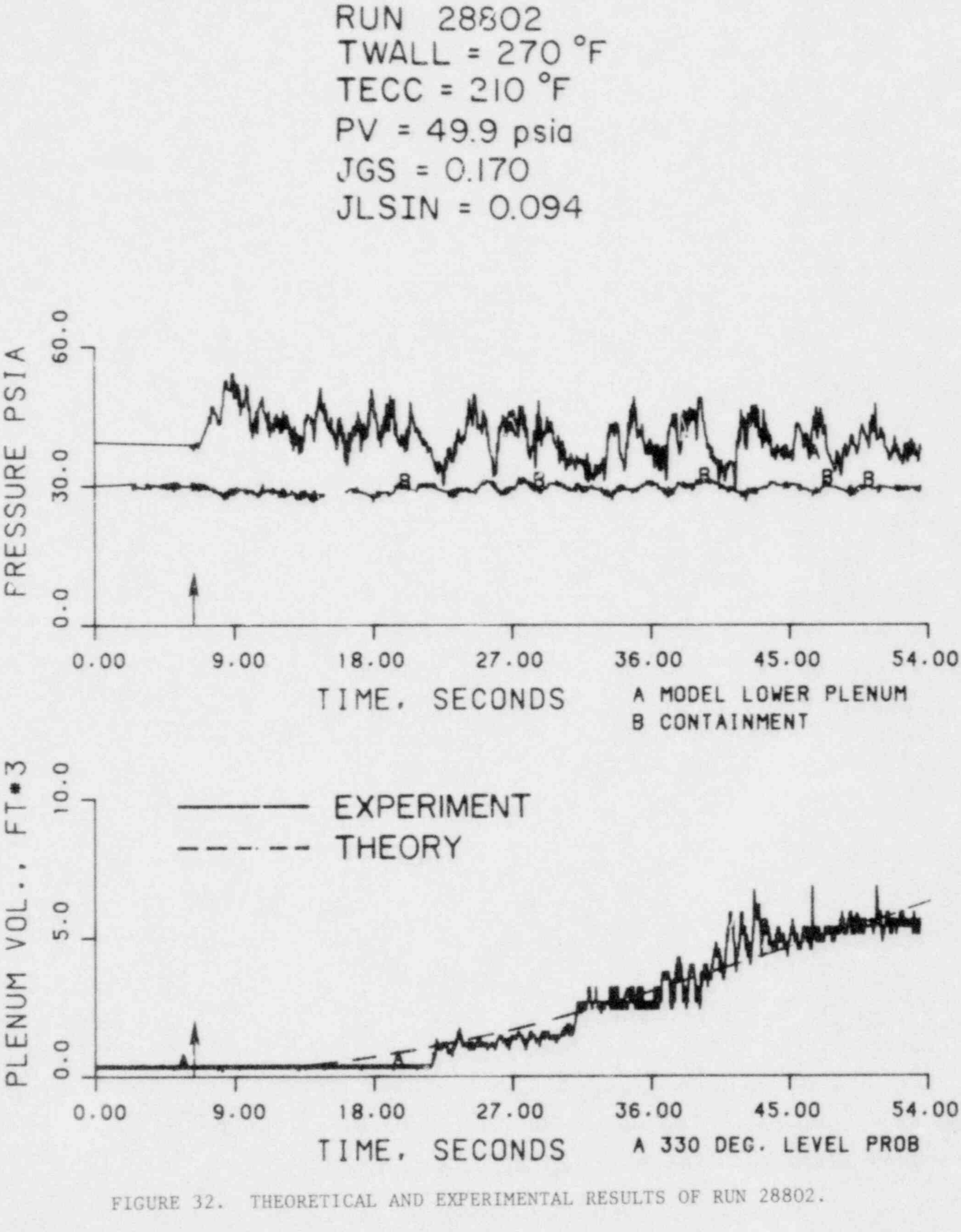

FIGURE 32. THEORETICAL AND EXPERIMENTAL RESULTS OF RUN 28802.

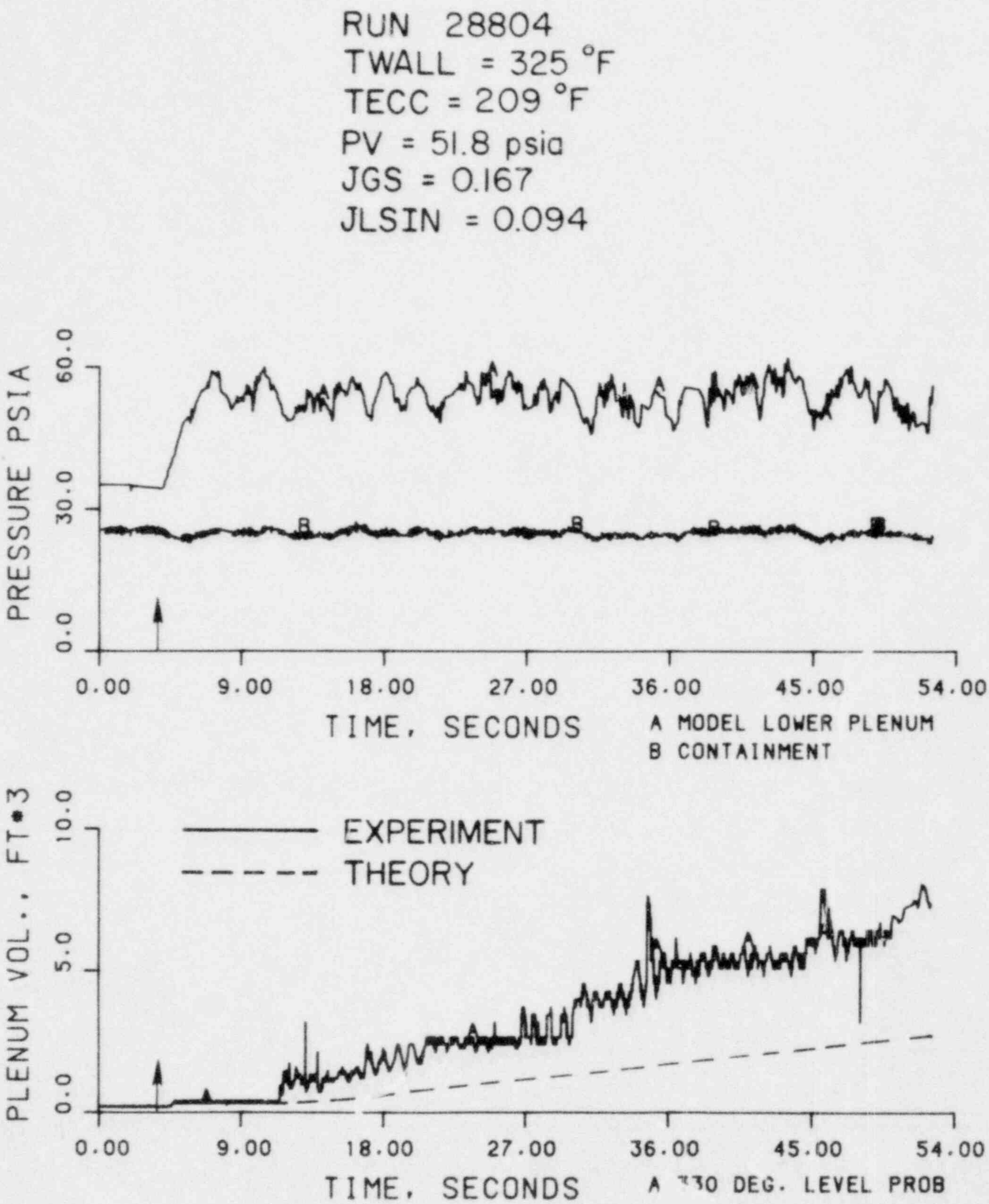

FIGURE 33. THEORETICAL AND EXPERIMENTAL RESULTS OF RUN 28804.

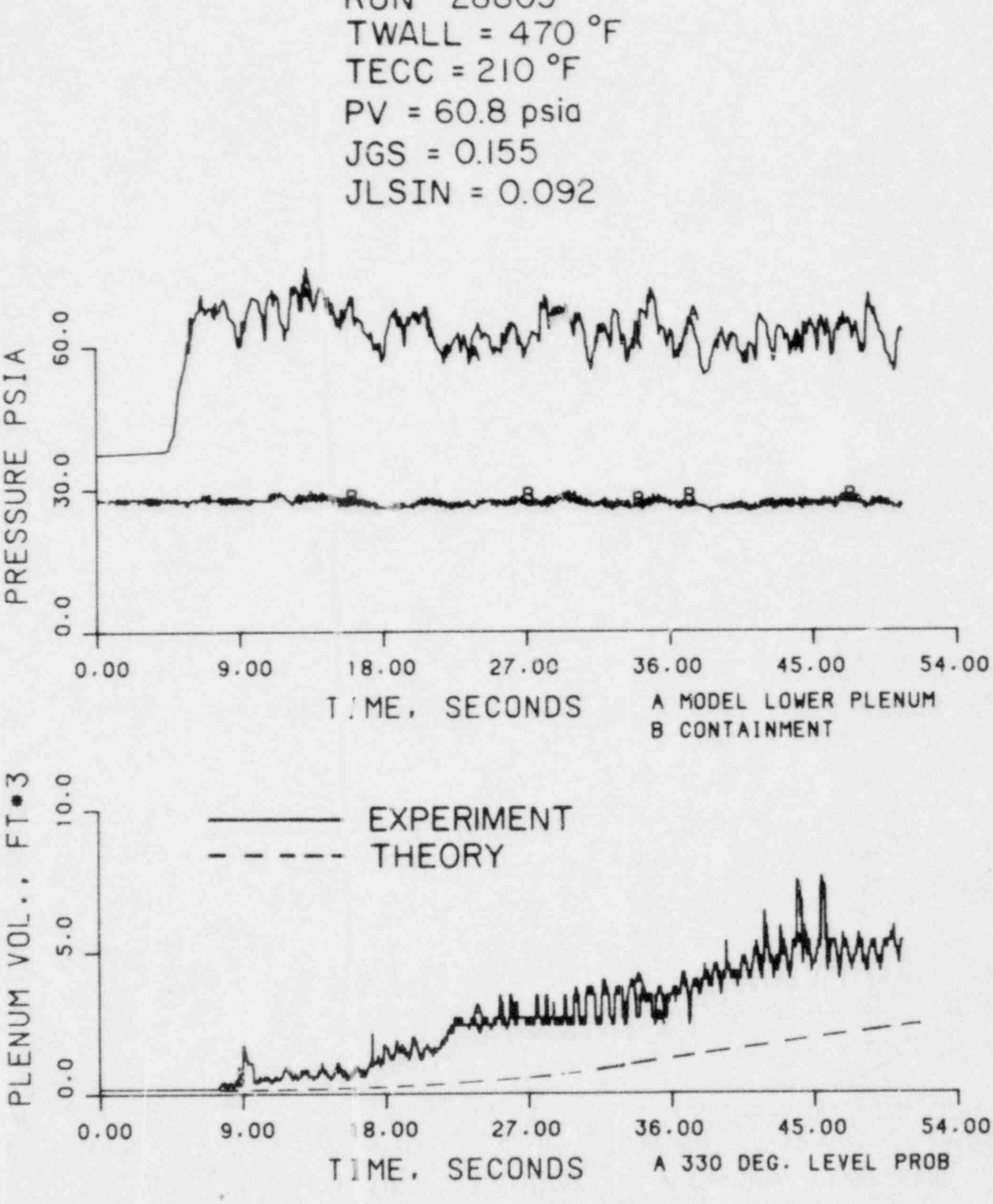

FIGURE 34. THEORETICAL AND EXPERIMENTAL RESULTS OF RUN 28805.

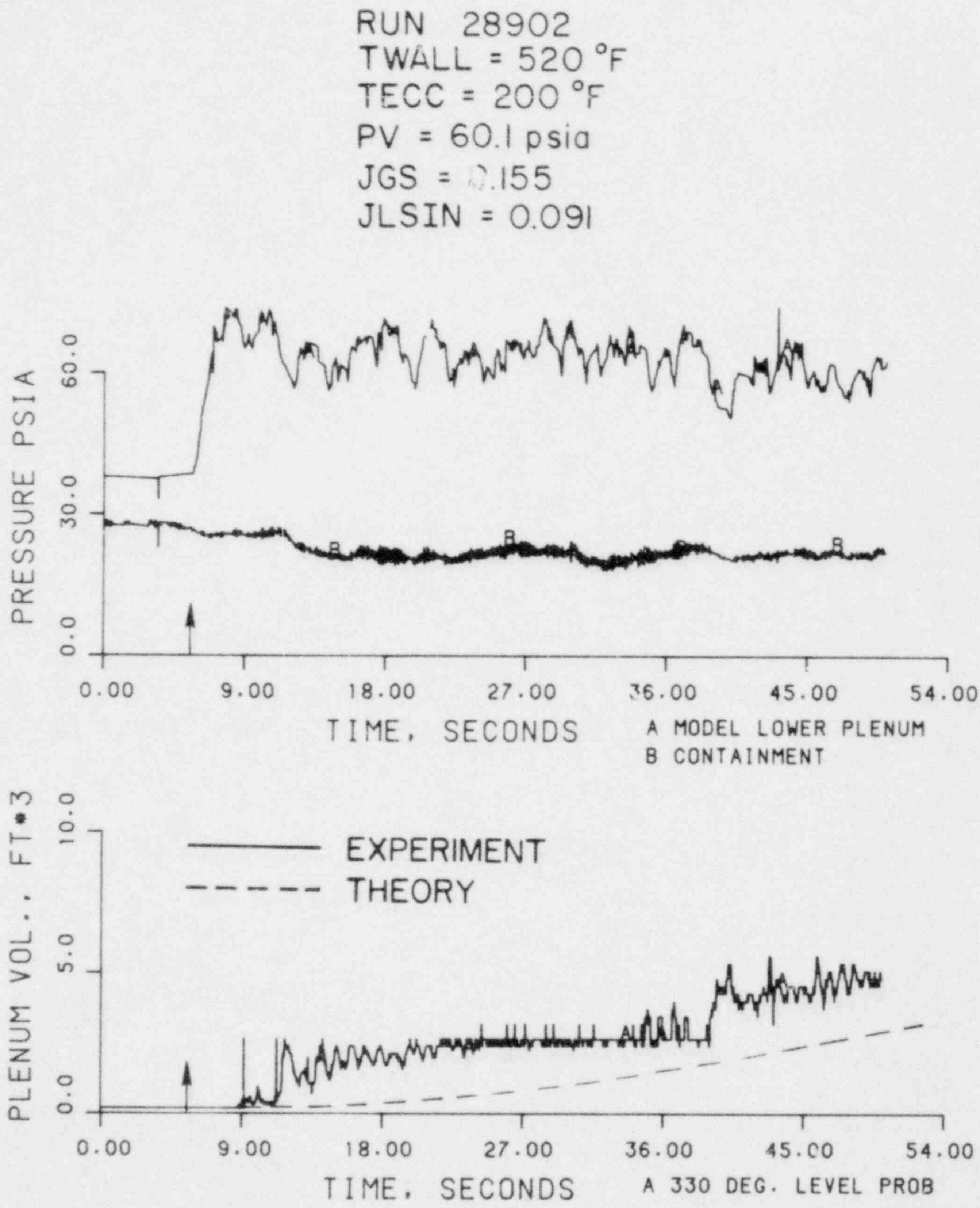

FIGURE 35. THEORETICAL AND EXPERIMENTAL RESULTS OF RUN 28902.

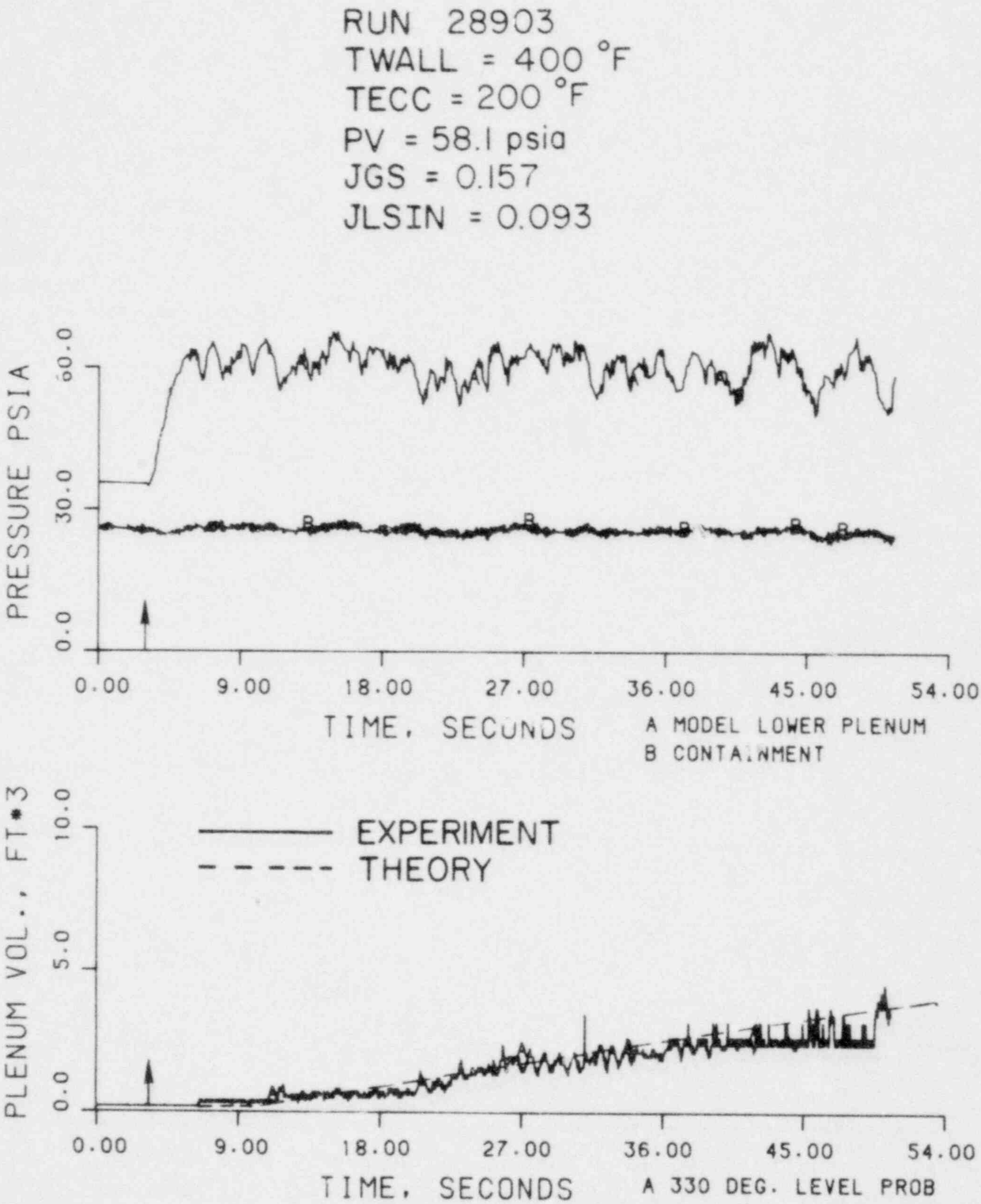

FIGURE 36. THEORETICAL AND EXPERIMENTAL RESULTS OF RUN 28903.

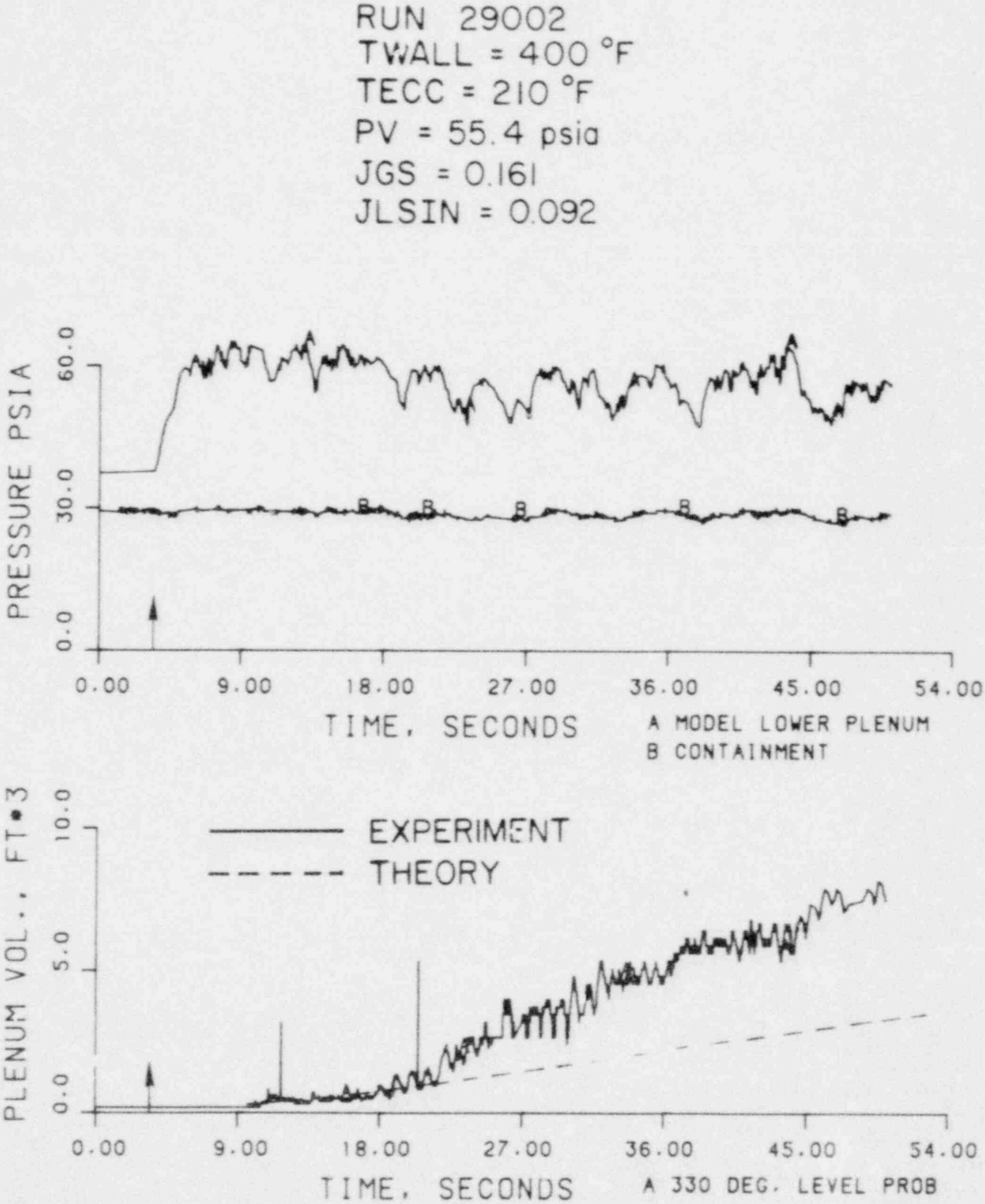

FIGURE 37. THEORETICAL AND EXPERIMENTAL RESULTS OF RUN 29002.

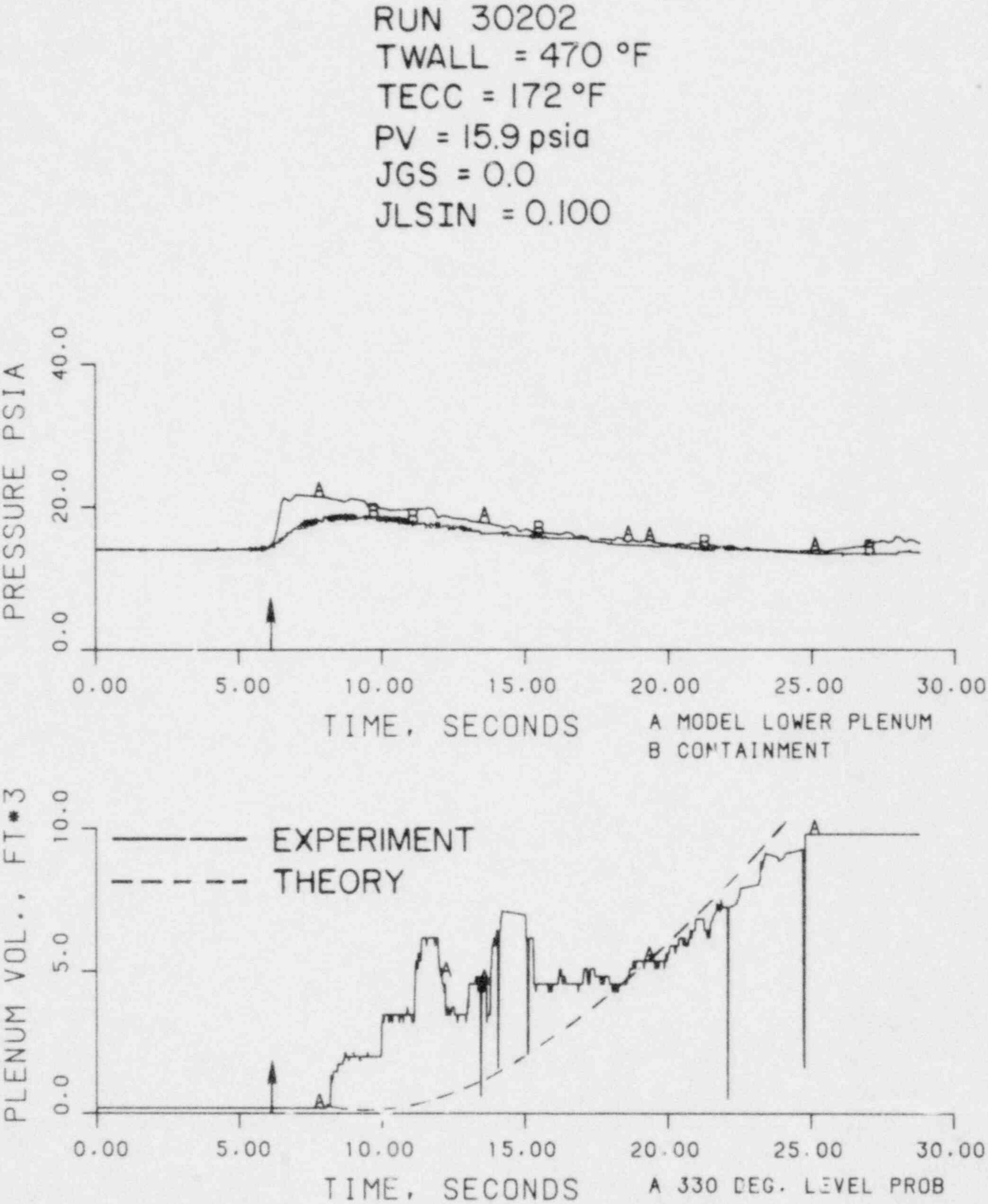

FIGURE 38. THEORETICAL AND EXPERIMENTAL RESULTS OF RUN 30202.

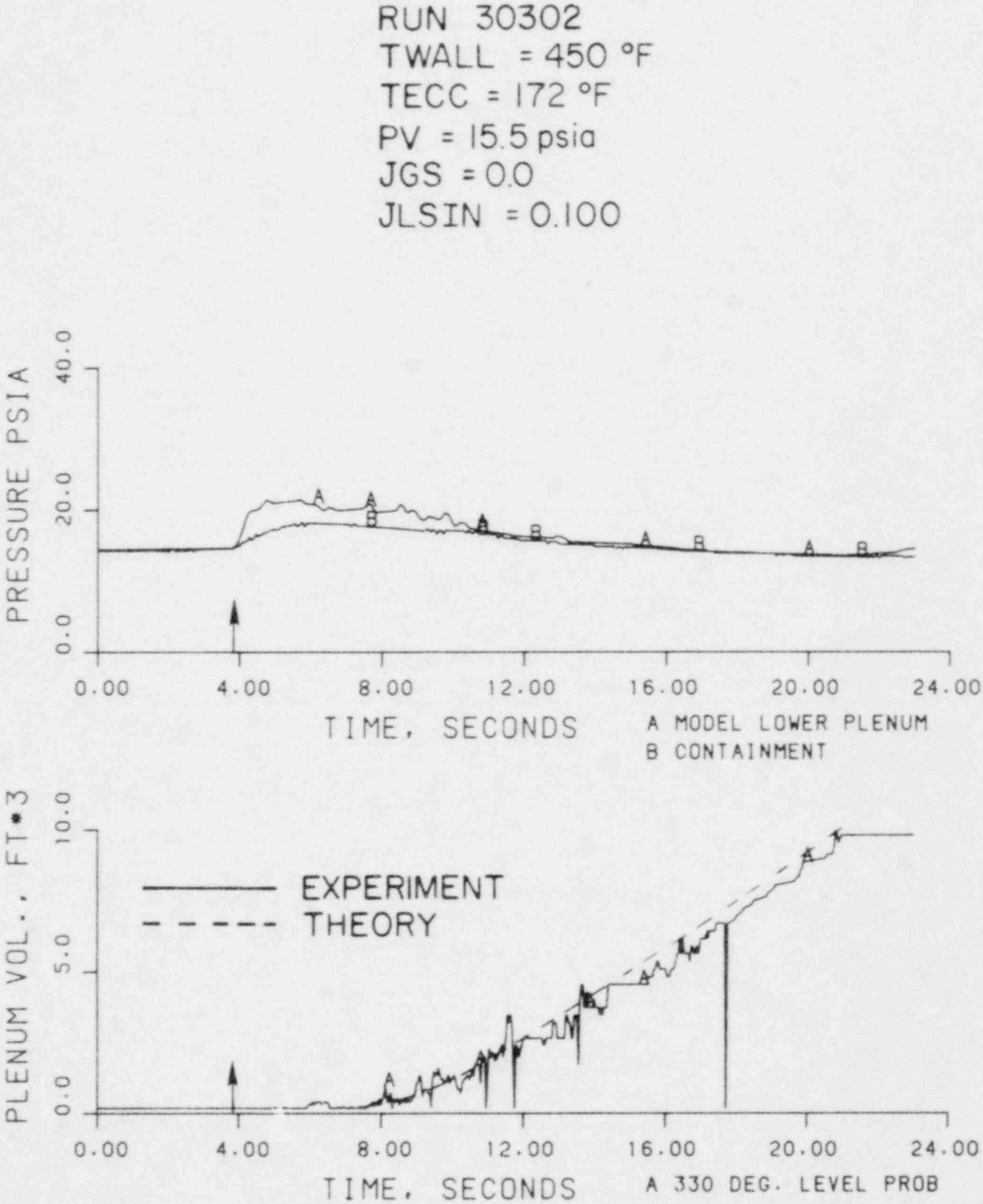

FIGURE 39. THEORETICAL AND EXPERIMENTAL RESULTS OF RUN 30302.

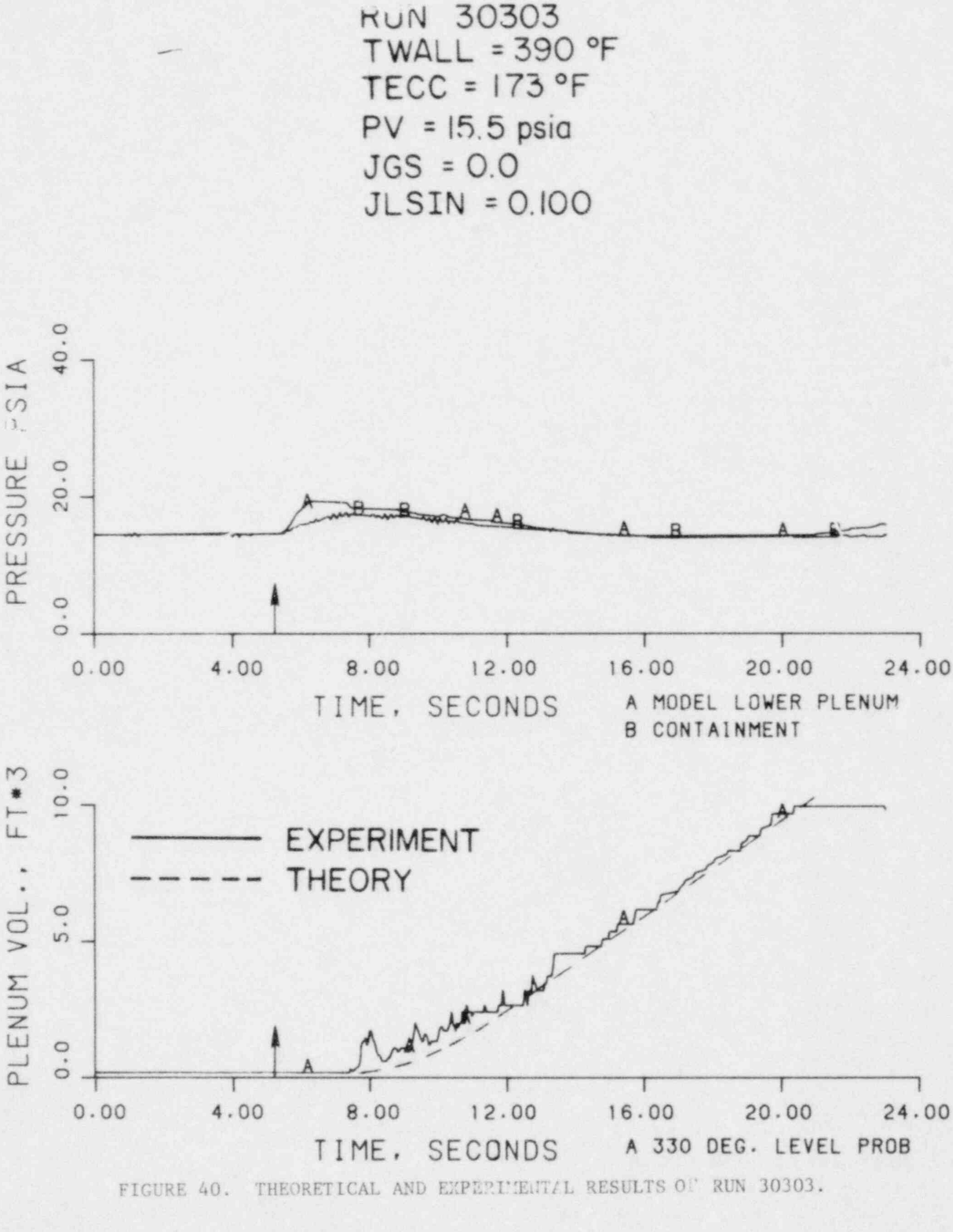

FIGURE 40. THEORETICAL AND EXPERIMENTAL RESULTS OF RUN 30303.

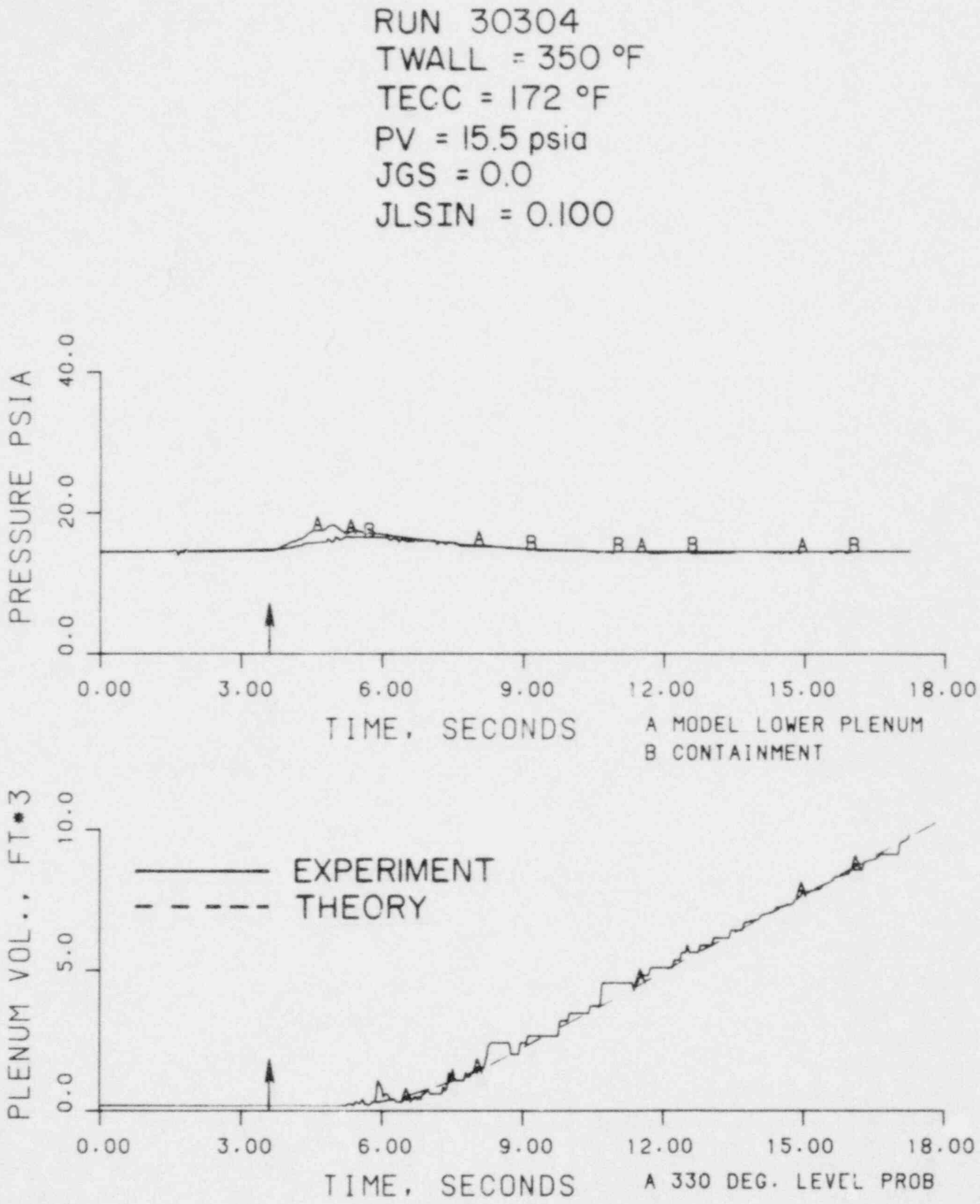

FIGURE 41. THEORETICAL AND EXPERIMENTAL RESULTS OF RUN 30304.

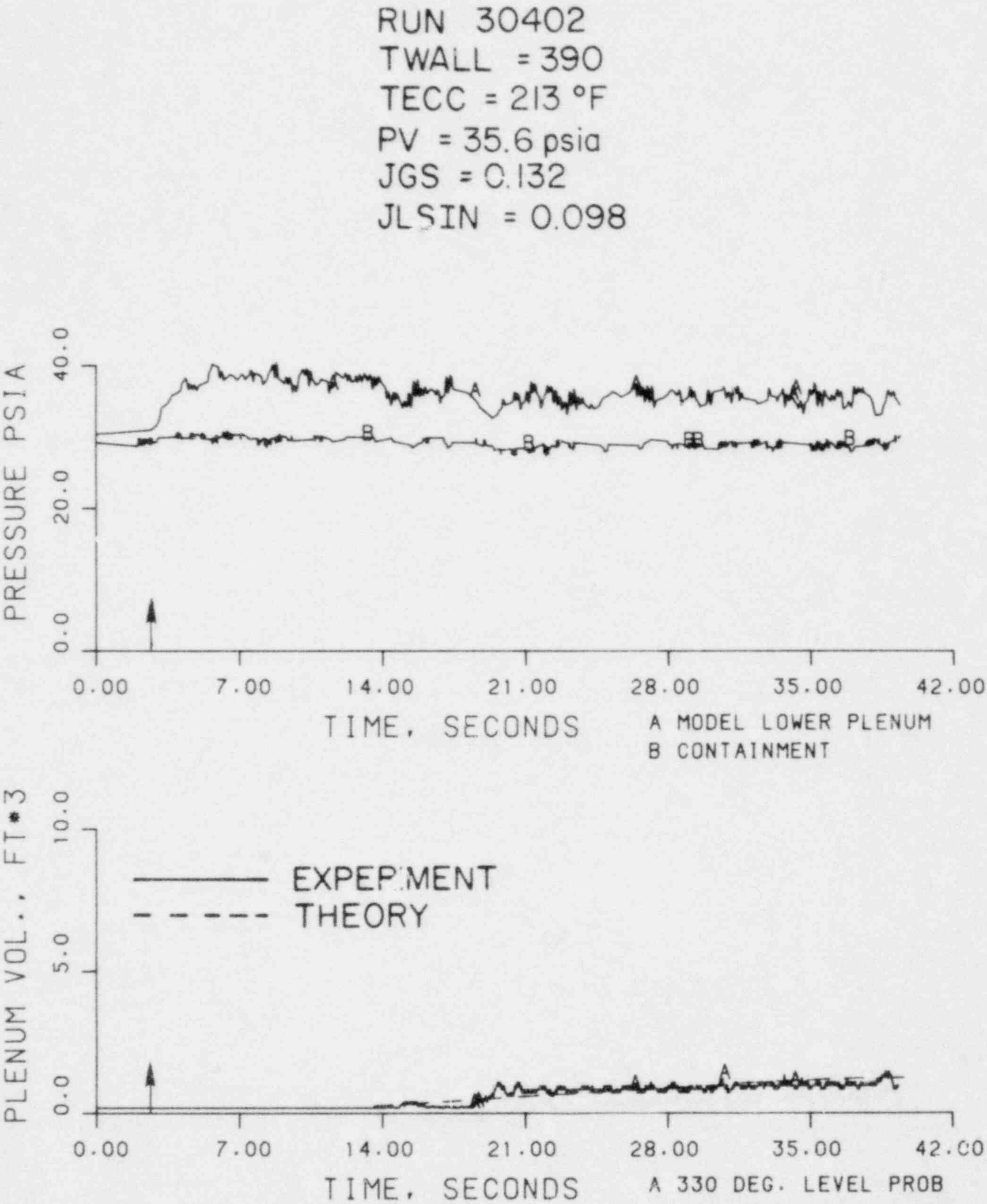

FIGURE 42. THEORETICAL AND EXPERIMENTAL RESULTS OF RUN 30402.

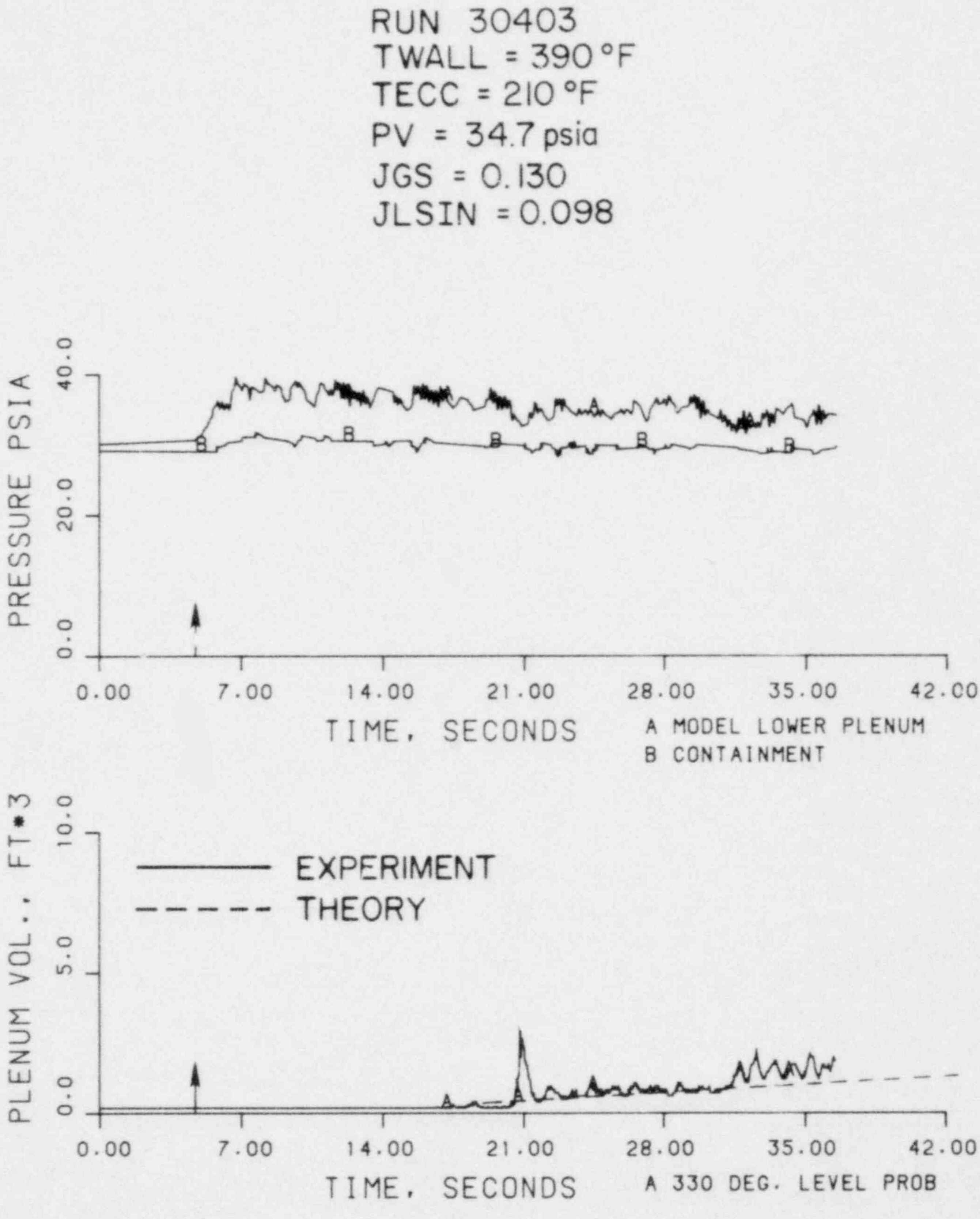

FIGURE 43. THEORETICAL AND EXPERIMENTAL RESULTS OF RUN 30403.

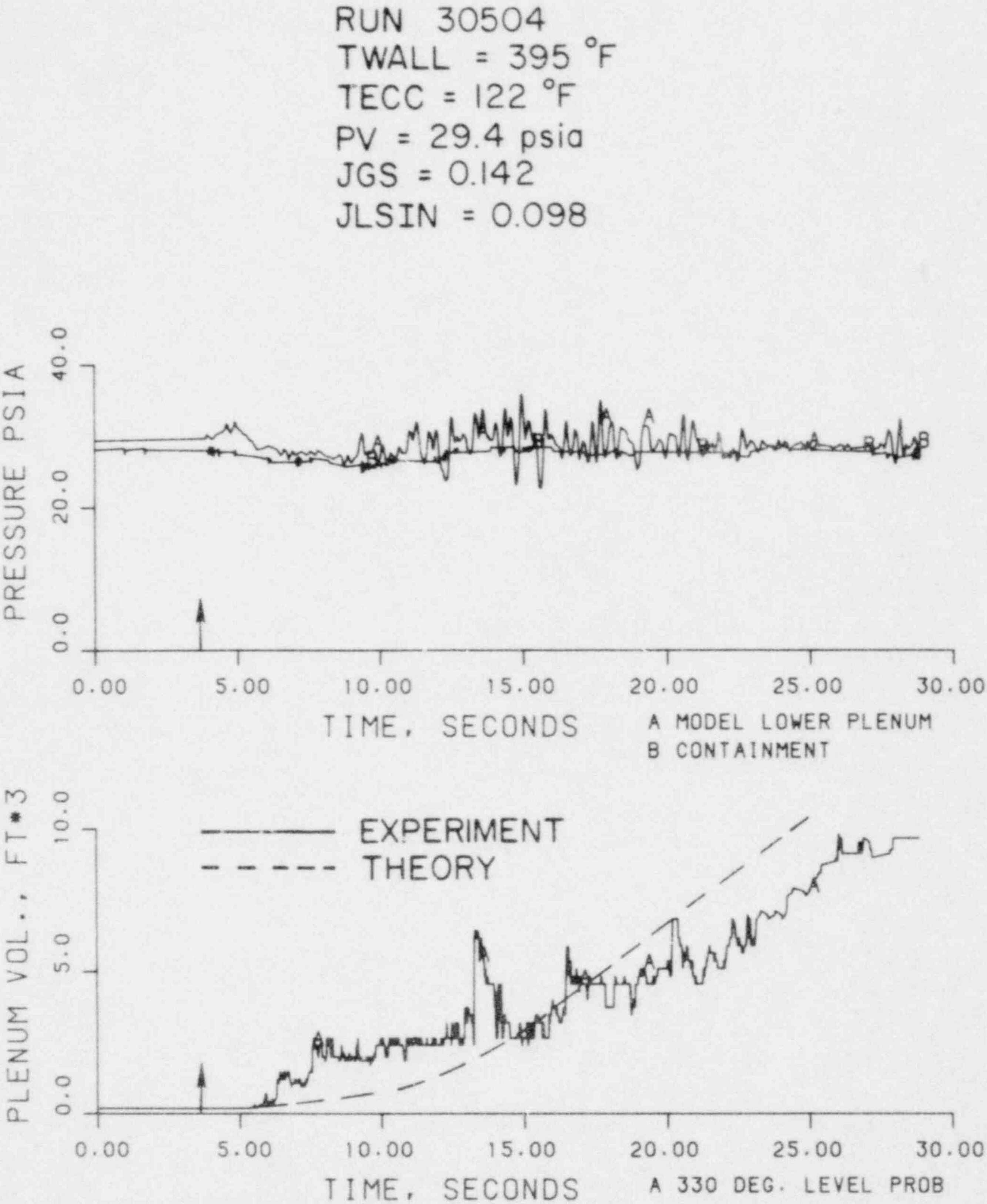

FIGURE 44. THEORETICAL AND EXPERIMENTAL RESULTS OF RUN 30504.

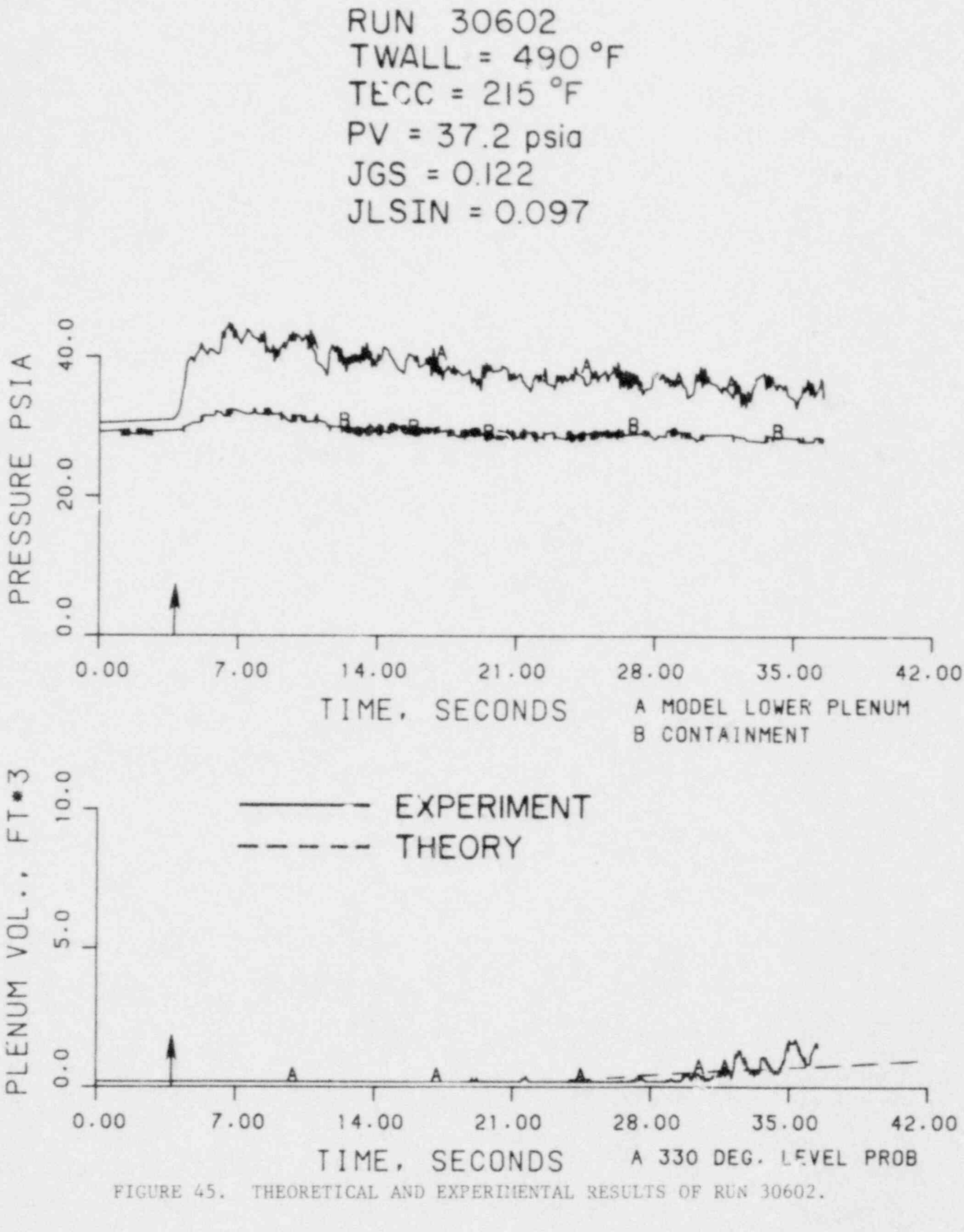

FIGURE 45. THEORETICAL AND EXPERIMENTAL RESULTS OF RUN 30602.

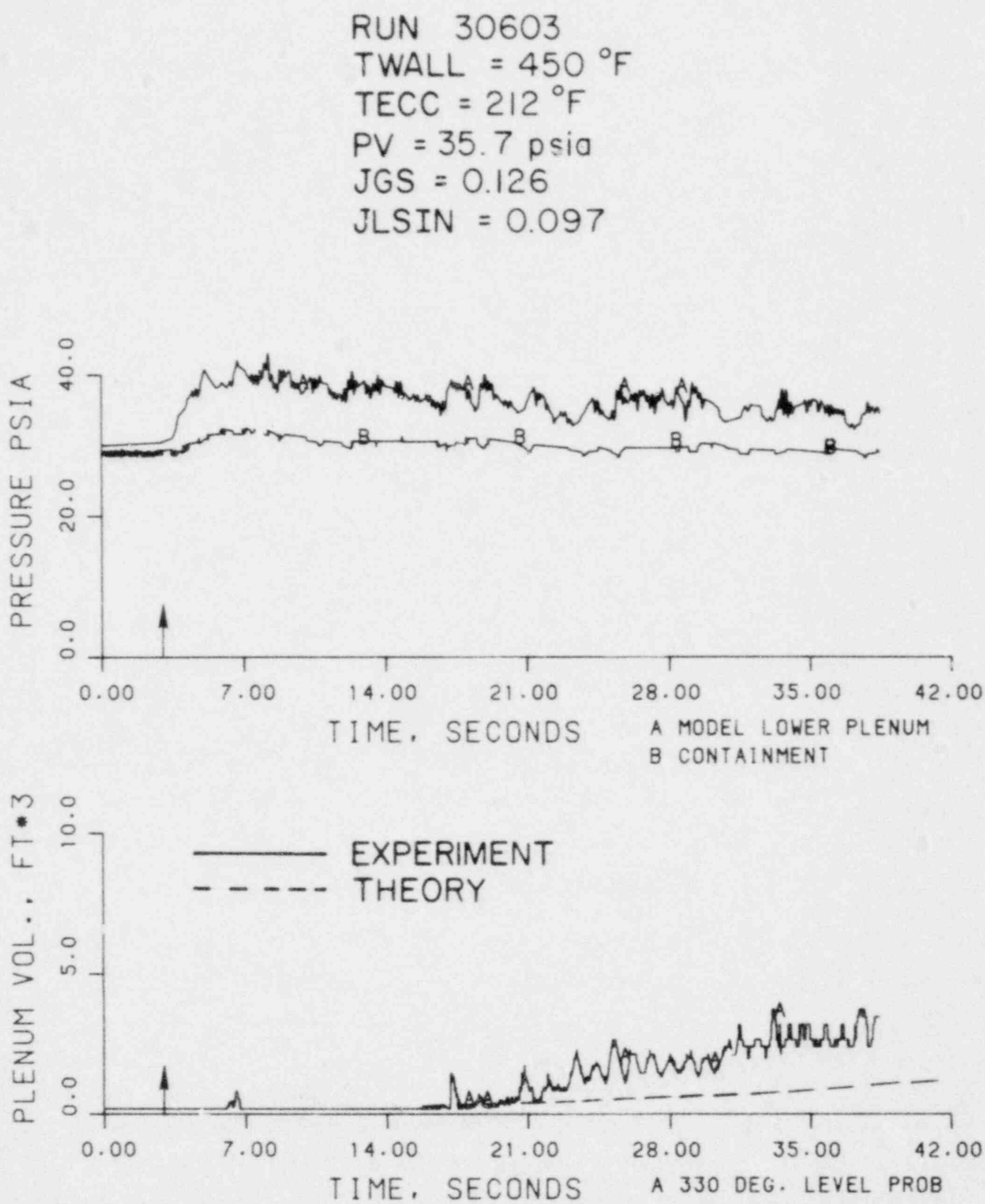

FIGURE 46. THEORETICAL AND EXPERIMENTAL RESULTS OF RUN 30603.

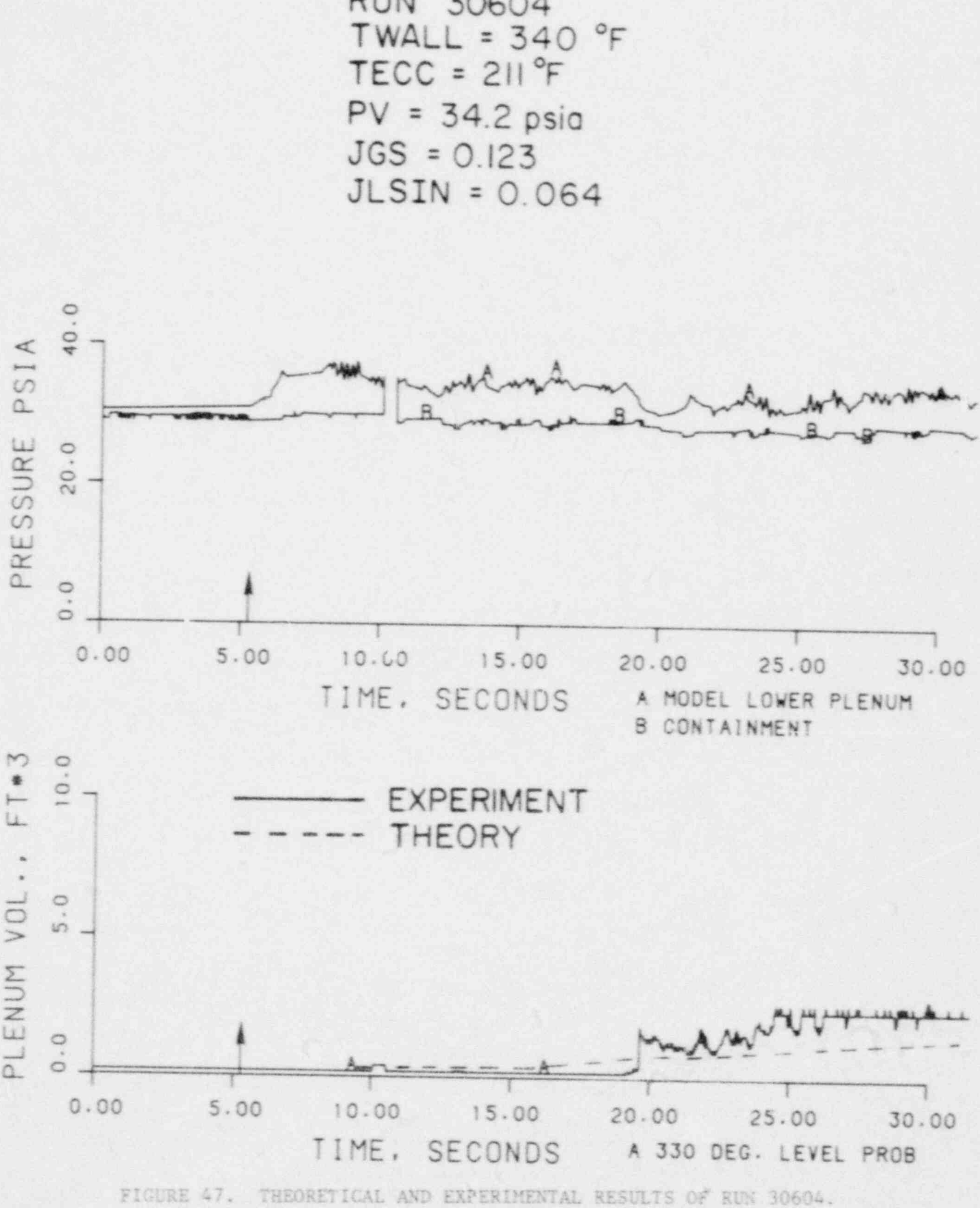

FIGURE 47. THEORETICAL AND EXPERIMENTAL RESULTS OF RUN 30604.

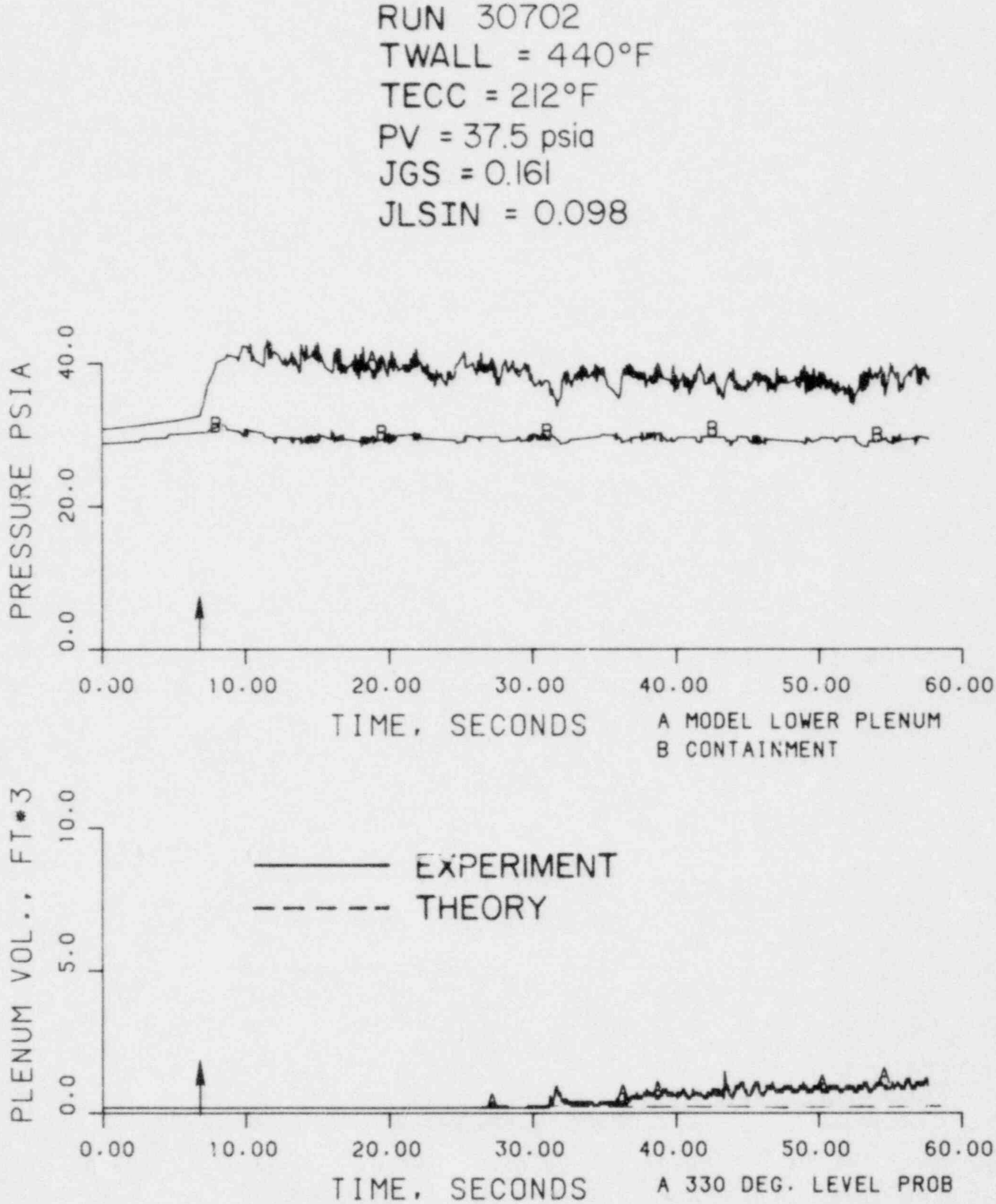

FIGURE 48. THEORETICAL AND EXPERIMENTAL RESULTS OF RUN 30702.

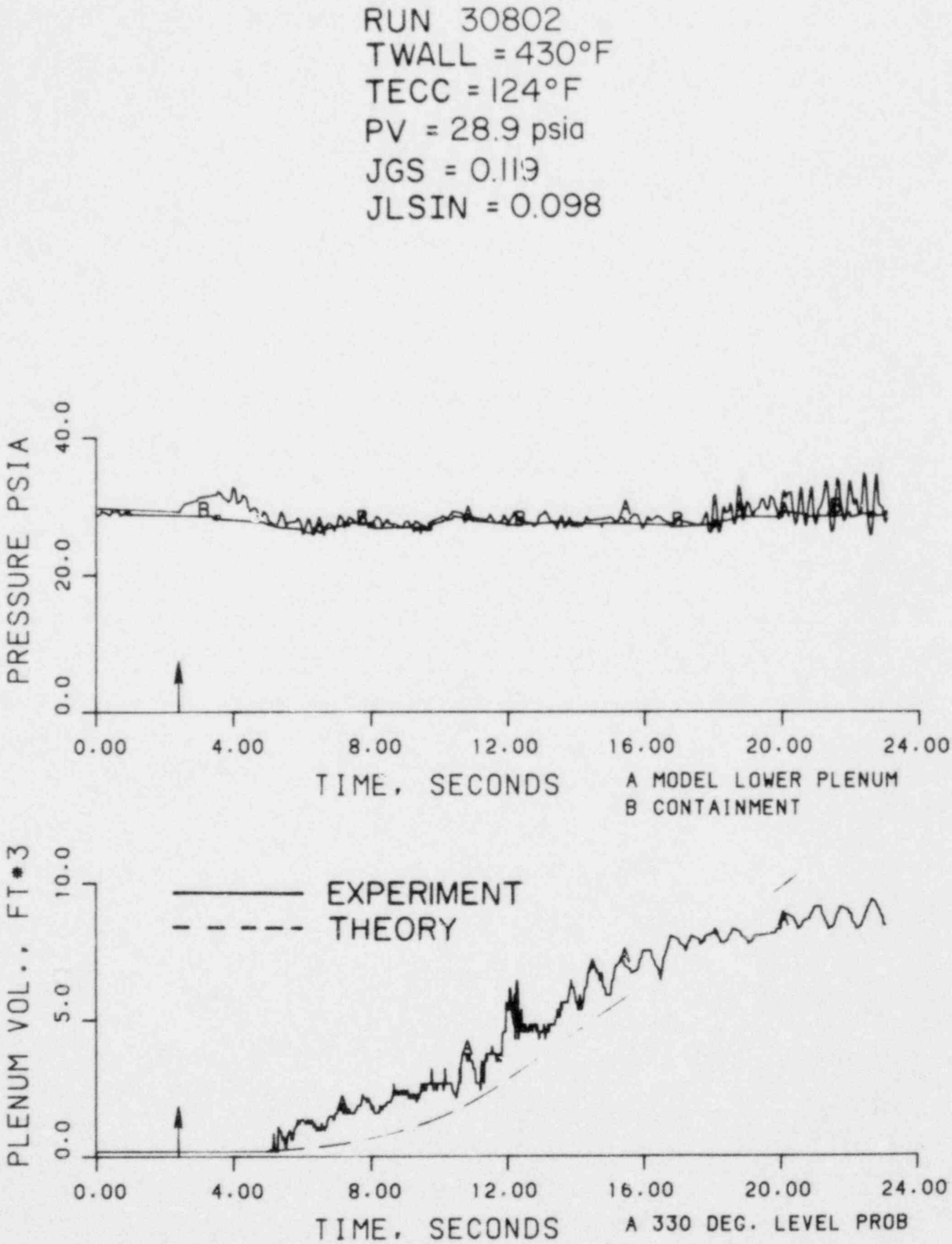

FIGURE 49. THEORETICAL AND EXPERIMENTAL RESULTS OF RUN 30802.

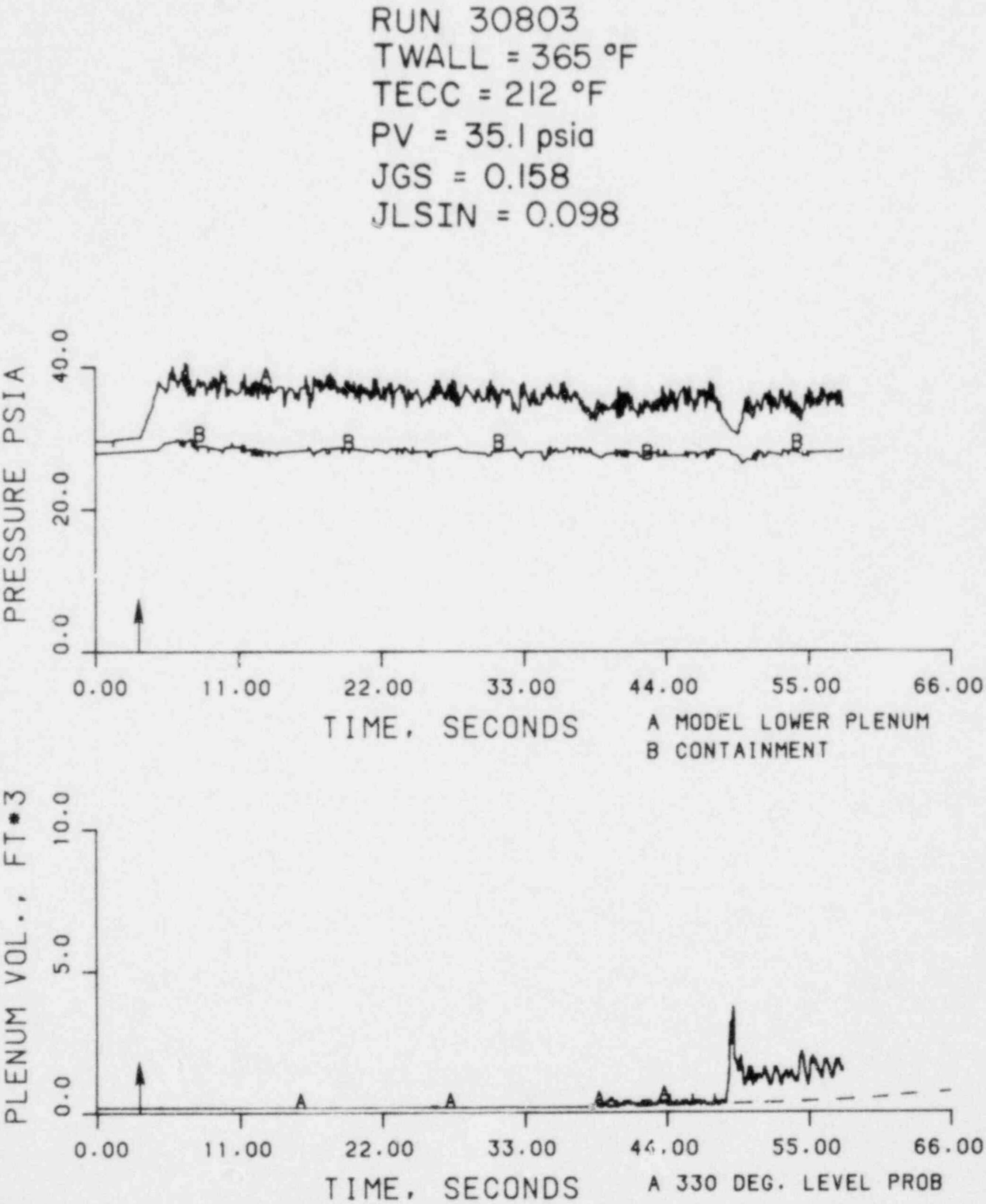

FIGURE 50. THEORETICAL AND EXPERIMENTAL RESULTS OF RUN 30803.

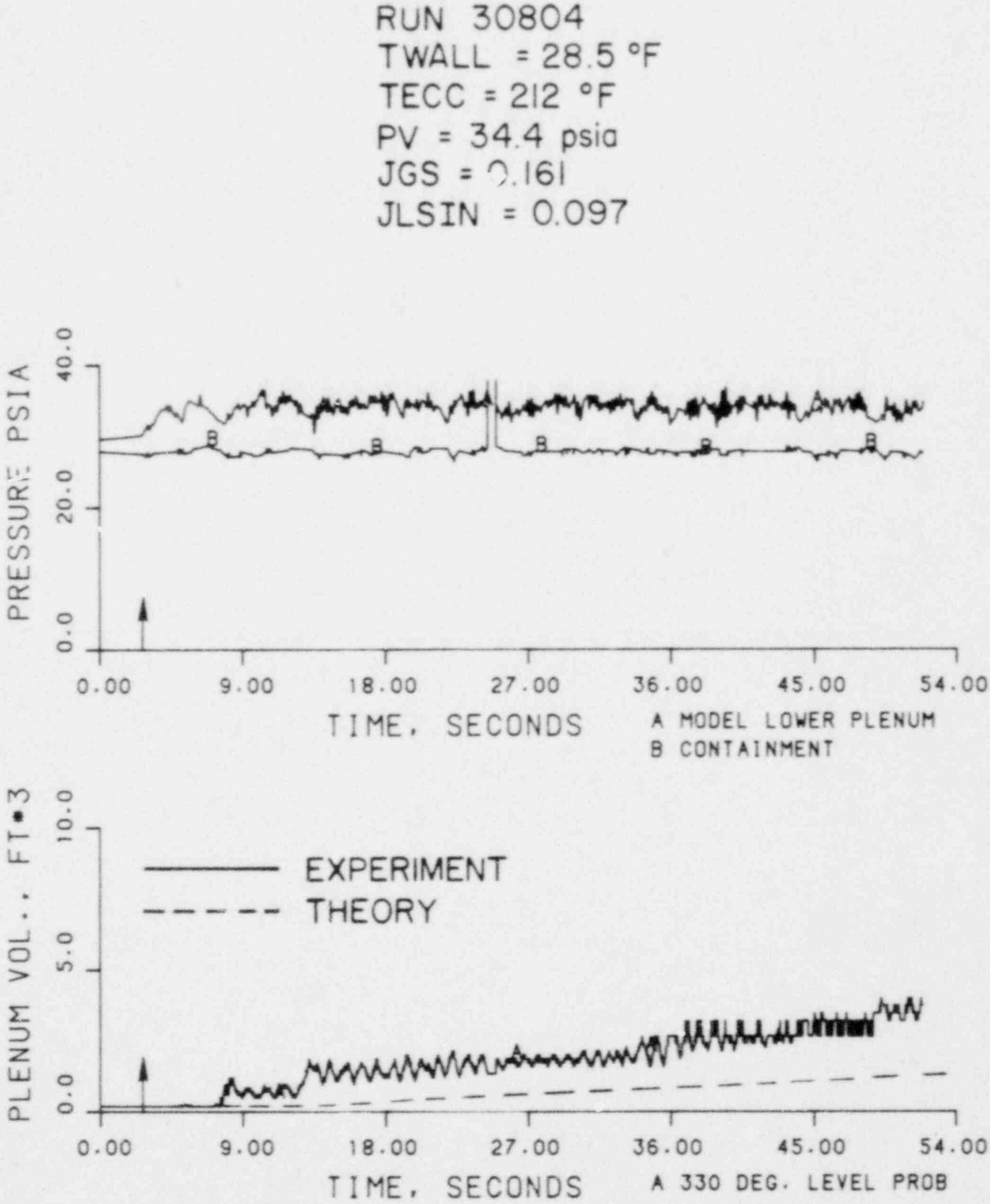

FIGURE 51. THEORETICAL AND EXPERIMENTAL RESULTS OF RUN 30804.

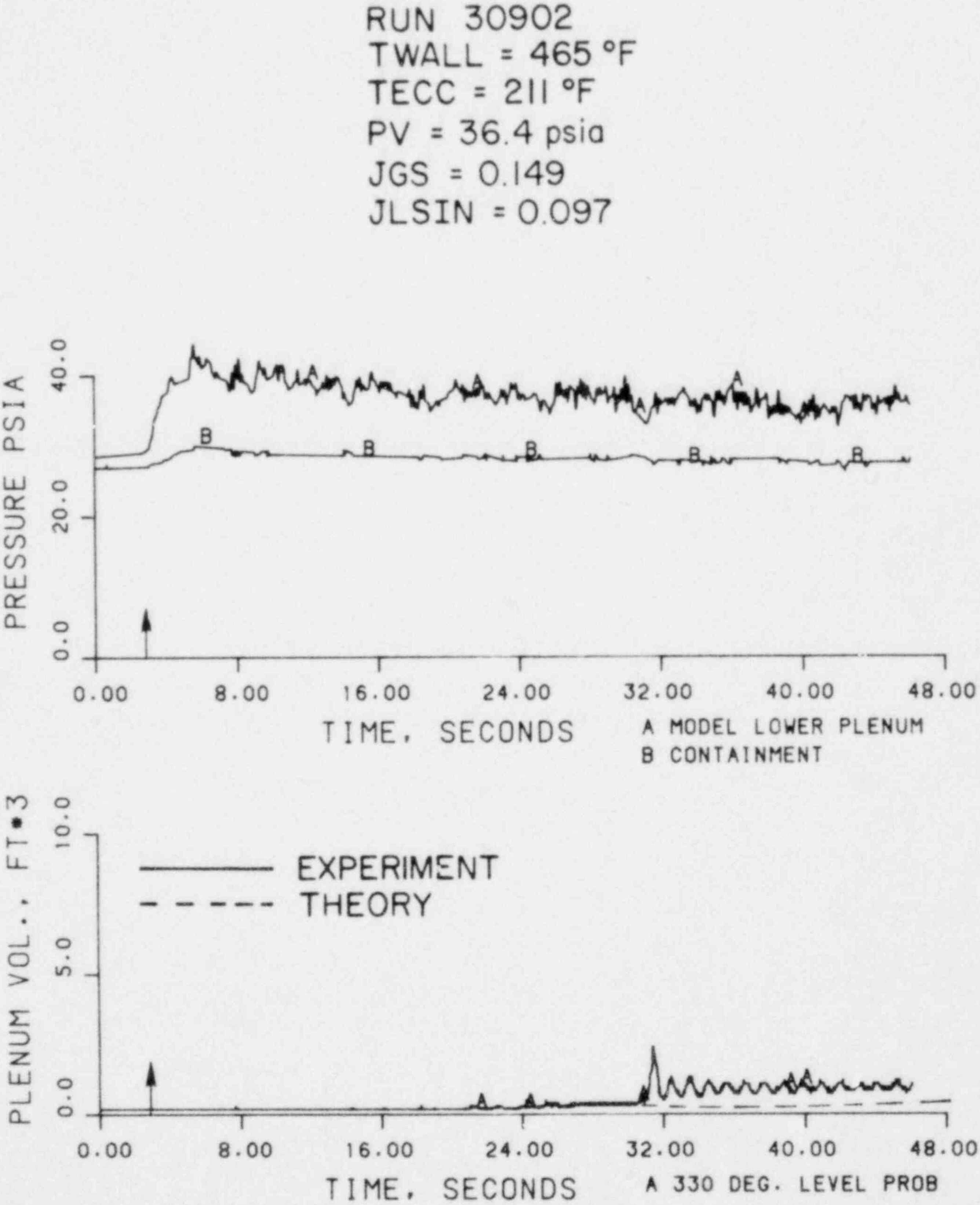

FIGURE 52. THEORETICAL AND EXPERIMENTAL RESULTS OF RUN 30902.

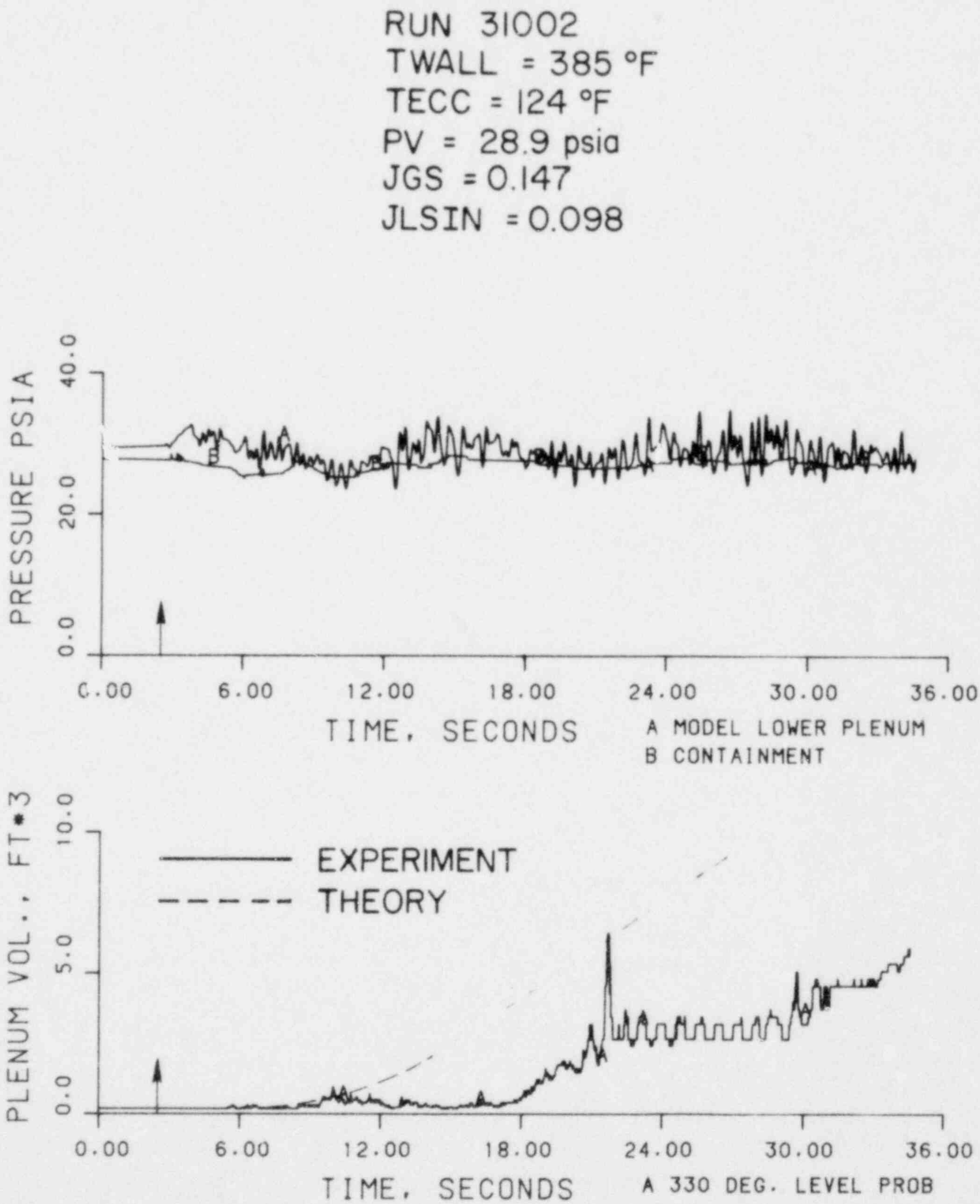

FIGURE 53. THEORETICAL AND EXPERIMENTAL RESULTS OF RUN 31002.

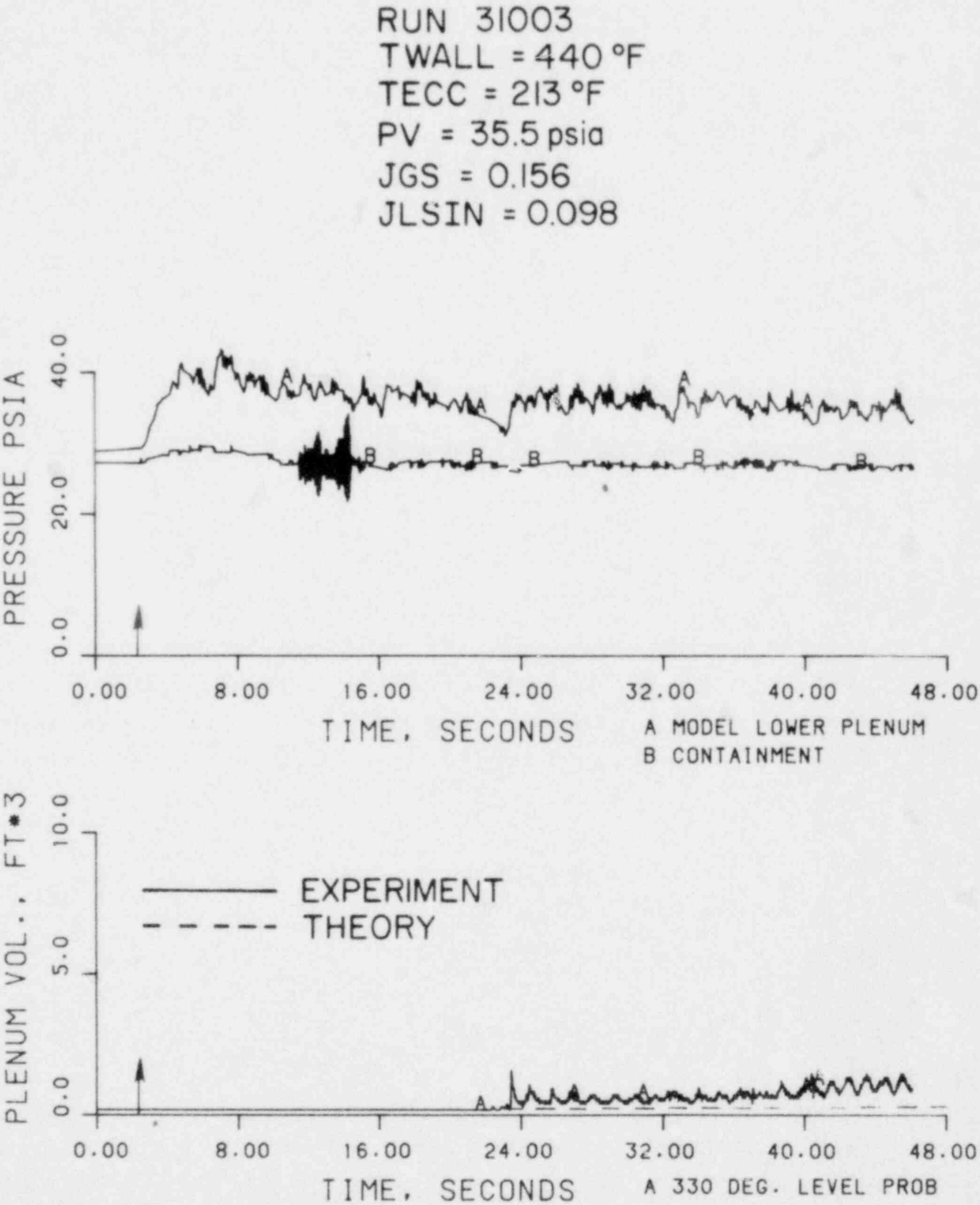

FIGURE 54. THEORETICAL AND EXPERIMENTAL RESULTS OF RUN 31003.

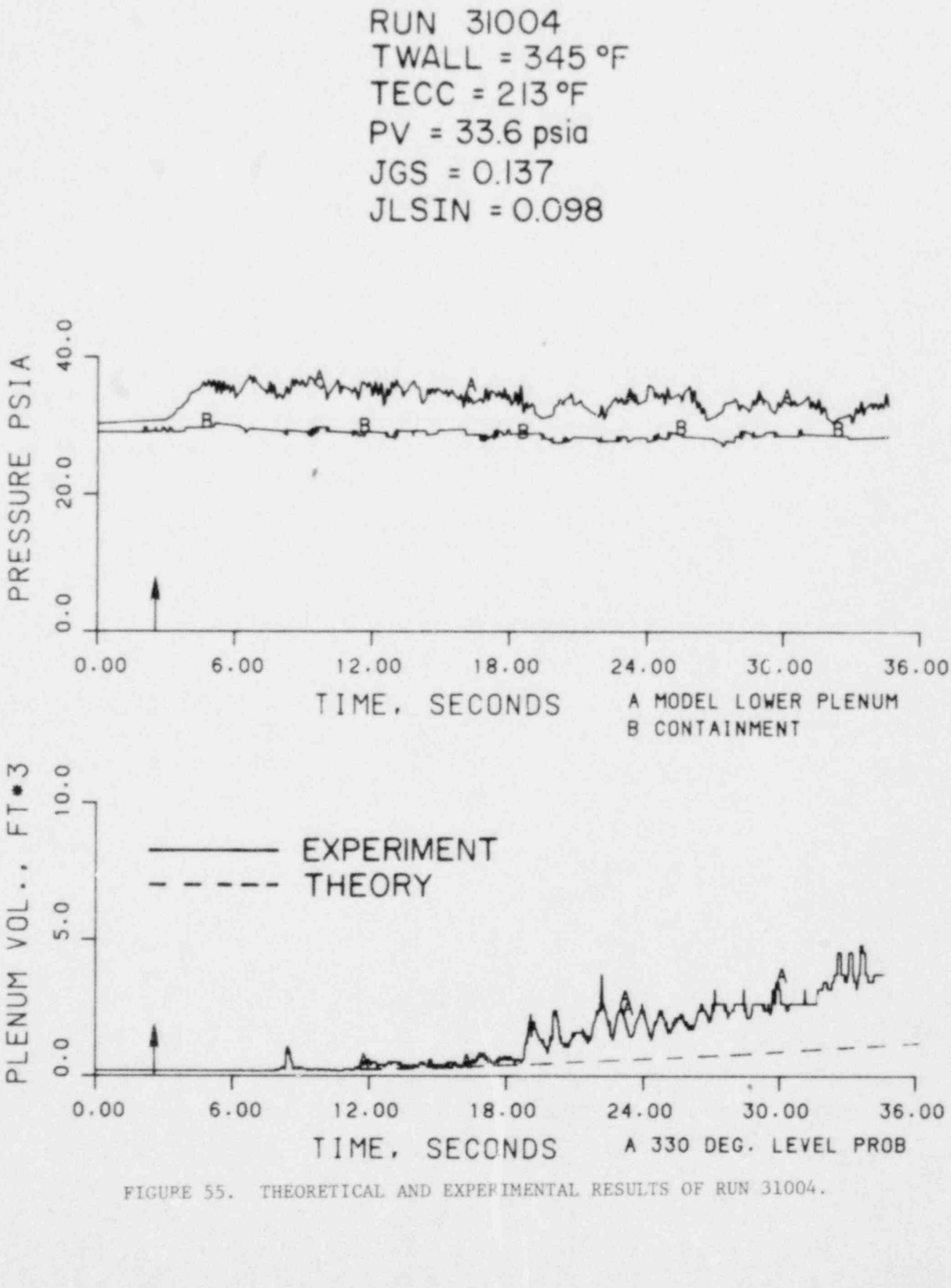

FIGURE 55. THEORETICAL AND EXPERIMENTAL RESULTS OF RUN 31004.

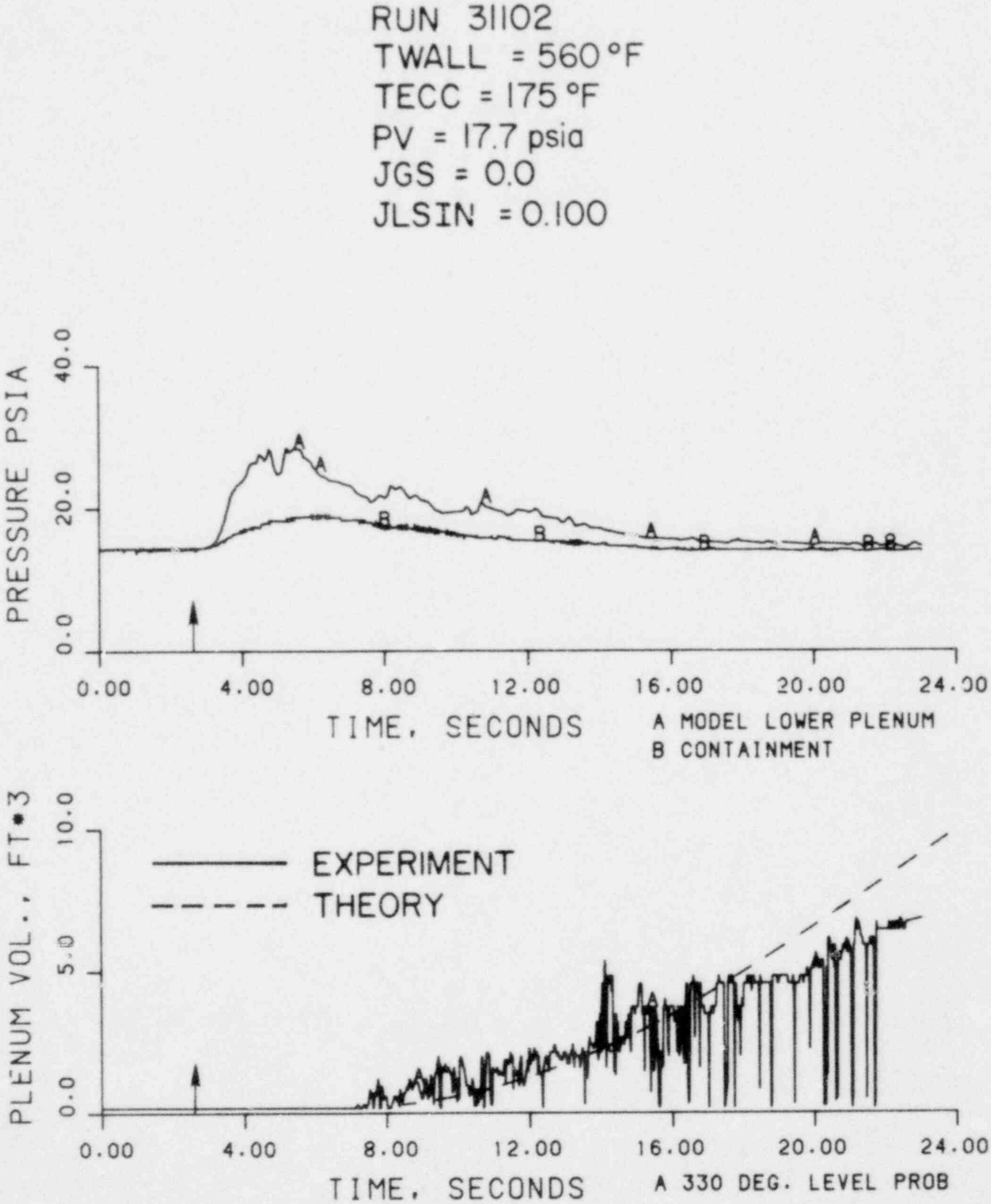

FIGURE 56. THEORETICAL AND EXPERIMENTAL RESULTS OF RUN 31102.

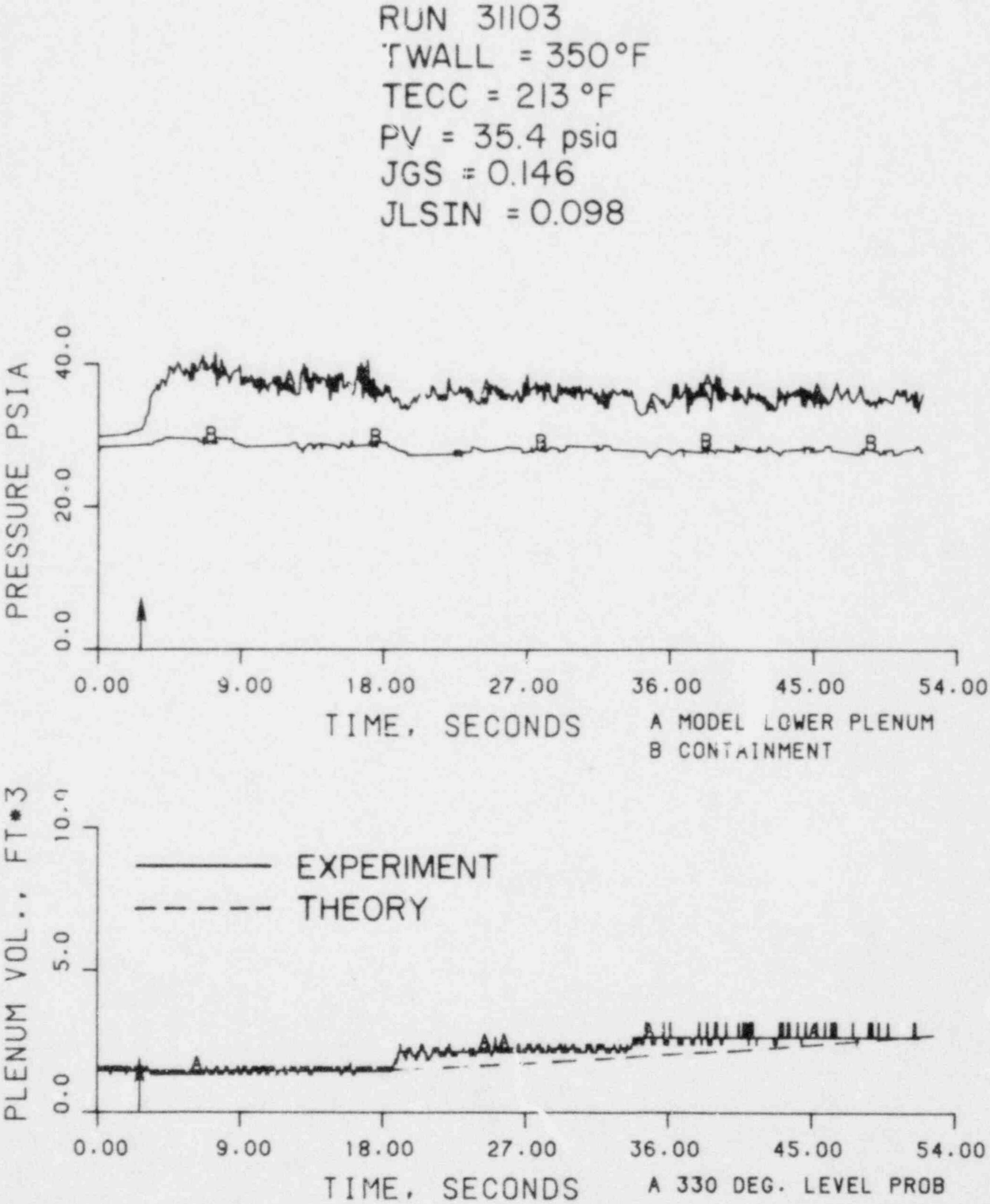

FIGURE 57. THEORETICAL AND EXPERIMENTAL RESULTS OF RUN 31103.

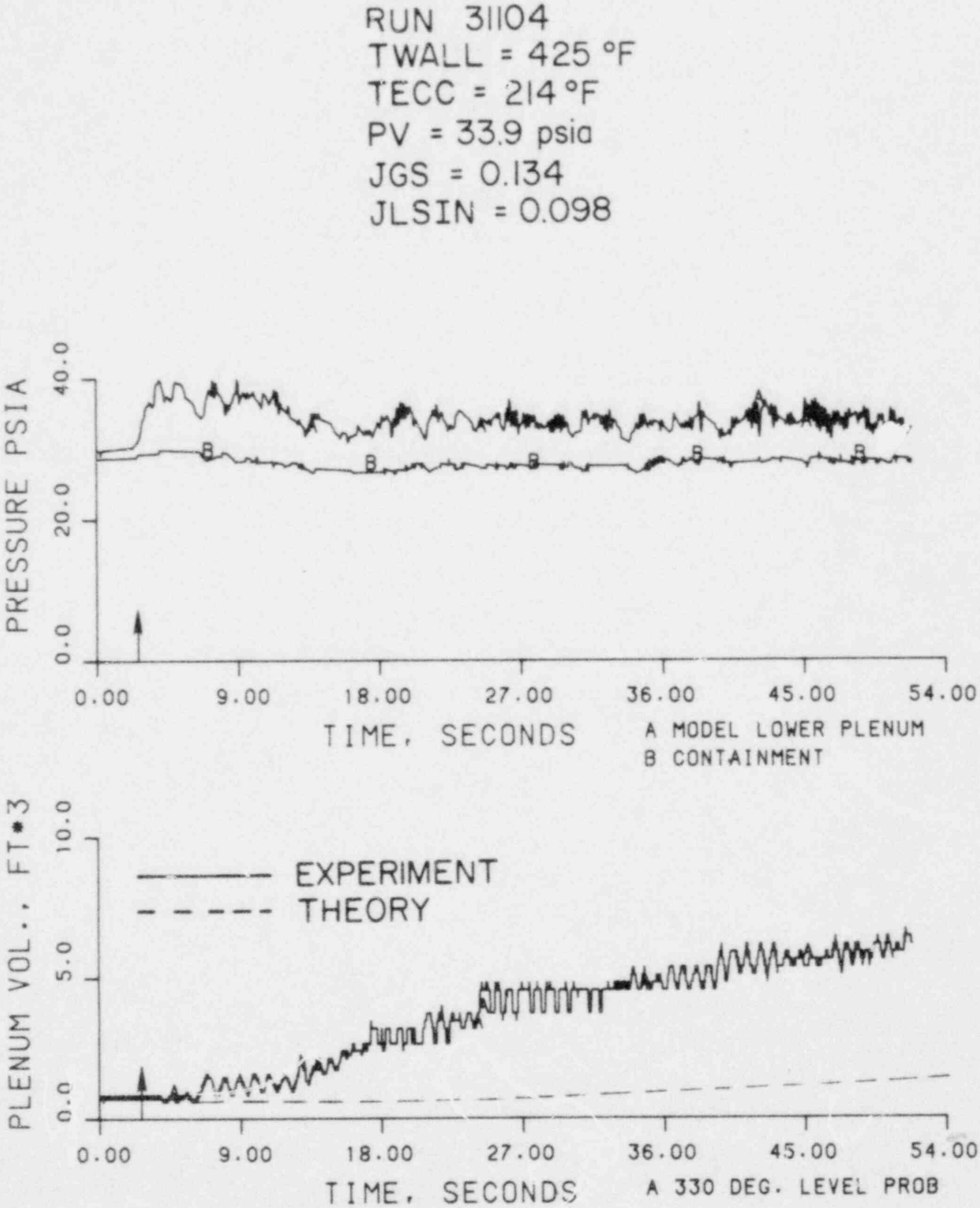

FIGURE 58. THEORETICAL AND EXPERIMENTAL RESULTS OF RUN 31104.

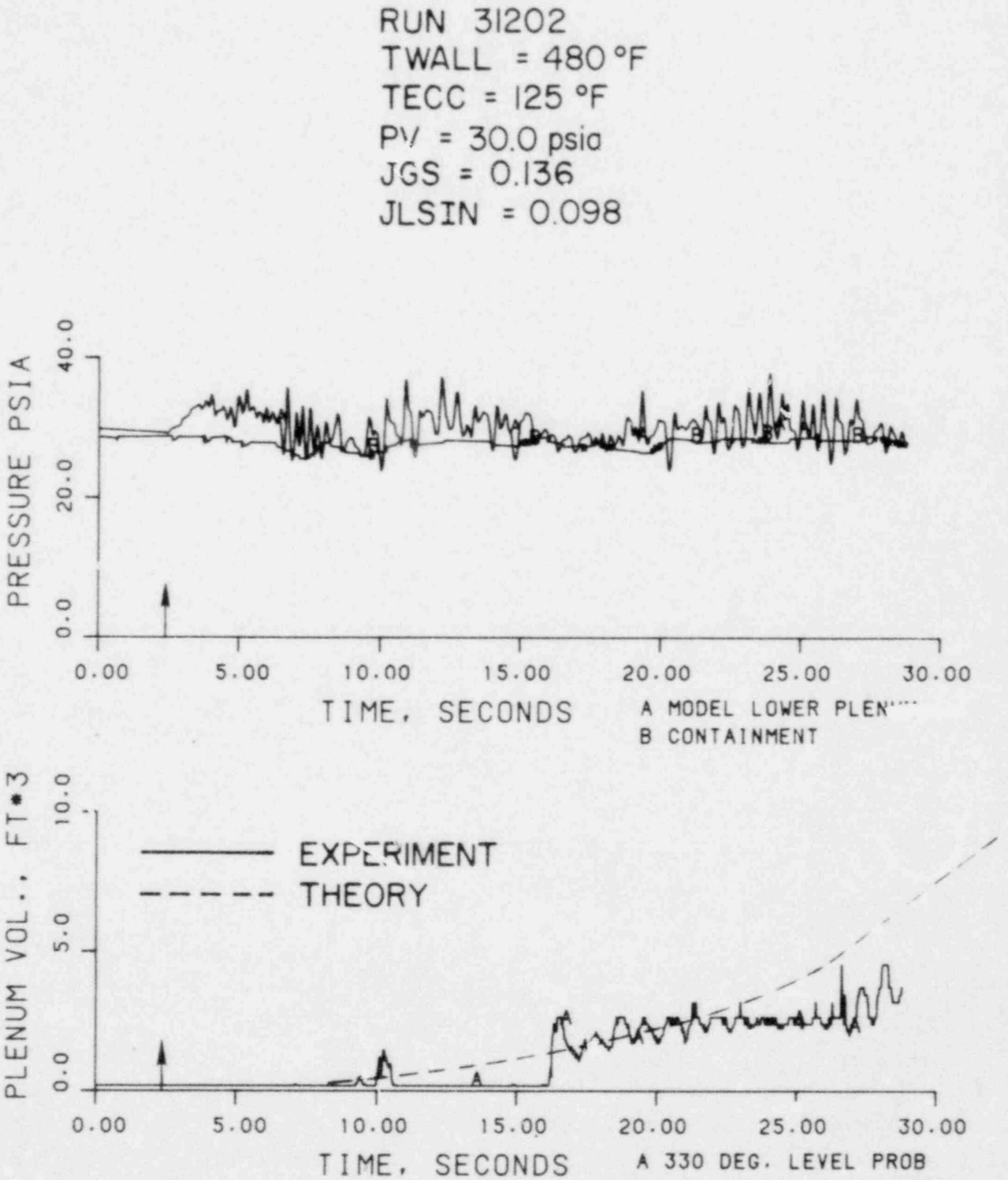

FIGURE 59. THEORETICAL AND EXPERIMENTAL RESULTS OF RUN 31202.

RUN 31302
TWALL = 420 °F
TECC = 125 °F
PV = 28.8 psia
JGS = 0.133
JLSIN = 0.098

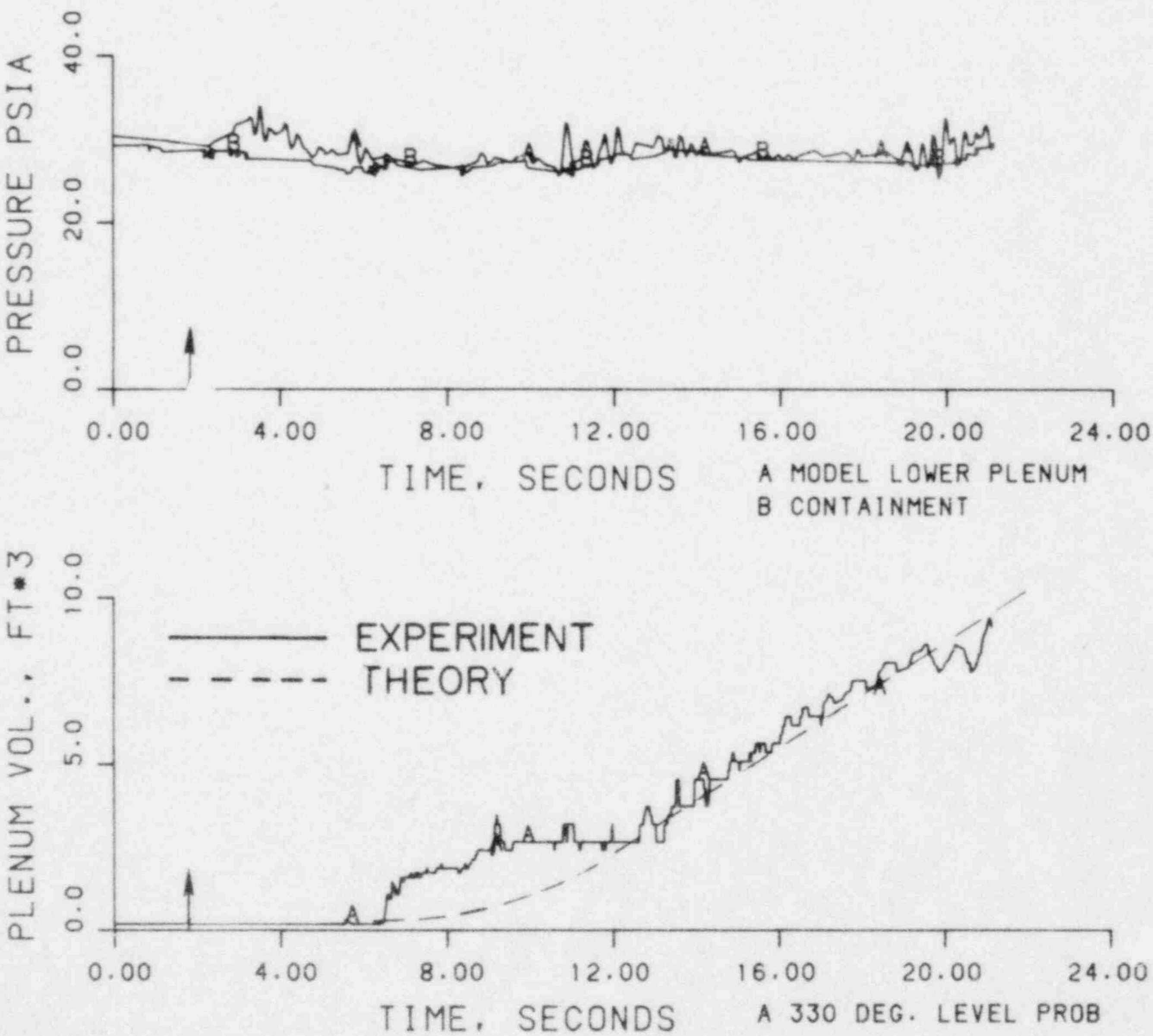

FIGURE 60. THEORETICAL AND EXPERIMENTAL RESULTS OF RUN 31302.

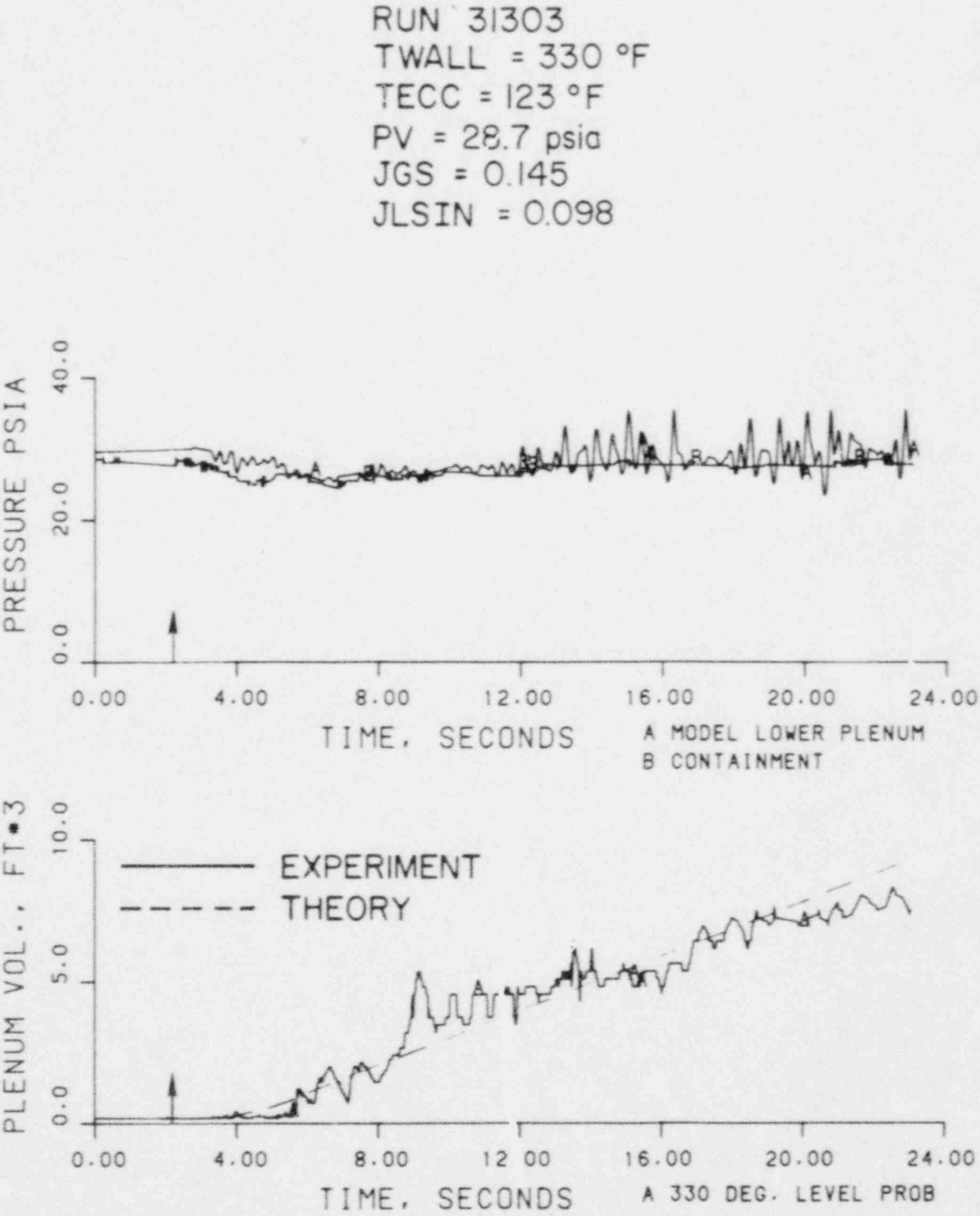

FIGURE 61. THEORETICAL AND EXPERIMENTAL RESULTS OF RUN 31303.

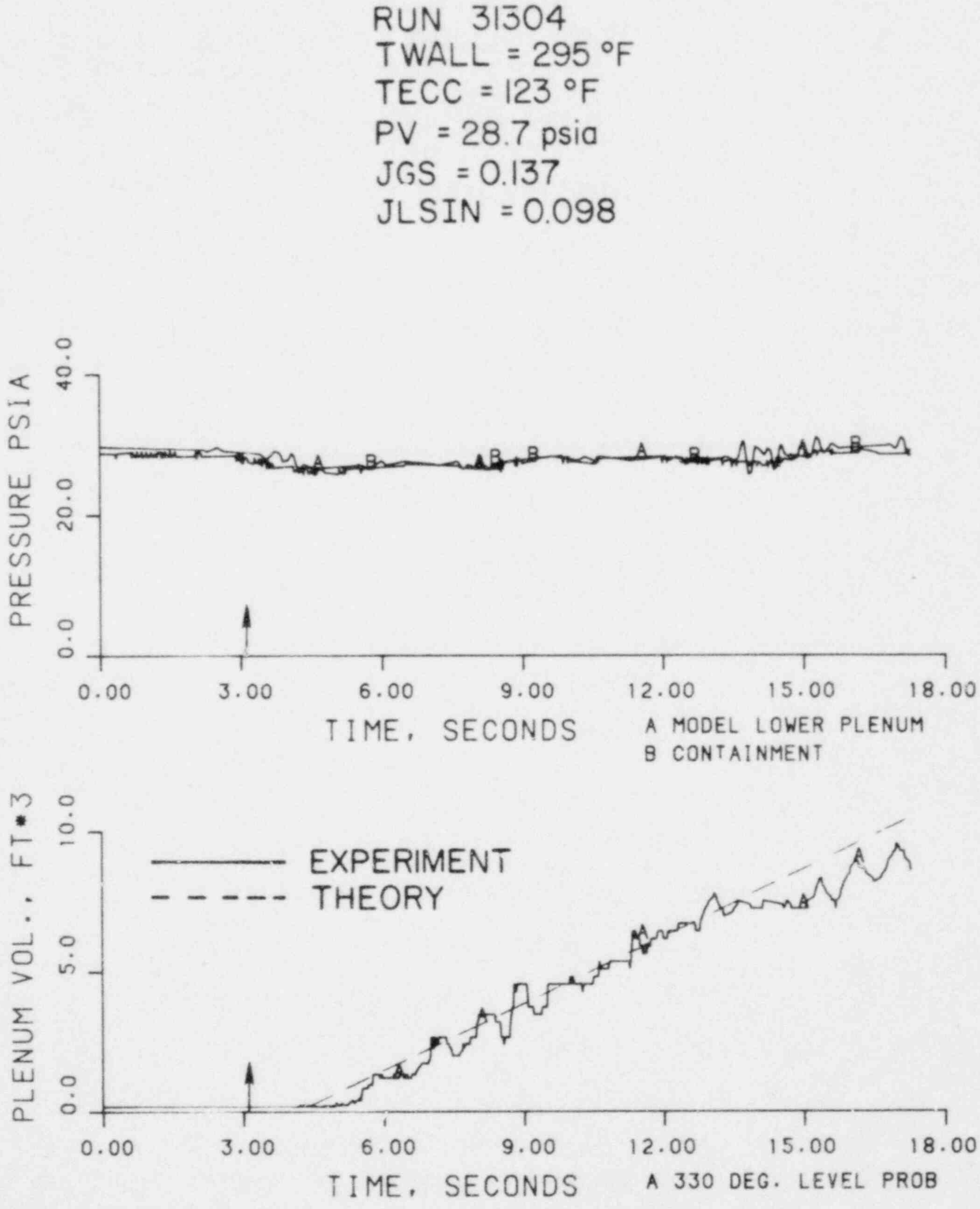

FIGURE 62. THEORETICAL AND EXPERIMENTAL RESULTS OF RUN 31304.

REFERENCES

(1) Segev, A., et al, "Steam-Water Mixing and System Hydrodynamics Program, Task 4", Quarterly Progress Report, January-March, 1980, NUREG/CR-1742, BMI-2065 (September, 1980).*

(2) Segev, A., Flanigan, L. J., and Collier, R. P., "Steam-Water Mixing and System Hydrodynamics Program, Task 4", Quarterly Progress Report, April-June, 1980, NUREG/CR-1743, BMI-2067 (September, 1980).*

(3) Segev, A., and Collier, R. P., "Topical Report on Development of a Mechanistic Model for ECC Penetration in a PWR Downcomer", NUREG/CR-1426, BMI-2051 (June, 1980).*

(4) Crowley, C. J., Block, J. A., and Cary, C. N., "Downcomer Effects in a 1/15-Scale PWR Geometry-Experimental Data Report", NUREG-0281, Creare TN-252 (February, 1977).*

(5) Segev, A., et al, "Countercurrent Steam Condensation and its Application to ECC Penetration" in Experimental and Analytical Modeling of LWR Safety Experiments, L. E. Hochreiter and G. L. Sozzi, ed., pp 101-108, ASME, New York (1980).

(6) Saha, P., and Zuber, N., "Point of Net Vapor Generation and Vapor Void Fraction in Subcooled Boiling", Paper No. B4.7, Proc. Fifth Int. Heat Transfer Conf., Tokyo, Vol. IV (1974).

* Available from National Technical Information Service (NTIS), Springfield, Virginia, 22161. Also available from the NRC/GPO Sales Program, U. S. Nuclear Regulatory Commission, Washington, D.C. 20555.

NRC FORM 335 (7-77)

U.S. NUCLEAR REGULATORY COMMISSION

BIBLIOGRAPHIC DATA SHEET

1. REPORT NUMBER (Assigned by DDC)
NUREG/CR-1822
BMI-2069

4. TITLE AND SUBTITLE (Add Volume No., if appropriate)
Steam-Water Mixing and System Hydrodynamics Program,
Task 4 - Quarterly Progress Report
July 1, 1980 - September 30, 1980

2. (Leave blank)

3. RECIPIENT'S ACCESSION NO.

7. AUTHOR(S)
Aryeh Segev and Robert P. Collier

5. DATE REPORT COMPLETED

MONTH	YEAR
October	1980

DATE REPORT ISSUED

MONTH	YEAR
November	1980

9. PERFORMING ORGANIZATION NAME AND MAILING ADDRESS (Include Zip Code)
Battelle, Columbus Laboratories
505 King Avenue
Columbus, Ohio 43201

6. (Leave blank)

8. (Leave blank)

12. SPONSORING ORGANIZATION NAME AND MAILING ADDRESS (Include Zip Code)
Office of Nuclear Regulatory Research
U. S. Nuclear Regulatory Commission
Washington, D.C. 20555

10. PROJECT/TASK/WORK UNIT NO.

11. CONTRACT NO.
FIN No. A4048

13. TYPE OF REPORT
Quarterly Progress Report

PERIOD COVERED (Inclusive dates)
July 1, 1980 - September 30, 1980

15. SUPPLEMENTARY NOTES

14. (Leave blank)

16. ABSTRACT (200 words or less)

During this quarter we analyzed results from hot wall tests in the 2/15-scale model and compared the experiment filling curves to those predicted by the mechanistic model. The comparison shows a good agreement for both the large break tests and scaled size break tests.

17. KEY WORDS AND DOCUMENT ANALYSIS
ECC Bypass
Scaling
Condensation
Analysis
Experiments

17a. DESCRIPTORS

17b. IDENTIFIERS/OPEN-ENDED TERMS

18. AVAILABILITY STATEMENT
Unlimited

19. SECURITY CLASS (This report)
Unclassified

20. SECURITY CLASS (This page)

21. NO. OF PAGES

22. PRICE
$

NRC FORM 335 (7-77)